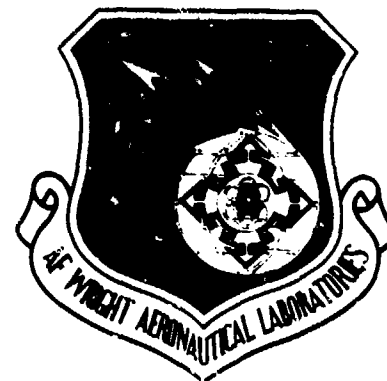


AD A130944

AFWAL TR-83-4018

## **OPTIMUM MICROSTRUCTURES FOR SPF USING HYDROVAC**

**S. M. L. Sastry  
R. J. Lederich  
J. E. O'Neal**



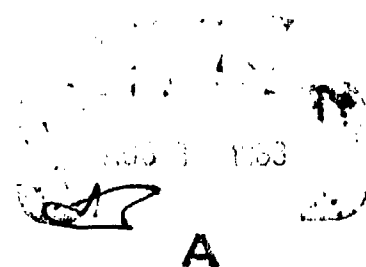
**McDonnell Douglas Research Laboratories  
St. Louis, Missouri 63166**

**February 1983  
Final Report for Period 1 September 1980 - 1 October 1982**

Approved for public release; distribution unlimited

DTIC FILE COPY

**MATERIALS LABORATORY  
AIR FORCE WRIGHT AERONAUTICAL LABORATORIES  
AIR FORCE SYSTEMS COMMAND  
WRIGHT-PATTERSON AIR FORCE BASE, OHIO 45433**



**A**

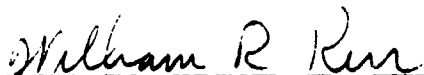
**83 08 02 005**

## NOTICE

When Government drawings, specifications, or other data are used for any purpose other than in connection with a definitely related Government procurement operation, the United States Government thereby incurs no responsibility nor any obligation whatsoever; and the fact that the government may have formulated, furnished, or in any way supplied the said drawings, specifications, or other data, is not to be regarded by implication or otherwise as in any manner licensing the holder or any other person or corporation, or conveying any rights or permission to manufacture use, or sell any patented invention that may in any way be related thereto.

This report has been reviewed by the Office of Public Affairs (ASD/PA) and is releasable to the National Technical Information Service (NTIS). At NTIS, it will be available to the general public, including foreign nations.

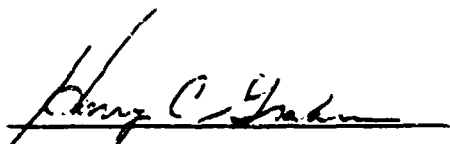
This technical report has been reviewed and is approved for publication.



WILLIAM R. KERR  
Project Engineer  
FOR THE COMMANDER



NORMAN M. GEYER  
Technical Area Manager  
Processing & High Temperature  
Materials Branch  
Metals & Ceramics Division



HENRY C. GRAHAM, Chief  
Processing & High Temperature  
Materials Branch  
Metals and Ceramics Division

"If your address has changed, if you wish to be removed from our mailing list, or if the addressee is no longer employed by your organization please notify AFWAL/MLLM, W-PAFB, OH 45433 to help us maintain a current mailing list".

Copies of this report should not be returned unless return is required by security considerations, contractual obligations, or notice on a specific document.

UNCLASSIFIED

SECURITY CLASSIFICATION OF THIS PAGE (When Data Entered)

REPORT DOCUMENTATION PAGE		READ INSTRUCTIONS BEFORE COMPLETING FORM
1. REPORT NUMBER AFWAL-TR-83-4018	2. GOVT ACCESSION NO. AD-A130944	3. RECIPIENT'S CATALOG NUMBER
4. TITLE (and Subtitle) OPTIMUM MICROSTRUCTURES FOR SPF USING HYDROVAC		5. TYPE OF REPORT & PERIOD COVERED FINAL REPORT 1 Sep 80 - 1 Oct 82
		6. PERFORMING ORG. REPORT NUMBER
7. AUTHOR(s) S. M. L. Sastry R. J. Lederich J. E. O'Neal		8. CONTRACT OR GRANT NUMBER(s) F33615-80-C-5118
9. PERFORMING ORGANIZATION NAME AND ADDRESS McDonnell Douglas Research Laboratories McDonnell Douglas Corporation St. Louis, Missouri 63166		10. PROGRAM ELEMENT, PROJECT, TASK AREA & WORK UNIT NUMBERS Project 2418
11. CONTROLLING OFFICE NAME AND ADDRESS Materials Laboratory Air Force Wright Aeronautical Laboratories Air Force Systems Command Wright-Patterson Air Force Base, Ohio 45433		12. REPORT DATE February 1983
		13. NUMBER OF PAGES 124
14. MONITORING AGENCY NAME & ADDRESS (if different from Controlling Office)		15. SECURITY CLASS. (of this report) Unclassified
		15a. DECLASSIFICATION/DOWNGRADING SCHEDULE
16. DISTRIBUTION STATEMENT (of this Report) Approved for public release; distribution unlimited		
17. DISTRIBUTION STATEMENT (of the abstract entered in Block 20, if different from Report)		
18. SUPPLEMENTARY NOTES		
19. KEY WORDS (Continue on reverse side if necessary and identify by block number)		
forming	Eutectoid decomposition	Creep
Diffusion bonding	Fatigue	Microstructure
Superplastic	Sheet metal	Hydrogen additions
Ti-6Al-4V	Subgrain strengthening	Internal hydrogen
Ti-6Al-2Sn-4Zr-2Mo	Titanium	Tensile properties
		Beta transus
20. ABSTRACT (Continue on reverse side if necessary and identify by block number)		
<p>The effects of the addition of up to 1.0 wt% hydrogen as a transient alloying element on the mechanical properties, superplastic forming (SPF), and diffusion bonding (DB) of fine-grained equiaxed Ti-6Al-4V and duplex-annealed Ti-6Al-2Sn-4Zr-2Mo were determined.</p> <p>Uniquely fine microstructures were obtained in Ti-6Al-4V and Ti-6Al-2Sn-4Zr-2Mo by hydrovac processing which consists of adding = 1.0 wt% hydrogen to the alloy, beta annealing above 810°C, eutectoidly transforming at = 600°C, and dehydro-</p>		

DD FORM 1 JAN 73 1473

EDITION OF 1 NOV 65 IS OBSOLETE

UNCLASSIFIED

SECURITY CLASSIFICATION OF THIS PAGE (When Data Entered)

genating at 660-700°C.

Formkote T50 and Deltaglaze 349M coatings were used to prevent the evolution of hydrogen during the beta anneal and eutectoid decomposition treatment. Although the hydrogen content was maintained, excessive oxygen pickup occurred in the coated samples. Samples which were sealed in vacuum capsules during the transformation showed no oxygen contamination and exhibited increases in tensile strengths of  $\approx 100$  MPa and decreases in creep rates of an order-of-magnitude over conventionally processed alloys. Despite their initial fine microstructure, the hydrovac processed alloys did not exhibit improved superplastic formability and diffusion bondability because of rapid grain-growth at the forming/bonding temperatures.

Small amounts of internal hydrogen greatly improve the SPF of the alloys. Formability at 720-900°C was evaluated by an instrumented cone-forming test with continuous monitoring of strain with time. Argon/1% hydrogen and argon/4% hydrogen gas mixtures were used for charging the alloys with hydrogen as well as for superplastic forming. Hydrogen additions lower the beta-transus of alpha-beta titanium alloys, and the proportions of the alpha and beta phases required for optimum superplasticity can thus be obtained at lower temperatures in hydrogen-modified alloys than in standard alloys. The increased amount of beta phase in the hydrogen-modified titanium alloys increases diffusion rates and reduces the grain growth rates at forming temperature, thus reducing the time-dependent decrease in superplastic strain rate at a constant stress and the increase in flow stress at constant strain rate. Processing parameters for superplastic forming of Ti-6Al-4V and Ti-6Al-2Sn-4Zr-2Mo using argon-hydrogen gas mixtures were determined.

The evolution of hydrogen during forming improves the superplastic formability to a lesser extent than when hydrogen is maintained in the samples. Diffusion bondability is unaffected by either the presence or the evolution of internal hydrogen. Ti-6Al-4V and Ti-6Al-2Sn-4Zr-2Mo panels containing hydrogen were formed into large trough shapes without degradation of final mechanical properties after dehydrogenation.

## PREFACE

This report presents the results of the work performed from 1 September 1980 to 1 October 1982 by McDonnell Douglas Research Laboratories (MDRL) under Air Force contract F33615-80-C-5118 on Optimum Microstructures for Superplastic Forming Using Hydrovac, Project 2418 - Metallic Structural Materials. Mr. W. R. Kerr, AFWAL-ML, was the program manager.

The principal investigator was Dr. Shankar M. L. Sastry; co-investigators were Mr. Richard J. Lederich and Mr. James E. O'Neal. The work was performed in the Solid State Sciences Department under the direction of Dr. Charles R. Whitsett.

A rectangular administrative stamp with a grid of boxes. A large handwritten "A" is written across the bottom left portion of the stamp. A checkmark is visible in the top right box.

# TABLE OF CONTENTS

SECTION		PAGE
I	INTRODUCTION	1
II	TECHNICAL BACKGROUND	2
	1. Phase Transformation in Ti-H Alloys	2
	2. Effect of Internal Hydrogen on Superplastic Forming and Diffusion Bonding of Ti Alloys	8
III	OBJECTIVES AND APPROACH	12
	1. Objectives	12
	2. Program Plan	12
	3. Selection of Alloys	14
	4. Production of Fine Microstructures by Hydrovac Processing	15
	5. Microstructure and Property Characterization of Hydrovac-Processed Alloys	18
	6. Superplastic Formability Determination	19
	7. Superplastic Forming and Diffusion Bonding of Specimens Containing and Evolving Hydrogen	21
	8. Superplastic Forming of Trough-Shaped Specimens Containing Internal Hydrogen	21
IV	MICROSTRUCTURES, MECHANICAL PROPERTIES, AND SUPERPLASTIC FORMABILITY OF HYDROVAC-PROCESSED TITANIUM ALLOYS	23
	1. Effects of Surface Coatings on Hydrogen Retention and Oxygen Pick-Up in Hydrovac-Processed Ti Alloys	23
	2. Microstructures of Hydrovac-Processed Ti-6Al-4V and Ti-6Al-2Sn-4Zr-2Mo	26
	3. Tensile and Creep Properties of Hydrovac-Processed Ti-6Al-4V and Ti-6Al-2Sn-4Zr-2Mo	36
	4. Superplastic Forming and Diffusion Bonding of Hydrovac-Processed Ti Alloys	40
V	SUPERPLASTIC FORMING AND DIFFUSION BONDING OF Ti-ALLOYS CONTAINING INTERNAL HYDROGEN	56
	1. Effects of Internal Hydrogen on SPF/DB of Titanium Alloys	56
	2. Effects of Hydrogen Evolution on SPF/DB of Titanium Alloys	69
VI	PROPERTIES OF SUPERPLASTICALLY FORMED Ti-ALLOY TROUGHS	73
VII	CONCLUSIONS	81
VIII	RECOMMENDATIONS	93

# TABLE OF CONTENTS (Continued)

SECTION		PAGE
IX	REPORTS AND PUBLICATIONS RESULTING FROM THIS CONTRACT	84
	APPENDIX A PRACTICAL ASPECTS OF HYDROVAC PROCESSING ON A PRODUCTION SCALE	85
	APPENDIX B ANALYSES OF BIAXIAL-STRESS CONE FORMING	91
	APPENDIX C MECHANICAL PROPERTIES OF ALLOYS HYDROVAC-PROCESSED BY OREMET USING FORMKOTE T50 COATING AND 810°C BETA-ANNEALING TREATMENT	103
REFERENCES		113

# LIST OF ILLUSTRATIONS

FIGURE		PAGE
1	Phase diagram for the Ti-H system	2
2	Equilibrium pressure-temperature-concentration relations for the Ti-H system	3
3	Phase boundaries in Ti-6Al-4V with hydrogen	4
4	Time-temperature-transformation curves for Ti-6Al-4V-1.35H	5
5	Microstructures of Ti-6Al-4V-1.0H beta treated at 870°C, transformed at 590°C for 4 h, and dehydrogenated at 650°C, 700°C, and 760°C	6
6	Transmission electron micrographs of Ti-6Al-4V-1.0H beta treated at 870°C, transformed at 590°C for 4 h, and dehydrogenated at 650°C, 675°C, and 760°C	7
7	Effects of alloy chemistry on the strain-rate dependences of flow stress and strain-rate sensitivity of flow stress of titanium alloys at 875°C	9
8	Strain-rate dependence of flow stress for Ti-8Al-1Mo-1V, Ti-6Al-4V, and Ti-3Al-2.5V showing the unique dependence of flow stress at constant strain rate on $T/T_g$	10
9	Temperature and strain-rate dependence of strain-rate sensitivity for alpha-beta titanium alloys	10
10	Flow chart showing scope of Phase I of the program	13
11	Scope of Phase II of the program	14
12	Experimental arrangement for laboratory cone-forming tests	19
13	Trough-shaped die used in the superplastic forming of large panels	22
14	Effect of oxygen concentration on Rockwell-C hardness values for hydrovac-processed Ti-6Al-4V	25
15	Transmission electron micrographs showing the transformation products at various stages of hydrovac processing	27
16	Effect of dehydrogenation temperature on substructure formation in Ti-6Al-4V-1.2H beta annealed at 870°C for 0.5 h, cooled to 595°C, transformed at 595°C for 4 h, and dehydrogenated at 665°C for 20 h, 682°C for 20 h, 705°C for 6 h, and 705°C for 20 h	28
17	Scanning electron micrographs of equiaxed- $\alpha$ Ti-6Al-4V before and after hydrovac processing	30
18	Scanning electron micrographs of Widemanstätten Ti-6Al-4V before and after hydrovac processing	31

# LIST OF ILLUSTRATIONS (Continued)

FIGURE		PAGE
19	Scanning electron micrographs of duplex-annealed Ti-6Al-2Sn-4Zr-2Mo before and after hydrovac processing	32
20	High-magnification scanning electron micrographs of hydrovac-processed Ti-6Al-4V, Widmanstätten Ti-6Al-4V, and duplex-annealed Ti-6Al-2Sn-4Zr-2Mo	33
21	(0002) and (1010) pole figures of equiaxed- $\alpha$ Ti-6Al-4V and (0002) and (1010) pole figures of hydrovac-processed Ti-6Al-4V	34
22	(0002) and (1010) pole figures of duplex-annealed Ti-6Al-2Sn-4Zr-2Mo and (0002) and (1010) pole figures of hydrovac-processed Ti-6Al-2Sn-4Zr-2Mo	35
23	Effect of temperature on the 0.2% yield stress of as-received and hydrovac-processed equiaxed- $\alpha$ Ti-6Al-4V	37
24	Effect of temperature on the 0.2% yield stress of as-received and hydrovac-processed duplex-annealed Ti-6Al-2Sn-4Zr-2Mo	38
25	Effect of temperature on the ultimate tensile strength of as-received and hydrovac-processed equiaxed- $\alpha$ Ti-6Al-4V	39
26	Effect of temperature on the ultimate tensile strength of as-received and hydrovac-processed duplex-annealed Ti-6Al-2Sn-4Zr-2Mo	39
27	Stress dependence of steady-state creep rate for equiaxed- $\alpha$ Ti-6Al-4V in as-received condition and hydrovac condition at 600°C, 520°C, 435°C, and 350°C	40
28	Stress dependence of steady-state creep rate for duplex-annealed Ti-6Al-2Sn-4Zr-2Mo in as-received condition and hydrovac condition at 600°C, 520°C, 435°C, and 350°C	41
29	Ti-6Al-4V cones formed at 900°C and at various pressures	42
30	Photographs of cross sections of cones superplastically formed at 900°C: Ti-6Al-4V at 3.2 MPa, Ti-6Al-4V at 6.6 MPa, Ti-6Al-4V at 9.7 MPa, Ti-6Al-4V at 18.8 MPa, and Widmanstätten Ti-6Al-4V at 18.8 MPa	43
31	Time dependence of strain rate of equiaxed- $\alpha$ Ti-6Al-4V superplastically formed at 18.8 MPa and 900°C, 830°C, 800°C, 780°C, 760°C, and 720°C	44
32	Microstructures of equiaxed- $\alpha$ Ti-6Al-4V and hydrovac-processed equiaxed- $\alpha$ Ti-6Al-4V after cone forming at 720°C, 760°C, 780°C, 800°C, 830°C, and 900°C	45
33	Time dependence of strain of Widmanstätten and hydrovac-process Widmanstätten Ti-6Al-4V superplastically formed at 830°C and 18.8 MPa	47

# LIST OF ILLUSTRATIONS (Continued)

FIGURE		PAGE
34	Time dependence of strain of duplex-annealed and hydrovac-processed Ti-6Al-2Sn-4Zr-2Mo superplastically formed at 830°C and 18.8 MPa	48
35	Time dependence of strain of equiaxed- $\alpha$ Ti-6Al-4V and equiaxed- $\alpha$ hydrovac-processed Ti-6Al-4V superplastically formed at 900°C and 18.8 MPa with no preheat-treatment and with a 900°C, 4 h, preheat-treatment	49
36	Photomicrographs of interface regions of specimens diffusion-bonded for 3 h at 850°C and 1.0 MPa	50
37	Photomicrographs of interface regions of specimens diffusion-bonded for 3 h at 900°C and 1.3 MPa	51
38	Photomicrographs of interface regions of specimens diffusion-bonded for 3 h at 850°C and 1.0 MPa and annealed at 900°C for 5 h	52
39	Photomicrographs of interface regions of specimens diffusion-bonded for 3 h at 900°C and 1.3 MPa and annealed at 900°C for 5 h	53
40	Photomicrographs of interface regions of specimens diffusion-bonded for 3 h at 900°C and 2.0 MPa	54
41	Photomicrographs of interface regions of specimens diffusion-bonded for 3 h at 900°C and 2.0 MPa	55
42	Cross sections of equiaxed- $\alpha$ Ti-6Al-4V cones containing 0.34 and 0.39 wt% hydrogen and superplastically formed at 300°C and 18.8 MPa	57
43	Cross sections of equiaxed- $\alpha$ Ti-6Al-4V cones superplastically formed at 760°C and 18.8 MPa for 2 h uncharged and charged to 0.11 wt% hydrogen	57
44	Effect of internal hydrogen on superplastic forming of equiaxed- $\alpha$ Ti-6Al-4V at 860°C and 18.8 MPa	58
45	Effect of internal hydrogen on superplastic forming of equiaxed- $\alpha$ Ti-6Al-4V at 300°C and 18.8 MPa	59
46	Effect of internal hydrogen on superplastic forming of equiaxed- $\alpha$ Ti-6Al-4V at 760°C and 18.8 MPa	60
47	Effect of hydrogen concentration on the superplastic forming properties of Ti-6Al-4V at various temperatures	61
48	Forming time required to achieve a true strain of 1.25 in equiaxed- $\alpha$ Ti-6Al-4V for temperature/hydrogen-concentration combinations	62
49	Effect of internal hydrogen on superplastic forming of duplex-annealed Ti-6Al-2Sn-4Zr-2Mo at 900°C and 18.8 MPa	63
50	Effect of internal hydrogen on superplastic forming of duplex-annealed Ti-6Al-2Sn-4Zr-2Mo at 330°C and 18.8 MPa	64

# LIST OF ILLUSTRATIONS (Continued)

FIGURE		PAGE
51	Effect of internal hydrogen on superplastic forming of duplex-annealed Ti-6Al-2Sn-4Zr-2Mo at 800°C and 18.8 MPa	65
52	Cross sections of duplex-annealed Ti-6Al-2Sn-4Zr-2Mo cones superplastically formed at 830°C and 18.8 MPa for 2 h uncharged and charged to 0.11 wt% hydrogen	65
53	Effect of hydrogen concentration on the superplastic forming properties of duplex-annealed Ti-6Al-2Sn-4Zr-2Mo at various temperatures	66
54	Time dependence of strain of equiaxed- $\alpha$ Ti-6Al-4V, hydrogen-charged Ti-6Al-4V, and hydrogen-charged, hydrovac-processed Ti-6Al-4V superplastically formed at 760°C and 18.8 MPa	68
55	Percentage of bonded interface when duplex-annealed Ti-6Al-2Sn-4Zr-2Mo and equiaxed- $\alpha$ Ti-6Al-4V are exposed to a pressure of 1.9 MPa for 3.5 h and hydrogen is maintained in solution	70
56	Effect of internal-hydrogen evolution on superplastic forming of equiaxed- $\alpha$ Ti-6Al-4V at 760°C and 18.8 MPa	71
57	Percentage of bonded interface when duplex-annealed Ti-6Al-2Sn-4Zr-2Mo and equiaxed- $\alpha$ Ti-6Al-4V are exposed to a pressure of 1.9 MPa for 3.5 h and hydrogen is allowed to evolve as samples are heated to bonding temperatures	72
58	Percentage of bonded interface when duplex-annealed Ti-6Al-2Sn-4Zr-2Mo and equiaxed- $\alpha$ Ti-6Al-4V are exposed to a pressure of 1.9 MPa for 3.5 h and hydrogen is maintained in solution until the bonding temperature is reached and then allowed to evolve.	72
59	Three views of a hydrogen-charged Ti-6Al-4V panel (9) formed at 800°C	75
60	Three views of a hydrogen-charged Ti-6Al-2Sn-4Zr-2Mo panel (12) formed at 875°C	77
61	Scanning electron micrographs of duplex-annealed Ti-6Al-2Sn-4Zr-2Mo used in the forming of panel 12	79
62	Scanning electron micrographs of equiaxed- $\alpha$ Ti-6Al-4V used in the forming of panel 9	80
A-1	Relative positions and final hydrogen concentrations of batch-1 panels after hydrogenation by OREMET	86
A-2	Relative positions and final hydrogen concentrations of batch-2 panels after hydrogenation by OREMET	87
A-3	Relative positions and final hydrogen concentrations of batch-3 panels after hydrogenation by OREMET	88

# LIST OF ILLUSTRATIONS (Continued)

FIGURE		PAGE
A-4	Relative positions and final hydrogen concentrations of batch-4 panels after hydrogenation by OREMET	89
A-5	Relative positions and final hydrogen concentrations of batch-5 panels after hydrogenation by OREMET	89
B-1	Schematic cross-section of conical die	92
B-2	Time dependence of strain of equiaxed- $\alpha$ Ti-6Al-4V superplastically formed at 900°C at the indicated stresses	95
B-3	Time dependence of strain of equiaxed- $\alpha$ Ti-6Al-4V and duplex-annealed Ti-6Al-2Sn-4Zr-2Mo superplastically formed at 830°C and 18.8 MPa	96
B-4	Time dependence of strain of equiaxed- $\alpha$ Ti-6Al-4V and duplex-annealed Ti-6Al-2Sn-4Zr-2Mo superplastically formed at 900°C and 9.7 MPa	97
B-5	Time dependence of strain of equiaxed- $\alpha$ Ti-6Al-4V and duplex-annealed Ti-6Al-2Sn-4Zr-2Mo superplastically formed at 900°C and 18.8 MPa	98
B-6	Time dependence of strain of equiaxed- $\alpha$ Ti-6Al-4V superplastically formed at 900°C and 18.8 MPa as determined by tensile tests and cone-forming tests	99
B-7	Time dependence of strain of equiaxed- $\alpha$ Ti-6Al-4V superplastically formed at 830°C and 31 MPa, 25 MPa, 19 MPa, and 10 MPa	100
B-8	True-stress/true-strain relation of equiaxed- $\alpha$ Ti-6Al-4V at 830°C determined from tensile specimens deformed at a constant strain rate	101
C-1	Effect of temperature on the 0.2% yield stress of as-received and OREMET batch-1, hydrovac-processed, equiaxed- $\alpha$ Ti-6Al-4V	104
C-2	Effect of temperature on the 0.2% yield stress of as-received and OREMET batch-1, hydrovac-processed Ti-6Al-2Sn-4Zr-2Mo	104
C-3	Effect of temperature on the ultimate tensile strength of as-received and OREMET batch-1, hydrovac-processed, equiaxed- $\alpha$ Ti-6Al-4V	105
C-4	Effect of temperature on the ultimate tensile strength of as-received and OREMET batch-1, hydrovac-processed Ti-6Al-2Sn-4Zr-2Mo	105
C-5	Stress dependence of steady-state creep rate for equiaxed- $\alpha$ Ti-6Al-4V in as-received condition and OREMET batch-1 hydrovac condition at 600°C, 520°C, 435°C, and 350°C	106

# LIST OF ILLUSTRATIONS (Continued)

FIGURE		PAGE
C-6	Stress dependence of steady-state creep rate for duplex-annealed Ti-6Al-2Sn-4Zr-2Mo in as-received condition and OREMET batch-1 hydrovac condition at 600°C, 520°C, 435°C, and 350°C	107
C-7	Fatigue-crack-growth rate of equiaxed- $\alpha$ Ti-6Al-4V at room temperature in ambient air as determined by triplicate tests	108
C-8	Fatigue-crack-growth rate of duplex-annealed Ti-6Al-2Sn-4Zr-2Mo at room temperature in ambient air as determined by duplicate tests	108
C-9	Fatigue-crack-growth rate of hydrovac-processed, equiaxed- $\alpha$ Ti-6Al-4V at room temperature in ambient air as determined by triplicate tests	109
C-10	Fatigue-crack-growth rate of hydrovac-processed, duplex-annealed Ti-6Al-2Sn-4Zr-2Mo at room temperature in ambient air as determined by triplicate tests	109
C-11	Fatigue-crack-growth rates of as-received and hydrovac-processed equiaxed- $\alpha$ Ti-6Al-4V at room temperature in ambient air	111

# LIST OF TABLES

TABLE		PAGE
1	Chemical Analyses of Alloy Lots	15
2	Effects of Surface Coatings on Hydrogen Retention in Ti-6Al-4V Charged with Hydrogen at 650°C, Annealed at 870°C for 0.5 h, and Cooled to 25°C	23
3	Carbon and Oxygen Concentrations of Selected Hydrovac-Processed Ti-6Al-4V Samples	24
4	Rockwell-C Hardness Values of Uncharged Ti-6Al-4V Samples Annealed at 865°C for 0.5 h	24
5	Effect of Dehydrogenation Temperature on Mechanical Properties of Hydrovac-Processed Equiaxed- $\alpha$ Ti-6Al-4V	29
6	Tensile Properties of As-Received Alloys	36
7	Tensile Properties of Hydrovac-Processed Alloys	37
8	Matrix of Superplastic-Forming Tests	42
9	Changes in Internal Hydrogen Concentrations Resulting from Diffusion-Bonding Tests	69
10	Forming Parameters and Actual Strains of Preliminary Trough-Forming Tests on Equiaxed- $\alpha$ Ti-6Al-4V Containing Hydrogen	73
11	Hydrogen Concentrations Obtained in Equiaxed- $\alpha$ Ti-6Al-4V Panels Under Different Charging Conditions and Strain Attained When Formed into Trough	74
12	Forming Parameters for Preliminary Trough-Forming Tests on Duplex-Annealed Ti-6Al-2Sn-4Zr-2Mo Containing Hydrogen	76
13	Comparison of Mechanical Properties of As-Received Panels, Conventionally Superplastically Formed Panels, and Superplastically Formed Panels with Internal Hydrogen	78
C-1	Tensile Properties of OREMET Batch-1 Hydrovac-Processed Alloys	103
C-2	Fatigue-Crack-Growth Parameters for Conventional and Hydrovac-Processed Ti-6Al-4V and Ti-6Al-2Sn-4Zr-2Mo	110
C-3	Minimum Stress-Intensity Amplitude Values for the Onset of Crack Growth in As-Received and Hydrovac-Processed Ti-6Al-4V and Ti-6Al-2Sn-4Zr-2Mo	111
C-4	Fracture Toughness Values Determined from Fatigue-Crack-Growth-Rate Tests of As-Received and Hydrovac-Processed Ti-6Al-4V and Ti-6Al-2Sn-4Zr-2Mo	112

## SECTION I

### INTRODUCTION

Superplastic forming with concurrent diffusion bonding (SPF/DB) has emerged as a practical cost- and material-saving method of titanium fabrication, and attention has begun to be focused on improving SPF/DB by optimizing the material and process parameters. A recent Air Force sponsored research program (Reference 1) addressed the dependence of Ti-alloy superplasticity on microstructural and texture variables as affected by variations in thermomechanical processing. The use of ancillary additions to control superplastically favorable microstructures in Ti alloys has received little attention.

A systematic study of superplastic formability of several alpha-beta titanium alloys (Reference 1) indicated that Ti alloys having lower beta-transus temperatures and containing higher volume fractions of beta phase required lower gas pressures and forming temperatures and exhibited higher strain-rate sensitivities and forming rates. Because small additions of hydrogen to titanium alloys stabilize the beta phase and produce a larger volume fraction of beta phase (Reference 2), the addition of hydrogen as a transient alloying addition to Ti alloys offers a method to improve superplasticity of Ti alloys. The transient hydrogen can be subsequently removed by vacuum annealing.

Recent phase-transformation studies in Ti-6Al-4V-H alloys (References 3 and 4) indicate yet another beneficial effect of hydrogen in Ti. An AFWAL-ML program investigating the effect of large concentrations of hydrogen on the heat treatment and processability of Ti alloys has shown that uniquely fine microstructures can be produced by beta annealing Ti-6Al-4V-1H, transforming by eutectoid decomposition, and dehydriding. Such fine microstructures are conducive to increased room-temperature strength and ductility and high-temperature creep resistance.

The results of a systematic study of the beneficial effects of hydrogen on superplasticity and tensile and creep properties of Ti alloys are presented in this report. The microstructural refinement and property improvement effected by the heat treatment of Ti alloys containing hydrogen and the effects of internal hydrogen on the superplastic forming and diffusion bonding of Ti alloys were determined.

## SECTION II

### TECHNICAL BACKGROUND

#### 1. PHASE TRANSFORMATION IN Ti-H ALLOYS

Hydrogen combines readily with titanium and has a solubility in Ti of up to 60 at.% at 600°C (1110°F) (Figure 1). Hydrogen additions reduce the beta-transus temperature and stabilize the more-open body-centered-cubic phase of Ti. The equilibrium pressure-temperature-concentration relations in the Ti-H system shown in Figure 2 indicate that the Ti-H solid solution formed by annealing Ti at 500°C (1110°F) in a > 10 Pa

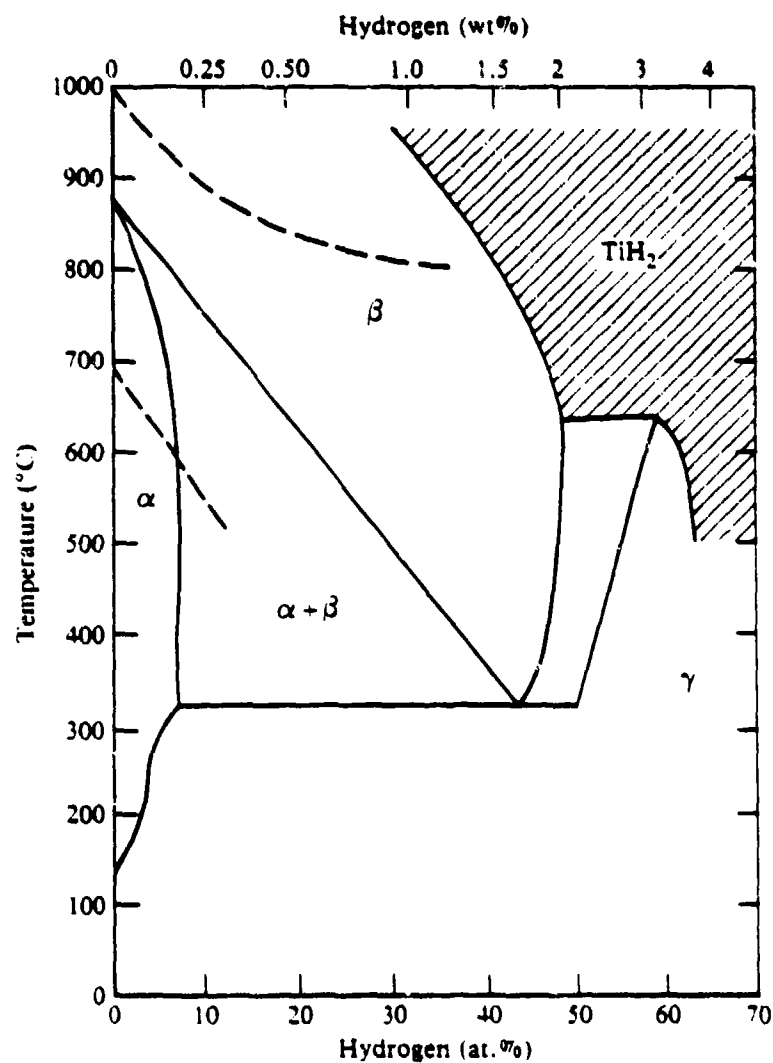


Figure 1. Phase diagram for the Ti-H system.

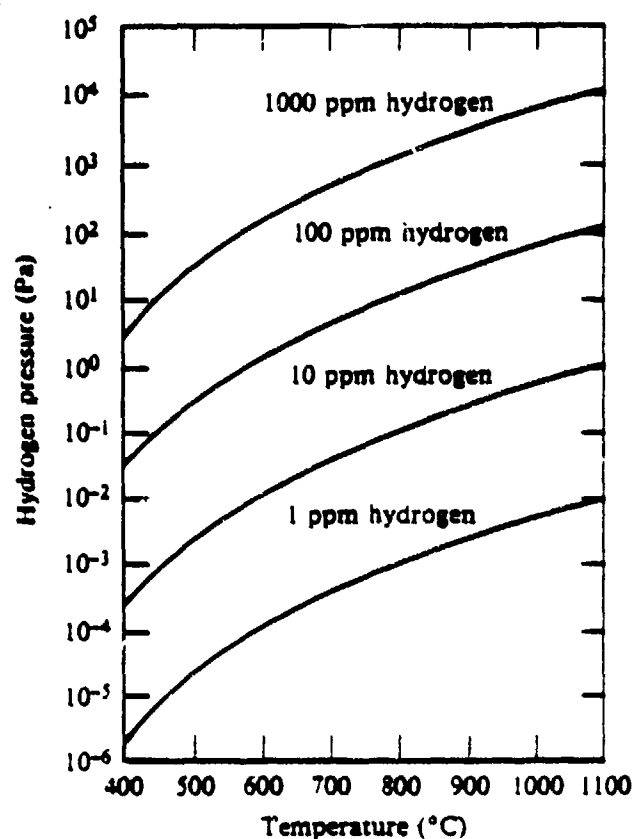


Figure 2. Equilibrium pressure-temperature-concentration relations for the Ti-H system.

( $7.5 \times 10^{-2}$  Torr) hydrogen atmosphere can be converted to hydrogen-free titanium by subsequent annealing in a vacuum of  $< 10^{-2}$  Pa ( $7.5 \times 10^{-5}$  Torr). This reversible process has been used successfully to produce titanium powders by the hydride-dehydride (HDH) method (Reference 5). Although the HDH process is a standard method for producing titanium powder, the implications of the method for producing fine microstructures were realized only recently (References 3, 4, and 6). With the objective of utilizing the fine microstructure for property improvements in Ti alloys, Kerr et al. (Reference 4) conducted a detailed study of the phase transformations in Ti-6Al-4V-H systems and determined the phase boundaries as shown in Figure 3. Several significant differences were noted between the Ti-H and Ti-6Al-4V-H systems. The addition of 1.0 wt% hydrogen decreased the beta transus temperature by only 200°C (360°F) in Ti-6Al-4V compared with a beta-transus temperature reduction of 550°C (990°F) in Ti. The eutectoid isotherm in Ti-6Al-4V was identi-

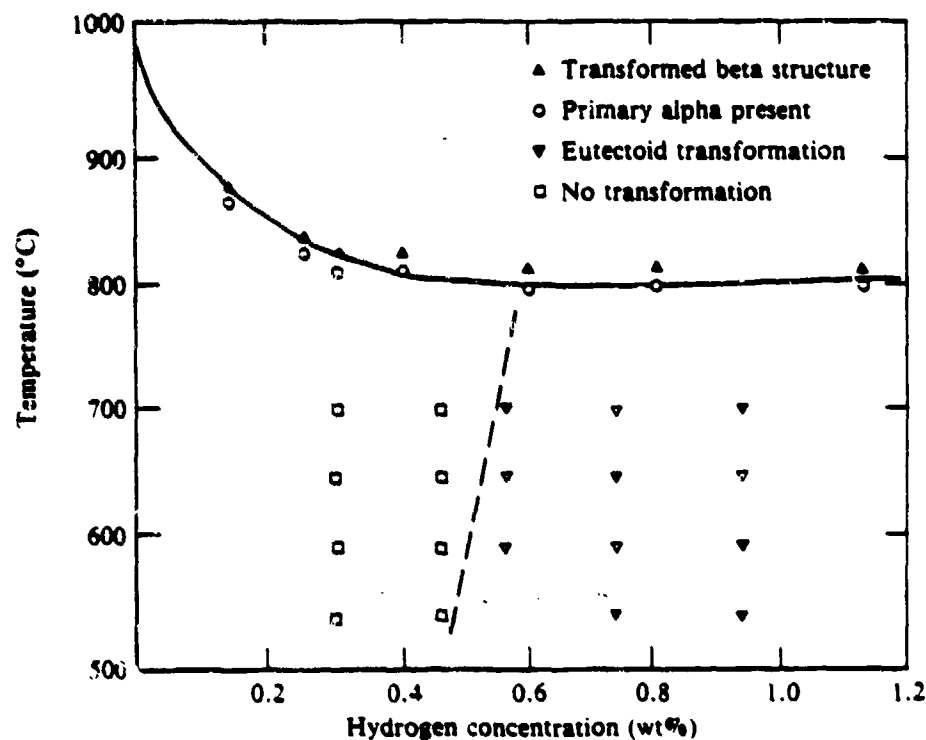


Figure 3. Phase boundaries in Ti-6Al-4V with hydrogen.

fied to be  $\approx 800^{\circ}\text{C}$  ( $1470^{\circ}\text{F}$ ), which is significantly higher than in Ti. The time-temperature-transformation curves for Ti-6Al-4V-1.35 wt% hydrogen shown in Figure 4 indicate that the transformation is slow below  $575^{\circ}\text{C}$  ( $1065^{\circ}\text{F}$ ).

The standard heat-treatment cycle used to produce fine microstructures in Ti-alloys consists of hydrogen charging the alloy at  $650\text{--}700^{\circ}\text{C}$  ( $1200\text{--}1290^{\circ}\text{F}$ ), beta annealing above  $800^{\circ}\text{C}$  ( $1470^{\circ}\text{F}$ ) for  $\sim 0.5$  h, transforming the beta-annealed alloy at  $\approx 600^{\circ}\text{C}$  ( $1100^{\circ}\text{F}$ ) for 8 h, and dehydrogenating the alloy in a vacuum of  $10^{-2}$  Pa ( $7.5 \times 10^{-5}$  Torr) at  $650\text{--}700^{\circ}\text{C}$  ( $1200\text{--}1290^{\circ}\text{F}$ ). At the transformation temperature, hydrogen-saturated beta phase decomposes isothermally to alpha phase and titanium hydride with some retained beta, and upon dehydrogenation the hydride transforms to alpha and beta. The heat-treatment process termed "hydrovac" produces fine microstructures of the type shown in Figures 5 and 6. The transformation temperature determines the size and spacing of the alpha and beta phases and the dehydrogenation temperature determines subgrain size and dislocation density produced by the removal

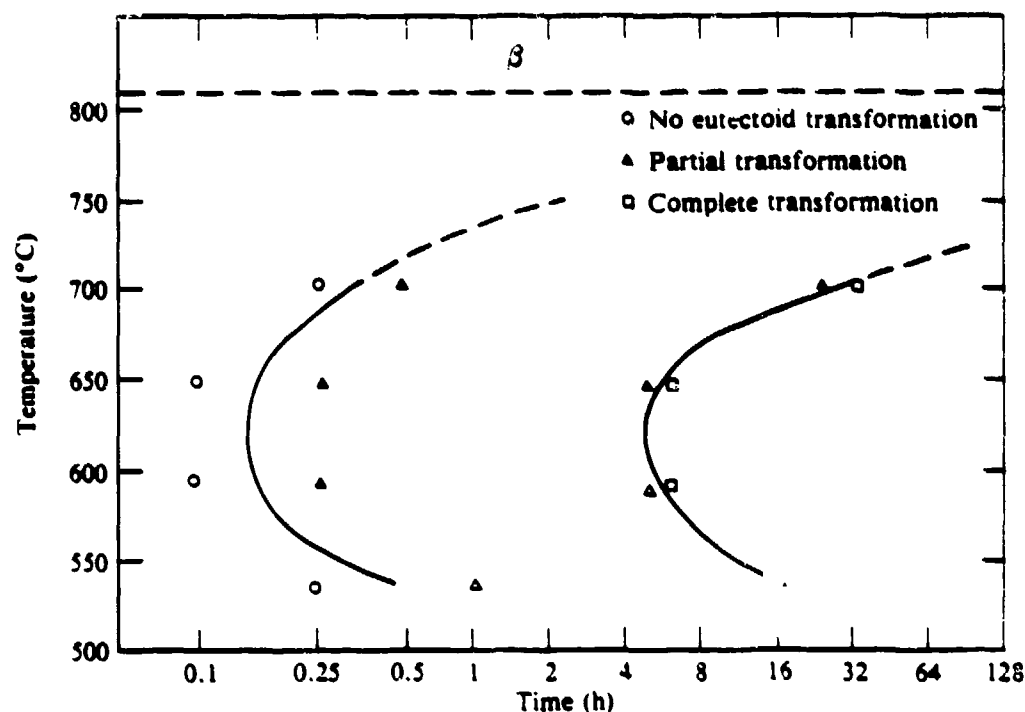


Figure 4. Time-temperature-transformation curves for Ti-6Al-4V-1.35H.

of hydrogen. For example, if the dehydrogenation is done at 650°C (1200°F), the substructure consists of highly tangled dislocations similar to those observed in cold-worked material (Figure 6a). With increasing dehydrogenation temperature, increased recovery and polygonization results in the formation of well-defined cells (Figures 6b and 6c). The fine subgrains resulting from hydrovac treatment increase the matrix strength ( $\sigma_0$ ) by acting as slip barriers. The overall tensile yield-stress ( $\sigma_y$ ) resulting from the superposition of the matrix yield-stress and subgrain-strengthening contributions is given (Reference 7) by  $\sigma_y = [\sigma_0^2 + (k\lambda^{-n})^2]^{1/2}$ , where  $k$  is a constant,  $\lambda$  is the subgrain size, and  $n$  has a value of 0.75-1.0. The subgrains significantly reduce the dislocation pile-up length and increase the ductility. The subgrains are effective in increasing the creep resistance of the alloys.

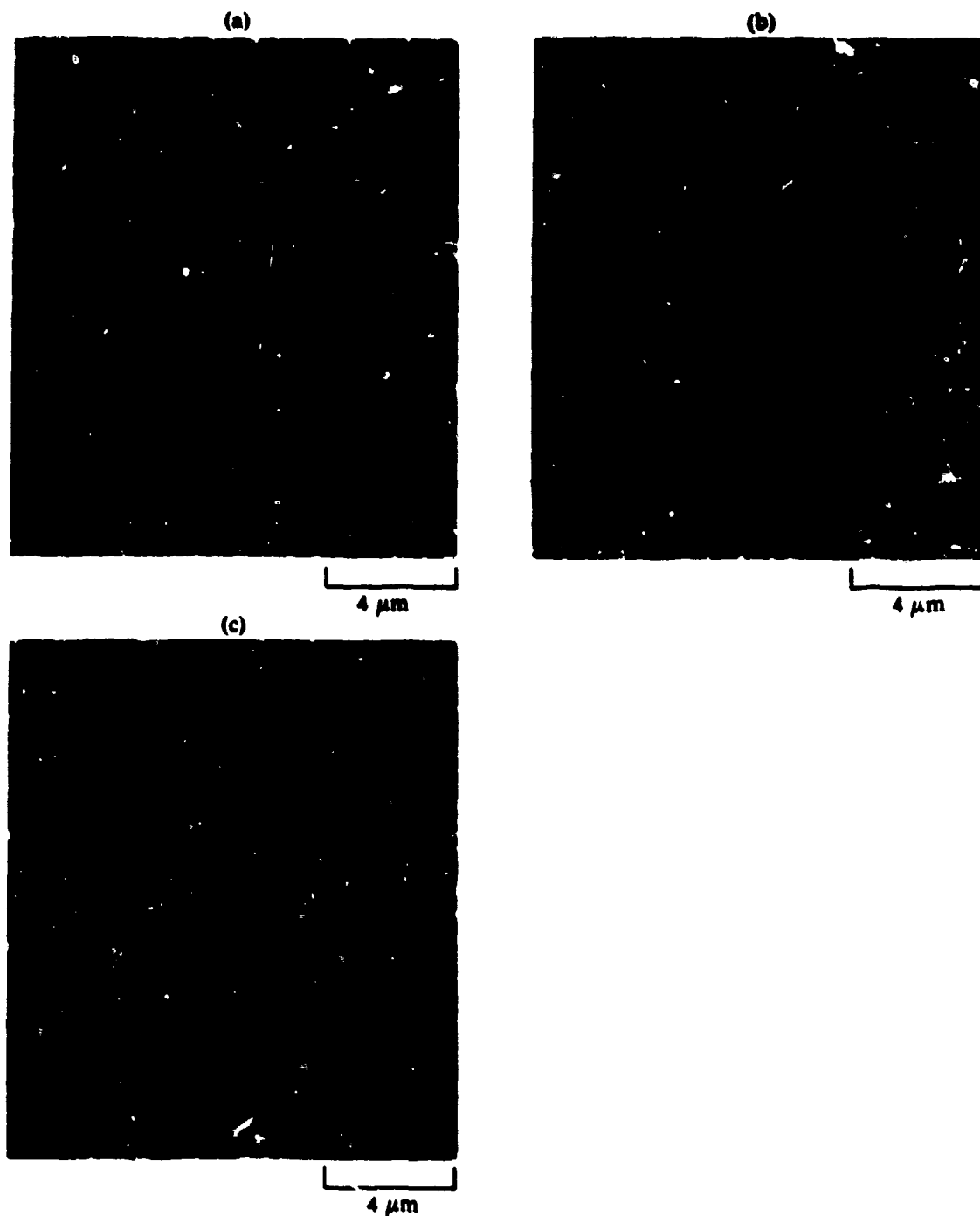


Figure 5. Microstructures of Ti-6Al-4V-1.0H beta treated at 870°C, transformed at 590°C for 4 h, and dehydrogenated at (a) 650°C, (b) 700°C, and (c) 760°C.



Figure 6. Transmission electron micrographs of Ti-6Al-4V-1.0H beta treated at 870°C, transformed at 590°C for 4 h, and dehydrogenated at (a) 650°C, (b) 675°C, and (c) 760°C.

## 2. EFFECT OF INTERNAL HYDROGEN ON SUPERPLASTIC FORMING AND DIFFUSION BONDING OF TI ALLOYS

A previous study has shown that the most important microstructural variables affecting the superplasticity of titanium alloys are grain-size, grain-shape, and volume-fractions of the constituent phases at temperature (Reference 1). The best combinations of flow stress and strain-rate sensitivity values for Ti-6Al-4V are obtained with optimum amounts of beta phase (Figure 7).

All data on the superplasticity of Ti alloys indicate that a fine-grain microstructure and grain-growth retardation during forming are desirable for improved superplasticity. The strain-rate dependences of flow stress and strain-rate sensitivity of Ti-6Al-4V, Ti-8Al-1Mo-1V, and Ti-3Al-2.5V, plotted for various ratios of the test temperature ( $T$ ) to the beta-transus temperature ( $T_\beta$ ) in Figures 8 and 9, indicate that the flow stress and strain-rate sensitivity at a constant strain rate of different alpha-beta alloys are uniquely related to  $T/T_\beta$ , which is a measure of the relative amounts of alpha and beta phases present. The effects of different compositions and microstructural modifications are implicit in the  $T/T_\beta$  ratio of a specific alloy. For a fixed  $T/T_\beta$  ratio and grain size, the logarithm of flow stress is the same function of the logarithm of the strain-rate for all alloy compositions. Therefore, by lowering the beta transus temperature and minimizing the in-process grain growth, superplastic forming (SPF) and diffusion bonding (DB) can be improved significantly.

Previous efforts to obtain fine-grain microstructures in Ti alloys have been by thermomechanical processing of the alloys, and few studies have addressed the problem of minimizing in-process grain growth, lowering the beta transus temperature, and increasing the beta phase. The effectiveness of hydrogen additions to alpha-beta Ti alloys for lowering the beta-transus temperature, controlling the alpha and beta phase proportions, and producing fine transformation microstructures indicate a potential for improving the superplastic formability as well as the creep resistance and room-temperature tensile properties of Ti alloys. The microstructural modifications effected by hydrogen additions to Ti

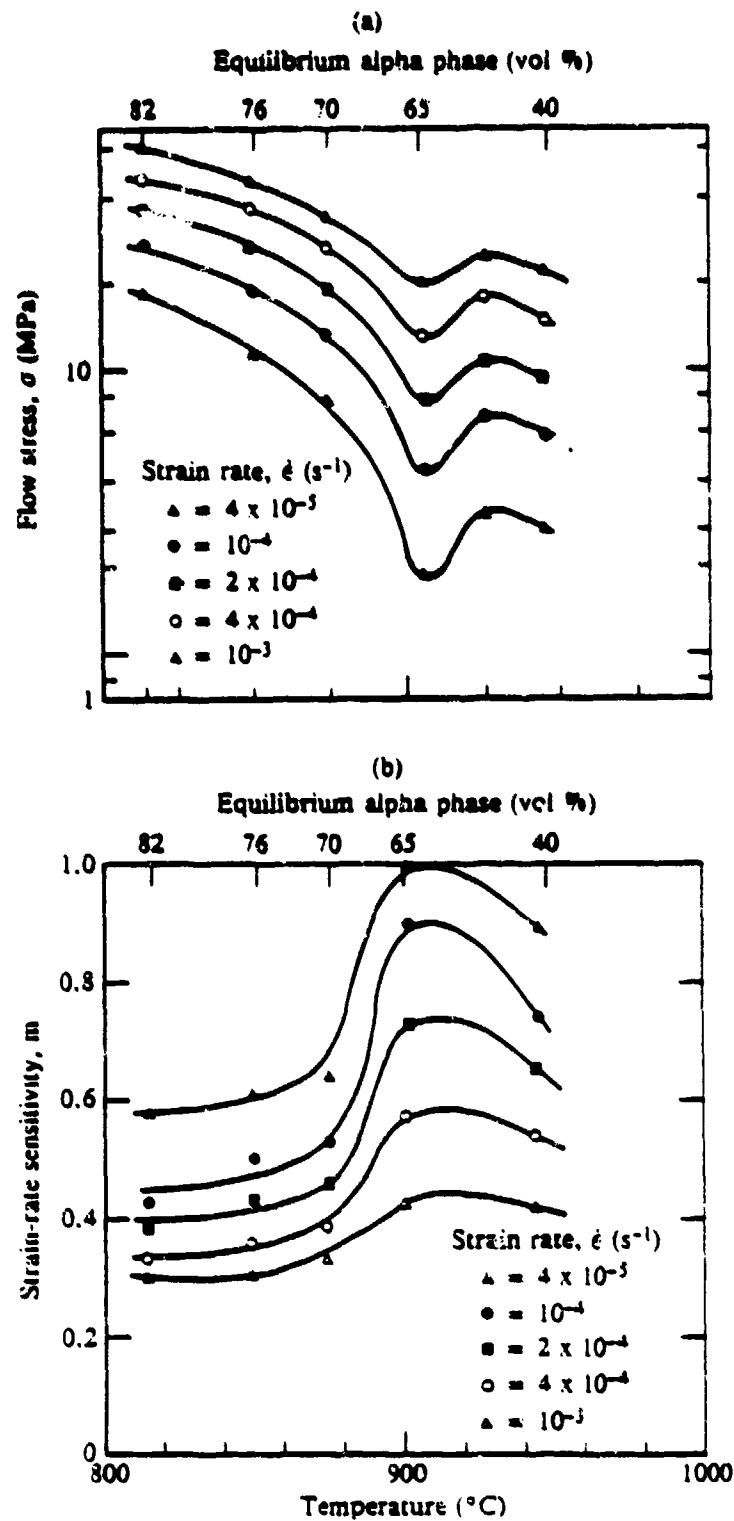


Figure 7. Effects of alloy chemistry on the strain-rate dependences of (a) flow stress and (b) strain-rate sensitivity of flow stress of titanium alloys at 875°C.

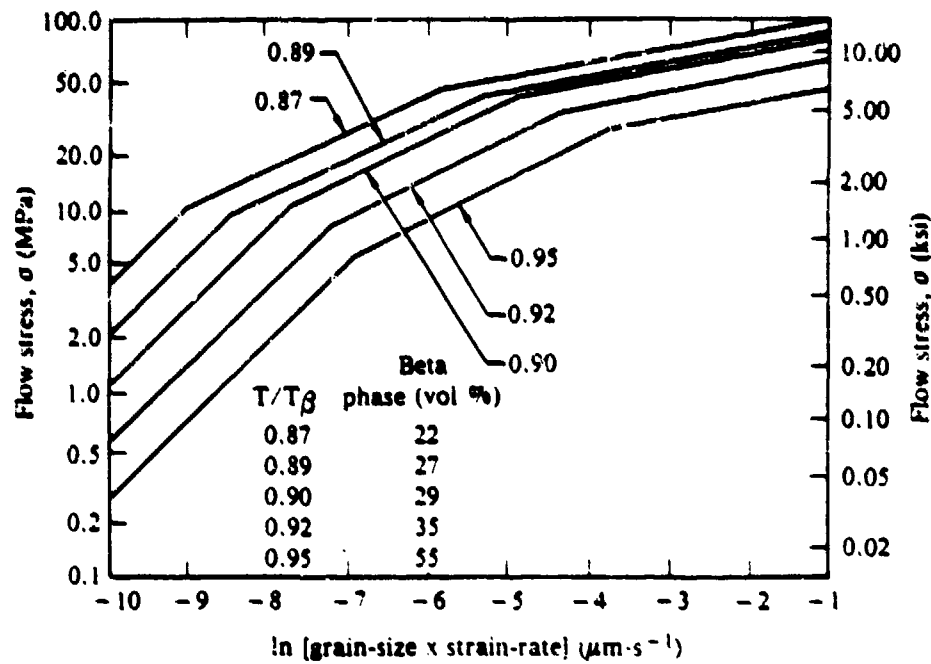


Figure 8. Strain-rate dependence of flow stress for Ti-8Al-1Mo-1V, Ti-6Al-4V, and Ti-3Al-2.5V showing the unique dependence of flow stress at constant strain rate on  $T/T_\beta$ .

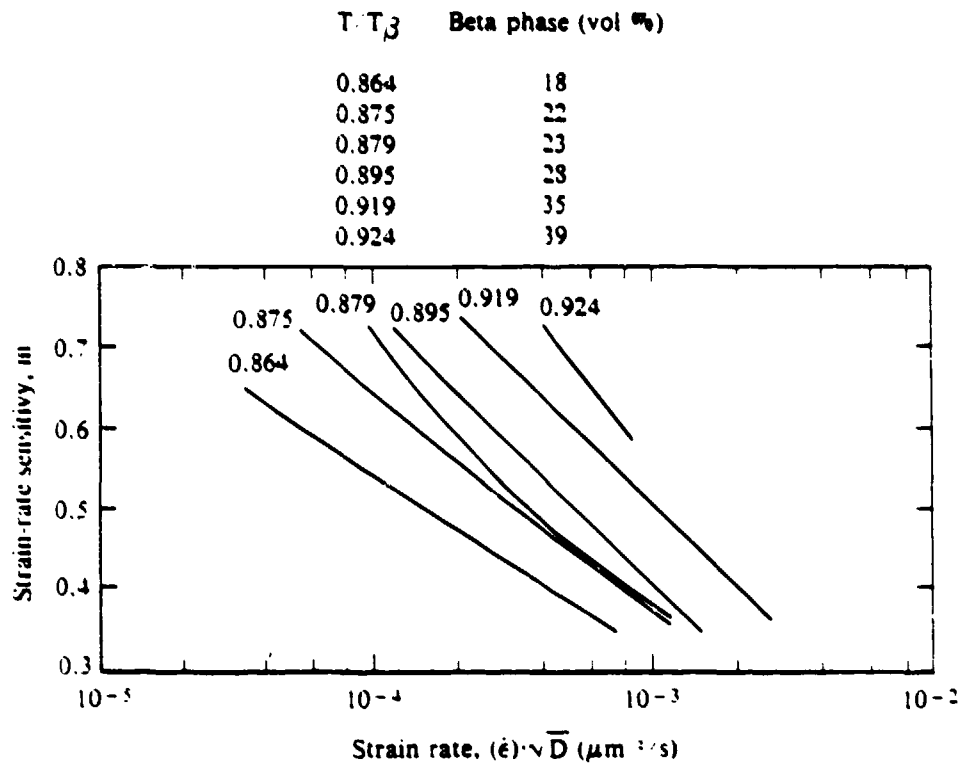


Figure 9. Temperature and strain-rate dependence of strain-rate sensitivity for alpha-beta titanium alloys.

decrease the high-temperature flow stress and increase the strain-rate sensitivity, both of which are conducive to superplasticity. Furthermore, because diffusion of Ti and H are significantly higher in the beta phase than in the alpha phase, hydrogen additions offer the possibility of improving diffusion bonding of Ti alloys. Kearns et al. (Reference 8) demonstrated significant improvements in the superplasticity of Zircalloy-4 with 0.08-0.3 wt% hydrogen additions. The hydrogen additions to Zircalloy-4 decreased the high-temperature flow stress and increased the strain-rate at which strain rate sensitivities indicative of superplasticity ( $n > 0.3$ ) were observed. The improved superplasticity in hydrogen-containing Zircalloy-4 was attributed to the presence of two-phase microstructures at temperatures for which the hydrogen-free alloy is normally single phase.

Production of favorable alpha-beta proportions and consequent SPF-DB at lower temperatures has the advantages of increased die life, shorter forming and/or bonding time, decreased temperature-induced microstructural degradation, and increased part complexity. Furthermore, the lattice-volume changes accompanying hydrogen removal from hydrogen-charged Ti specimens offers a method of generating a high density of lattice defects and increasing strain accommodation during high-temperature forming.

### SECTION III

#### OBJECTIVES AND APPROACH

##### 1. OBJECTIVES

The general objective of the program on optimum microstructures for superplastic forming using hydrovac was to determine the extent to which the addition of large amounts, up to 1.0 wt%, of hydrogen can be used to improve the tensile and creep properties and superplastic formability or diffusion bondability of titanium alloys by producing fine microstructures, reducing the forming temperature and flow stress, and minimizing microstructural changes during forming.

The specific objectives of this program were: (1) to characterize completely, in Ti-6Al-4V and Ti-6Al-2Sn-4Zr-2Mo, the unique fine microstructures that can be produced by hydrovac processing, (2) to characterize the hydrovac-processed material with respect to mechanical properties, including tensile characteristics, fatigue crack growth, creep, superplastic formability, and diffusion bondability, (3) to determine the superplastic formability and diffusion bondability of Ti-6Al-4V and Ti-6Al-2Sn-4Zr-2Mo containing different amounts of internal hydrogen, (4) to determine whether the evolution of hydrogen during superplastic forming or diffusion bonding will permit lower temperatures, lower flow stresses, and shorter times for superplastic forming or increased complexity of superplasticity formed parts, and (5) to determine the effect on final mechanical properties of superplastically-formed titanium alloys after removal of the previous large concentrations of hydrogen.

##### 2. PROGRAM PLAN

This program was organized into two phases. Phase I was concerned with producing, characterizing, and testing material in which the fine microstructures were produced by hydrovac processing. Phase II was concerned with determining the superplastic forming and diffusion bonding characteristics of material that contains hydrogen. Figures 10 and 11 are flow charts showing the scope of the program.

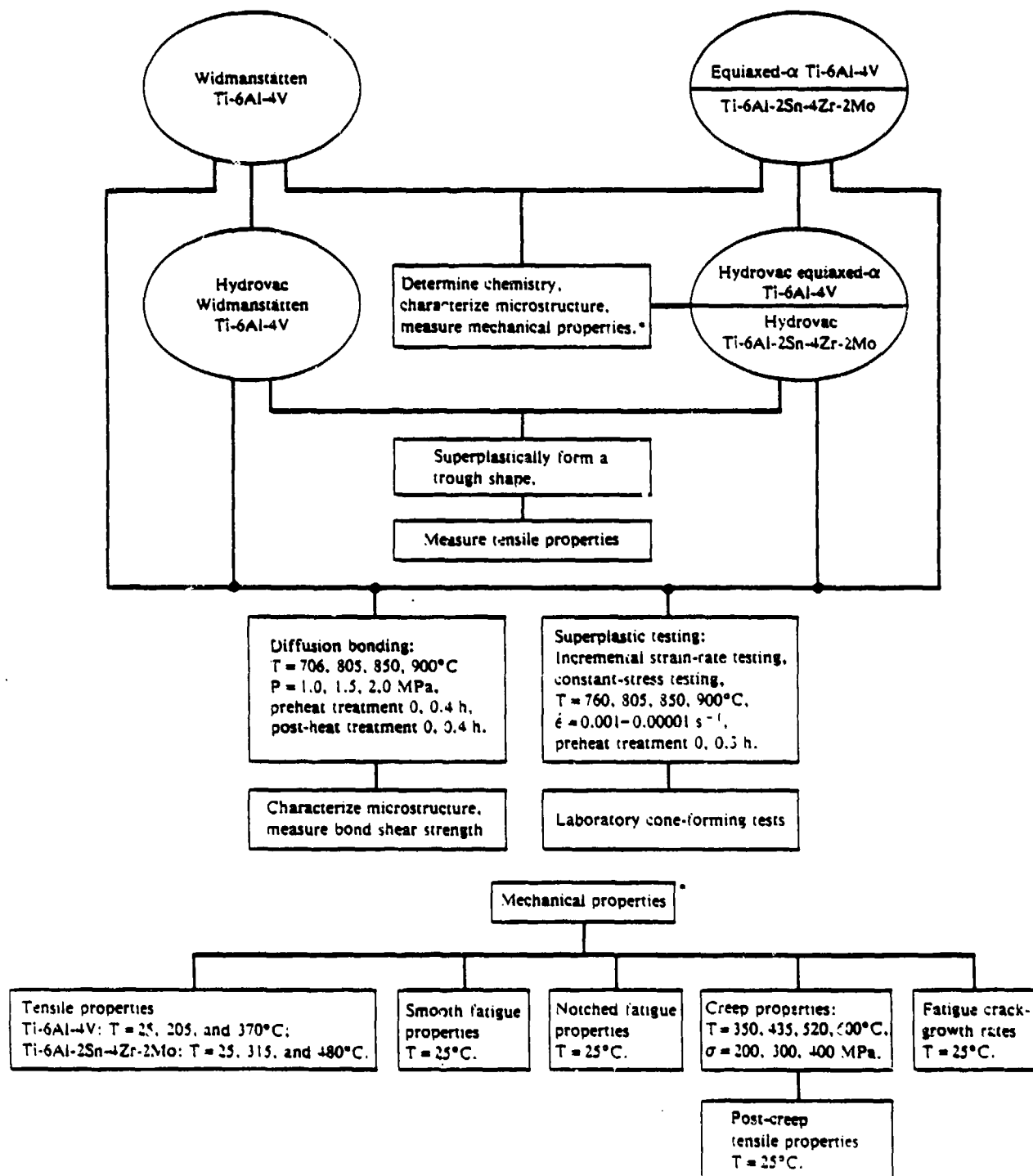


Figure 10. Flow chart showing scope of Phase I of the program.

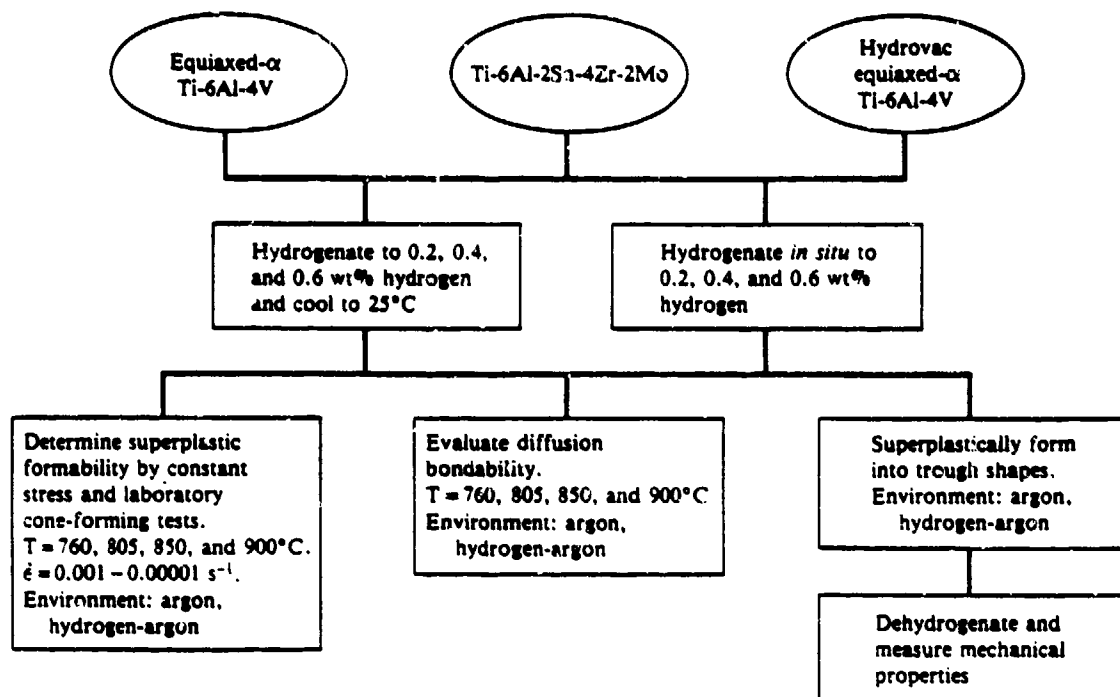


Figure 11. Scope of Phase II of the program.

### 3. SELECTION OF ALLOYS

Ti-6Al-4V and Ti-6Al-2Sn-4Zr-2Mo alloys were selected as representative of alpha + beta and near-alpha titanium alloys, respectively. The alloys were procured from RMI Co., Lawrence Aviation Industries, Inc., and TLMET. Table 1 lists the supplier, lot numbers, and suppliers' chemical analyses of the alloys used in the present study.

Two microstructural variations of Ti-6Al-4V were evaluated for the production of fine microstructures by hydrovac processing: equiaxed, fine-grained microstructure and elongated, alpha-beta (Widmanstätten) microstructure.

The conventionally processed Ti-6Al-4V was rolled and mill annealed at 787°C (1450°F) for 0.25 h and air cooled to 25°C (77°F) to produce a fine, equiaxed, alpha-plus-prior-beta microstructure, which is favorable for superplastic forming. Beta annealing at 1035°C (1895°F) for 0.5 h followed by air-cooling to 25°C (77°F) was used to produce a

**TABLE 1**  
**CHEMICAL ANALYSES OF ALLOY LOTS**

Element	Composition (wt%)		
	Ti-6Al-4V, RMI heat 885259-07	Ti-6Al-4V, LAI lot 955-6905	Ti-6Al-2Sn-4Zr-2Mo, TIMET lot no. P6853
Al	6.0	6.08	5.9
V	4.0	4.06	—
Sn	—	—	2.0
Zr	—	—	4.2
Mo	—	—	2.0
C	0.02	0.04	0.012
N	0.012	0.022	0.004
Fe	0.17	0.16	0.07
Y	<0.005	<0.001	<0.005
O	0.126	0.132	0.11
H	0.0043	0.0033	0.006
Mn	—	—	0.005
Si	—	—	0.07

Widmanstätten alpha-beta microstructure, which is unfavorable for superplastic forming. For convenience, the mill-annealed Ti-6Al-4V will be designated as equiaxed- $\alpha$  Ti-6Al-4V and the beta-annealed Ti-6Al-4V will be referred to as Widmanstätten Ti-6Al-4V.

Ti-6Al-2Sn-4Zr-2Mo was given a duplex-annealing treatment consisting of annealing at 900°C (1650°F) for 0.50 h, air cooling to 25°C (77°F), reannealing at 790°C (1450°F) for 0.25 h, and air cooling to 25°C (77°F).

#### 4. PRODUCTION OF FINE MICROSTRUCTURES BY HYDROVAC PROCESSING

Large alloy panels were hydrovac processed at Oregon Metallurgical Corporation (OREMET), and the small alloy specimens were hydrogen charged at Air Force Wright Aeronautical Laboratories and transformed and dehydrogenated at MDRL. The sequence of steps used in hydrovac processing consisted of hydrogenation at 650°C (1200°F) of alloy specimens to  $1.0 \pm 0.1$  wt% hydrogen, heating the specimens above the eutectoid temperature ( $\sim 810^\circ\text{C}$  (1490°F)) to produce an all-beta microstructure,

transforming the beta-annealed alloys below the eutectoid temperature to produce closely spaced, fine, eutectoid decomposition products, and dehydrogenating the alloy in a vacuum of  $\sim 10^{-2}$  Pa ( $7.5 \times 10^{-5}$  Torr) (Reference 9).

Small specimens were hydrogenated in a stainless-steel tube, 75 mm (3 in.) in diameter by 1.5 m (60 in.) long, sealed by flanges at both ends, and mounted in a laboratory furnace. One flange had inlets for the thermocouples and hydrogenating gas tubes. Specimens to be hydrogenated were placed in an unsealed box made of Ti-6Al-4V sheet, 0.42 mm (.016 in.) thick. This box aided in uniformity of hydrogen absorption during the run and reduced the contamination pick-up from the hydrogenating gas. The box containing the specimens was placed in the work zone at the center of the furnace where the temperature was uniform within  $\pm 10^{\circ}\text{C}$  ( $18^{\circ}\text{F}$ ) over a length of 250 mm (10 in.).

The furnace was evacuated and purged with argon three times, and then heated to the hydrogenation temperature with an atmosphere of flowing argon at a slight positive pressure in the tube. When the hydrogenation temperature,  $650^{\circ}\text{C}$  ( $1200^{\circ}\text{F}$ ), was attained, a flow of hydrogen was added to the argon stream and maintained for the hydrogenation time.

The hydrogen content of the specimens was controlled by the time of hydrogenation and the partial pressure of hydrogen. At the end of the hydrogenation time, a third gas, Ar + 4% H<sub>2</sub>, which is nonflammable but represents a partial pressure of hydrogen in equilibrium with a significant hydrogen content in Ti-6Al-4V (approximately 0.6 wt% at  $650^{\circ}\text{C}$  ( $1200^{\circ}\text{F}$ )), was added to the gas stream. Hydrogen and argon were then shut off, and the outlet from the furnace was closed. A slight positive pressure was maintained and specimens were allowed to equilibrate for 1 h at temperature and then cooled slowly.

The hydrogen content of specimens was determined by weighing specimens before and after hydrogenation to the nearest 0.1 mg. This method of analysis was verified by vacuum fusion analysis on selected specimens. After being analyzed for hydrogen, the samples were sealed in evacuated quartz tubes for subsequent heat treatment. The encapsulated specimens were beta treated by heating to  $870^{\circ}\text{C}$  ( $1600^{\circ}\text{F}$ ) for 0.5 h. The

specimens were then transferred to furnaces at 660-700°C (1220-1290°F) for eutectoid decomposition and air cooled to room temperature while still sealed in the quartz tubes.

After heat treatment, the specimens were removed from the quartz tubes and dehydrogenated in a vacuum furnace. The furnace was evacuated to  $< 7 \times 10^{-3}$  Pa ( $5 \times 10^{-5}$  Torr) before heating began. No hydrogen evolved below 500°C (930°F). Above this temperature, hydrogen evolution was usually at a rate that required by-passing the diffusion pump until sufficient hydrogen had been removed to decrease the chamber pressure to 7 Pa ( $5 \times 10^{-2}$  Torr). Dehydrogenation continued until the chamber pressure reached  $7 \times 10^{-3}$  Pa ( $5 \times 10^{-5}$  Torr). Vacuum fusion analysis of selected samples indicated hydrogen concentrations were  $< 10$  ppm.

Large-size panels were hydrovac processed by Oregon Metallurgical Corporation. Ten 250 x 375 mm (10 x 15 in.) panels were suspended vertically in a 500-mm (20 in.) diameter cylindrical furnace chamber which has a hydrogen gas inlet at the top and outlet at the bottom. A charging time of 72 h at 650°C (1200°F) yielded 1 wt% hydrogen. 25 x 25-mm (1 x 1 in.) tabs from two corners of each panel were analyzed for hydrogen content by measuring the change in weight of hydrogen-charged samples and uncharged control samples upon vacuum annealing at 950°C (1740°F) for 7 h. All samples formed a slight oxide film during annealing, which the uncharged samples demonstrated to result in a weight increase of approximately 0.08%. The weight changes of the hydrided samples were corrected for this slight increase from the oxide films. Vacuum extraction measurements by the MCAIR Process Control Laboratory of vacuum-annealed hydrided samples showed that the annealing reduces the hydrogen level to less than 25 ppm. The results indicated that large panels can be charged with required amounts of hydrogen with reasonable reproducibility. Appendix A describes further the practical aspects of hydrovac processing on a production scale.

A key element in the hydrovac processing of large panels was the selection of a suitable protective coating for hydrogenated panels for subsequent beta annealing and eutectoid decomposition. The surface coating as well as the beta-annealing temperature was extremely impor-

tant for maximizing hydrogen retention and minimizing oxygen pick-up during hydrovac processing. Formkote T50 (E/M Lubricants Inc., P. O. Box 2200, West Lafayette, IN 47906), Deltaglaze 349M (Acheson Colloids Co., P. O. Box 288, Port Huron, MI), and the naturally occurring surface oxide film were evaluated as protective coatings. Beta annealings were performed at 810, 830, and 870°C (1490, 1525, and 1600°F) to determine the effect of beta-annealing temperature on oxygen pick-up.

##### 5. MICROSTRUCTURE AND PROPERTY CHARACTERIZATION OF HYDROVAC-PROCESSED ALLOYS

The microstructures of hydrovac-processed alloys were determined by optical metallography and scanning and transmission electron microscopy. Tensile properties at 25-482°C (77-900°F), creep properties at 350-600°C (660-1110°F), and fatigue properties at 25°C (77°F) were determined. Duplicate, rectangular, tension-test specimens that comply with ASTM Standard E8-78 were tested in the longitudinal orientation. Ti-6Al-4V specimens were tested at room temperature, 205°C (400°F), and 371°C (700°F), and Ti-6Al-2Sn-4Zr-2Mo specimens were tested at room temperature, 315°C (600°F), and 482°C (900°F). All tensile tests were performed under uniaxial tension at a constant strain-rate of  $0.0001 \text{ s}^{-1}$ . The yield stress, ultimate tensile stress, and total elongation were determined. Creep tests were performed on duplicate specimens in the longitudinal orientation from 350 to 600°C (660-1110°F). At each test temperature, five creep stresses were applied progressively to a single specimen while the elongation was continuously monitored. The steady-state creep rate (minimum creep rate) was calculated for each alloy/temperature/stress combination. The stress and temperature dependences of the steady-state creep rate were established for each alloy studied.

Fatigue crack-growth rates of the hydrovac-processed materials were measured using standard compact-tension (CT) specimens oriented in the long-transverse (TL) direction. Fatigue tests were performed with constant-load-amplitude at room temperature in ambient air using an automated, closed-loop, hydraulically-actuated test system. Specimen design and test procedures conformed to ASTM Standard E647. An electrical-potential method was used to monitor crack growth. This

technique measures the average through-thickness crack length, and the output from the potentiometer can be used in the test-system control loop when appropriate. On-line data acquisition, processing, and storage was performed with a dedicated PDP 11/04 minicomputer. Empirical equations of fatigue crack-growth rate,  $da/dN$ , as a function of stress-intensity-factor range,  $\Delta K$ , were derived from the test results. The fracture surfaces of the fatigue specimens were analyzed by SEM to characterize pertinent metallurgical and microstructural features.

#### 6. SUPERPLASTIC FORMABILITY DETERMINATION

The superplastic formability of the alloys was evaluated using the cone-forming tester shown in Figure 12. The cone-forming tester enables the cone depth and strain to be measured as the specimen is being superplastically formed.

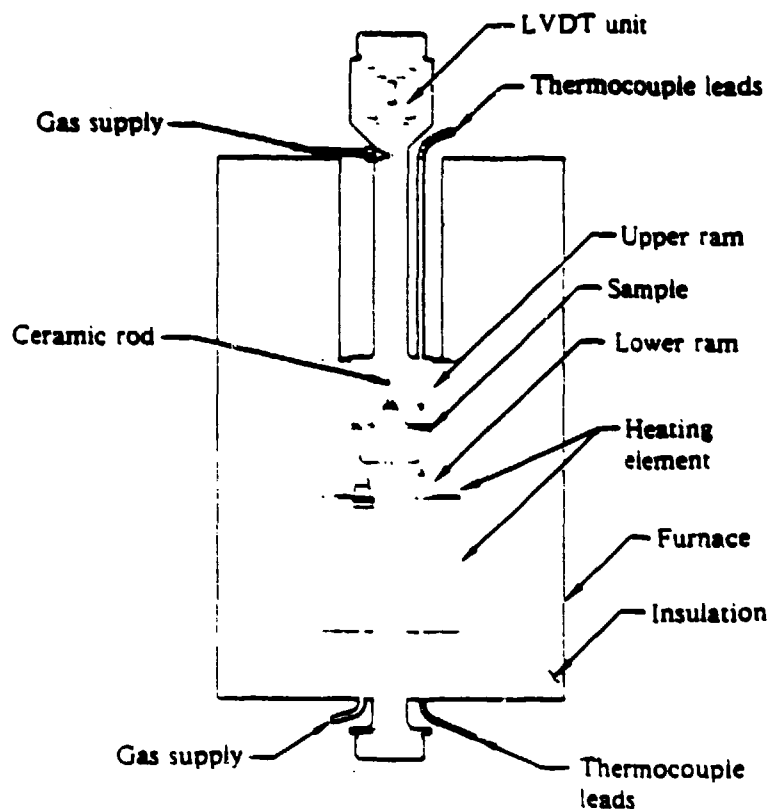


Figure 12. Experimental arrangement for laboratory cone-forming tests.

Applying the thin-membrane theory and assuming that the bulge shape is hemispherical until the sample contacts the die walls, the biaxial stress is given by

$$\sigma = \frac{xp}{2t} \quad (1)$$

where  $t$  is the membrane thickness,  $P$  is the applied pressure, and  $x$  is the radius of curvature of the membrane. The strain is given by

$$\epsilon = \ln(t/t_0) \quad (2)$$

where  $t_0$  is the initial thickness. For a conical angle of  $58^\circ$ , the ratio of thickness to radius of curvature ( $t/x$ ) is approximately constant as the cone forms (Reference 1), and hence forming occurs at a constant stress provided the pressure is maintained constant.

As explained in Appendix B, although the membrane thickness is small relative to the radius of curvature, the biaxial stress varies by 6% across the thickness. Equation (1) yields the average biaxial stress when the inner membrane radius is substituted for  $x$ . The strain-recording linear variable differential transformer (LVDT) shown in Figure 12 measures the instantaneous strain rate as a function of time at constant stress by means of the relation between strain and cone depth given in Appendix B. Constant stress prevails only after the sample contacts the die wall ( $\epsilon = 0.3$  for the present geometry).

As-received and hydrovac-processed alloys were cone formed under conditions generally used for superplastic forming in practice. Incremental-strain-rate, constant-stress, and constant-strain-rate tensile tests (Reference 10) were performed to establish the correspondence between biaxial cone-forming tests and uniaxial tensile tests.

## 7. SUPERPLASTIC FORMING AND DIFFUSION BONDING OF SPECIMENS CONTAINING AND EVOLVING HYDROGEN

The technical approach used for this task is outlined in Figure 11. Alloys with hydrogen concentrations of 0.01-0.1 wt% were investigated. The cone-forming tester shown in Figure 12 was used to hydrogenate the sample in situ, immediately heat it to the desired superplastic-forming temperature, and perform the superplastic-forming operation.

In-situ hydrogen charging was accomplished by applying equal pressures of a hydrogen-argon gas mixture to both sides of the sample disk. The clamping force on the disk was monitored and adjusted to permit controlled amounts of gas to escape, thus ensuring a continually fresh supply of hydrogen at each surface. Hydrogen charging was performed for 2 h at temperatures of 650-760°C (1200-1400°F) and at hydrogen partial pressures of 400-4000 Pa (3-30 Torr). After hydrogen charging, the hydrogen pressure was released from the conical-die side of the sample, and the pressure on the other side was increased to the desired level for forming. Internal hydrogen concentrations were determined by measuring the change in weight of formed samples upon vacuum annealing at 950°C (1740°F) for 4 h.

For investigating the effect of hydrogen evolution on formability, specimens were charged with hydrogen in situ and formed in an inert environment. The effect of internal hydrogen on diffusion bonding of Ti-alloys was investigated by charging small panels to various amounts of hydrogen, cutting the panels into 16 x 16 mm (0.6 x 0.6 in.) specimens, mechanically polishing the specimen surfaces on 400 grit paper, and diffusion bonding the specimens in a mixture of Ar with 4 wt% hydrogen at the desired temperature under an applied stress. Diffusion bonding experiments were performed in a vacuum/inert-gas chamber equipped with a furnace and a press.

## 8. SUPERPLASTIC FORMING OF TROUGH-SHAPED SPECIMENS CONTAINING INTERNAL HYDROGEN

Using optimum superplastic forming parameters determined from cone forming tests, large, 375 x 200 mm (15 x 8 in.) panels were in-situ

charged and superplastically formed into tough shapes using an Ar + 5 wt% hydrogen gas mixture. Superplastic forming evaluation was performed using the die configuration shown in Figure 13. Upon completion of forming, the toughs were dehydrogenated, and specimens were machined and tested for tensile properties.

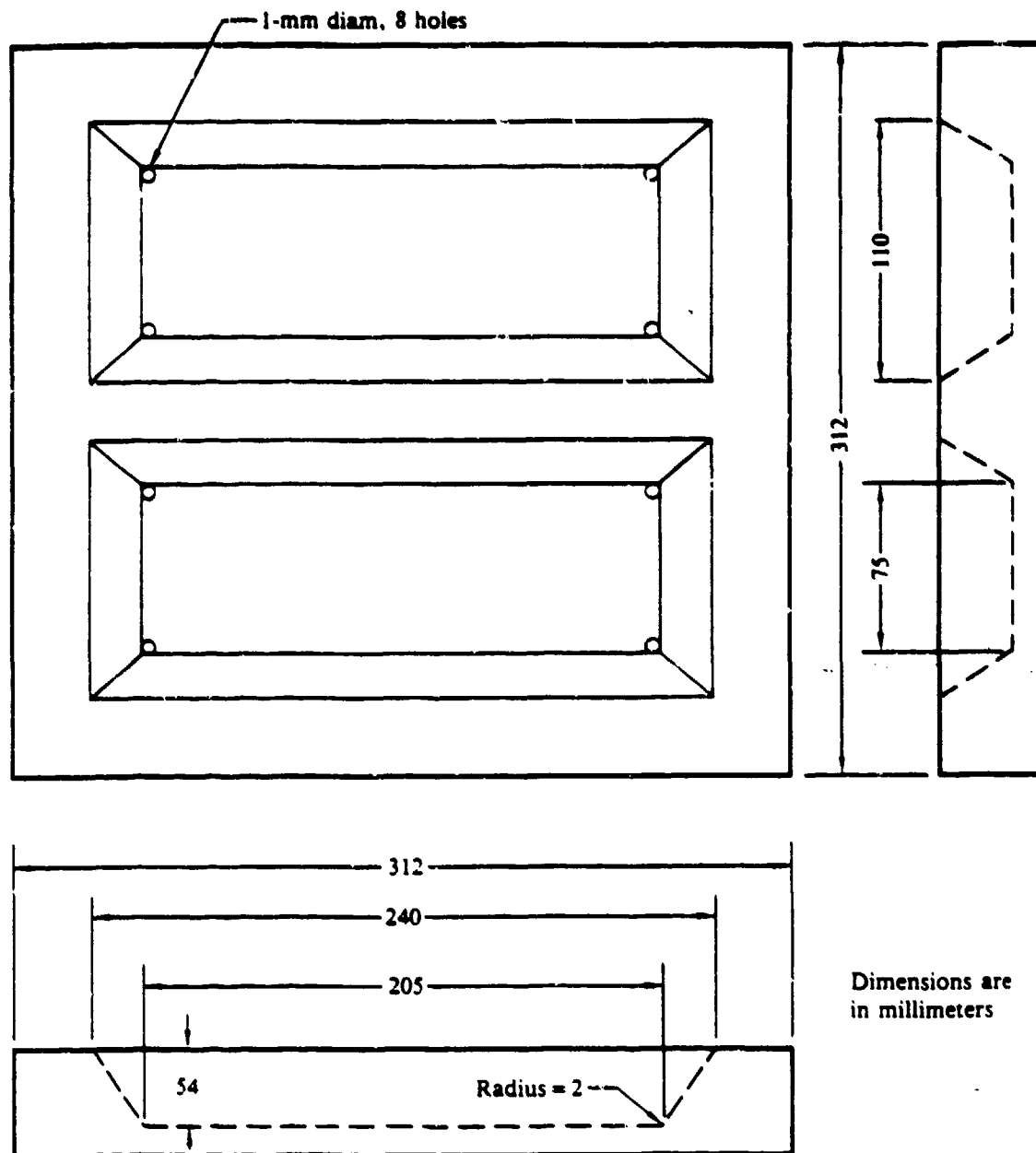


Figure 13. Trough-shaped die used in the superplastic forming of large panels.

SECTION IV  
MICROSTRUCTURES, MECHANICAL PROPERTIES, AND SUPERPLASTIC  
FORMABILITY OF HYDROVAC-PROCESSED TITANIUM ALLOYS

1. EFFECTS OF SURFACE COATINGS ON HYDROGEN RETENTION AND OXYGEN PICK-UP  
IN HYDROVAC-PROCESSED TI ALLOYS

A study was made of the effects of surface coatings on hydrogen retention and oxygen pick-up during hydrovac processing. Tables 2 and 3 list the retained hydrogen, carbon, and oxygen concentrations of hydrovac-processed Ti-6Al-4V. Oxygen pick-up is excessive in all but the vacuum encapsulated specimens. Although Formkote and Deltaglaze coatings are effective in retaining hydrogen, the specimens with these coatings had oxygen concentrations in excess of the maximum allowed under specification 9046H. The results were surprising since previous use of these coatings on uncharged Ti-alloys annealed in air at temperatures up to 1000°C (1830°F) did not result in oxygen pick-up. Hardness values of uncharged Ti alloys coated with Formkote and Deltaglaze and annealed at 860°C (1580°F) for 0.5 h are listed in Table 4. The hardness values are comparable to those of mill-processed, as-received Ti-6Al-4V, and oxygen concentrations determined from the calibration curve for hardness as a function of oxygen concentration shown in Figure 14 are well below the maximum allowable limits.

TABLE 2  
EFFECTS OF SURFACE COATINGS ON HYDROGEN RETENTION IN Ti-6Al-4V  
CHARGED WITH HYDROGEN AT 650°C (1200°F), ANNEALED AT 870°C (1600°F) FOR  
0.5h, AND COOLED TO 25°C (77°F)

Surface treatment	% hydrogen retained
Uncoated	79
Coated with Formkote T50	93
Coated with Deltaglaze 349	98
Vacuum encapsulated	100

**TABLE 3**  
**CARBON AND OXYGEN CONCENTRATIONS OF SELECTED HYDROVAC-PROCESSED**  
**Ti-6Al-4V SAMPLES**

Surface coating	Beta annealing temperature [°C (°F)]	Oxygen concentration (wt%)	Carbon concentration (wt%)
Formkote T50	870 (1600)	0.35	—
Formkote T50	870 (1600)	0.31	0.014
Formkote T50	810 (1490)	0.19	0.013
Deltaglaze 349	870 (1600)	0.21	—
Deltaglaze 349	830 (1526)	0.24	—
Uncoated	870 (1600)	0.28	—
Vacuum encapsulated	870 (1600)	0.14	0.017

Maximum allowable oxygen concentration in Ti-6Al-4V and Ti-6Al-2Sn-4Zr-2Mo alloy is 0.2 wt%.

**TABLE 4**  
**ROCKWELL C HARDNESS VALUES OF UNCHARGED Ti-6Al-4V SAMPLES ANNEALED**  
**AT 865°C FOR 0.5 h**

Surface treatment	Rockwell C hardness
Uncoated	35.5
Formkote T50	33.2
Deltaglaze 349	35.3
As-received (unannealed)	35.2

These results clearly demonstrate that in the presence of hydrogen, the coatings are ineffective barriers for oxygen diffusion into the specimens. However, whereas the coatings readily permit oxygen pick-up, they are effective in preventing hydrogen loss from the specimens. An understanding of the synergistic effects on oxygen pick-up of hydrogen and coating chemistry would require a detailed thermodynamic analysis and a large number of well-controlled experiments, which were beyond the scope of the present investigation. Reducing the beta-annealing temperature from 870°C (1600°F) to 810°C (1490°F) resulted in significant

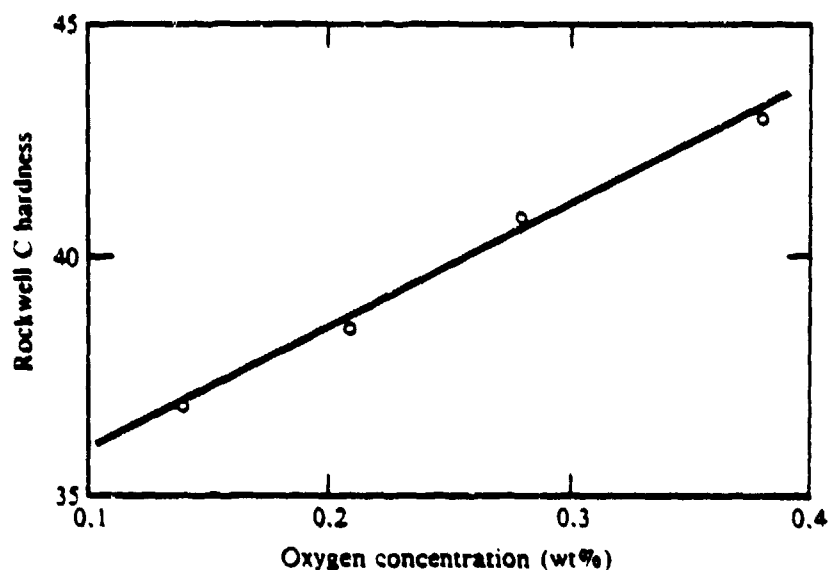


Figure 14. Effect of oxygen concentration on Rockwell C hardness values for hydrovac-processed Ti-6Al-4V.

decrease in oxygen pick-up in Ti-6Al-4V coated with Formkote T50 but did not produce a significant decrease in oxygen pick-up in Deltaglaze-coated Ti-6Al-4V.

The results shown in Table 3 indicate that vacuum encapsulation of specimens is the best choice for heat treating hydrogen-charged Ti alloys. Whereas this technique is well suited for small specimens, it is not cost effective for large panels. In the present investigation, all specimens for microstructure and mechanical property determinations were hydrovac processed using vacuum encapsulation for preventing hydrogen loss. The results obtained from such specimens are discussed in this section. Because Deltaglaze coating and Formkote coating combined with lower beta-annealing temperatures resulted in oxygen concentrations close to the specification limits, selected property measurements were made on alloy specimens that were hydrovac-processed using these coatings and lower beta-annealing temperatures. These results are presented in Appendix C.

## 2. MICROSTRUCTURES OF HYDROVAC-PROCESSED Ti-6Al-4V AND Ti-6Al-2Sn-4Zr-2Mo

Figures 15a-15d are transmission electron micrographs showing transformation products in Ti-6Al-4V at various stages of hydrovac processing. The conventionally processed Ti-6Al-4V has a partially recrystallized alpha-beta microstructure (Figure 15a). Hydrogenation at 665°C (1200°F) with 1.0 wt% hydrogen and annealing at 870°C (1600°F) produces a hydrogen-saturated beta phase. Water quenching of this beta phase produces a martensitic microstructure (Figure 15b). This martensite, identified by selected-area electron diffraction to be orthorhombic martensite ( $\alpha''$ ), is significantly different from the hexagonal martensite observed in  $\alpha + \beta$  alloys quenched from the beta field. The martensite plates are extensively twinned and contain large densities of dislocations. Upon annealing the alloy below 810°C (1490°F), the orthorhombic martensite transforms isothermally to  $\alpha$ -Ti and  $\text{TiH}_2$ ; the size and spacings of the decomposition products increasing with increase transformation temperature. Transformation at  $\sim 595^\circ\text{C}$  (1105°F) results in closely-spaced, fine, decomposition products (Figure 15c). Upon dehydrogenation of the alloy containing  $\alpha$ -Ti and  $\text{TiH}_2$ , the hydride phase transforms to  $\alpha + \beta$ . This transformation is associated with the formation of a high dislocation density in the alpha phase, as the conversion of titanium hydride to  $\alpha$ -Ti results in a  $\sim 17\%$  volume change and concomitant high strains. The dehydrogenated alloy contains a partially recovered dislocation substructure and low-angle boundaries (Figure 15d).

The effects of dehydrogenation temperature on substructure formation in Ti-6Al-4V-1.2 H alloy are shown in Figures 16a-16d. Dehydrogenation at 665°C (1200°F) results in partially recovered dislocation cell structure, and the dislocation subgrains coarsen with increasing dehydrogenation temperature and times.

The effect of the dehydrogenation temperature on tensile properties was determined for equiaxed Ti-6Al-4V samples with the objective of determining the dehydrogenation temperature that produces the best combination of strength and ductility. The mechanical properties of hydrovac-processed specimens dehydrogenated at 660 (1220) and 700°C

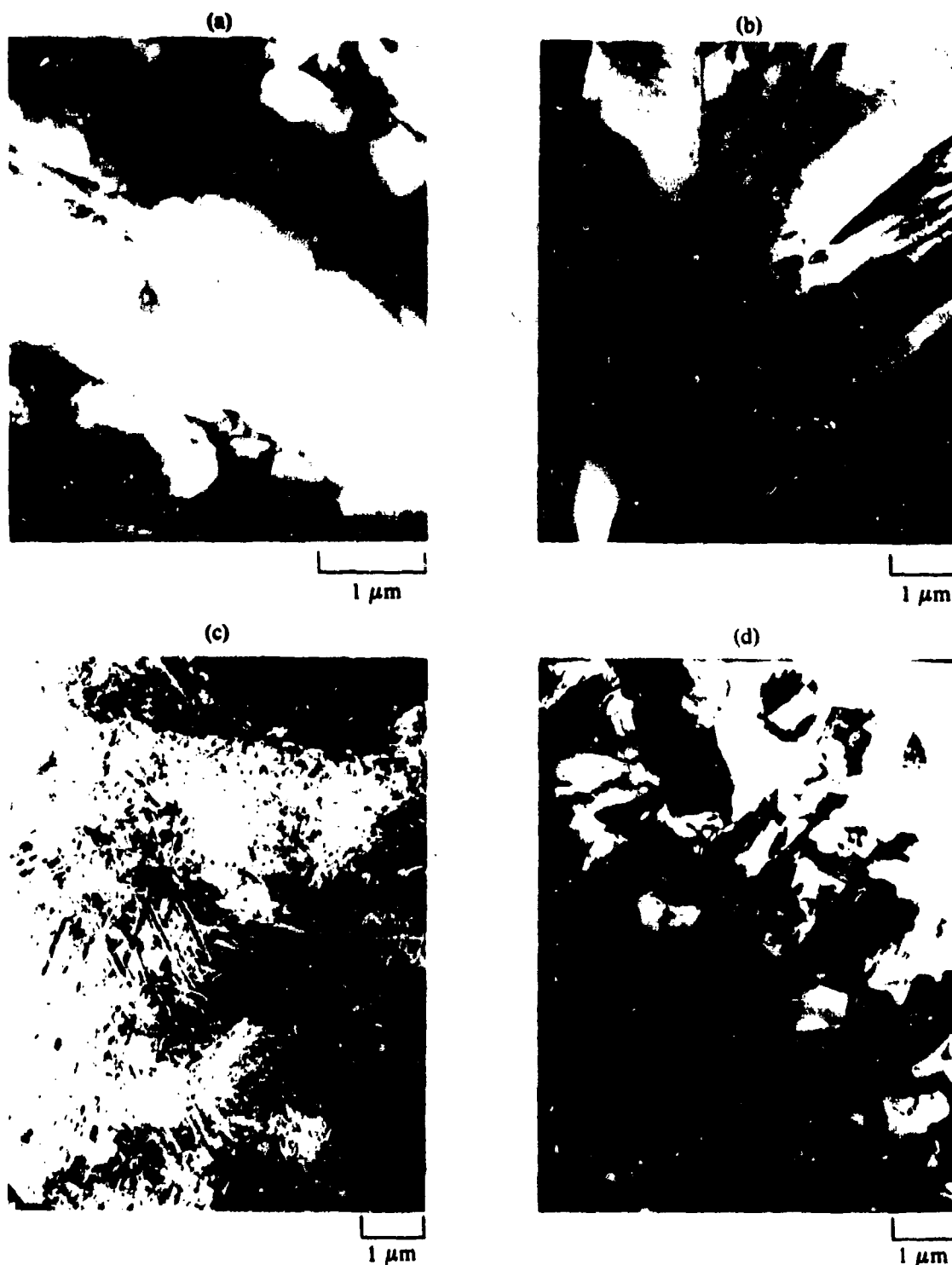


**Figure 15.** Transmission electron micrographs showing the transformation products at various stages of hydrovac processing: (a) conventionally processed Ti-6Al-4V; (b) hydrogen-charged at 665°C, beta-annealed at 870°C for 5 h and water quenched; (c) hydrogen-charged at 660°C, annealed at 870°C for 0.5 h, cooled to 595°C, and annealed at 595°C for 4 h; and (d) as in (c) followed by dehydrogenation at 700°C for 6 h.

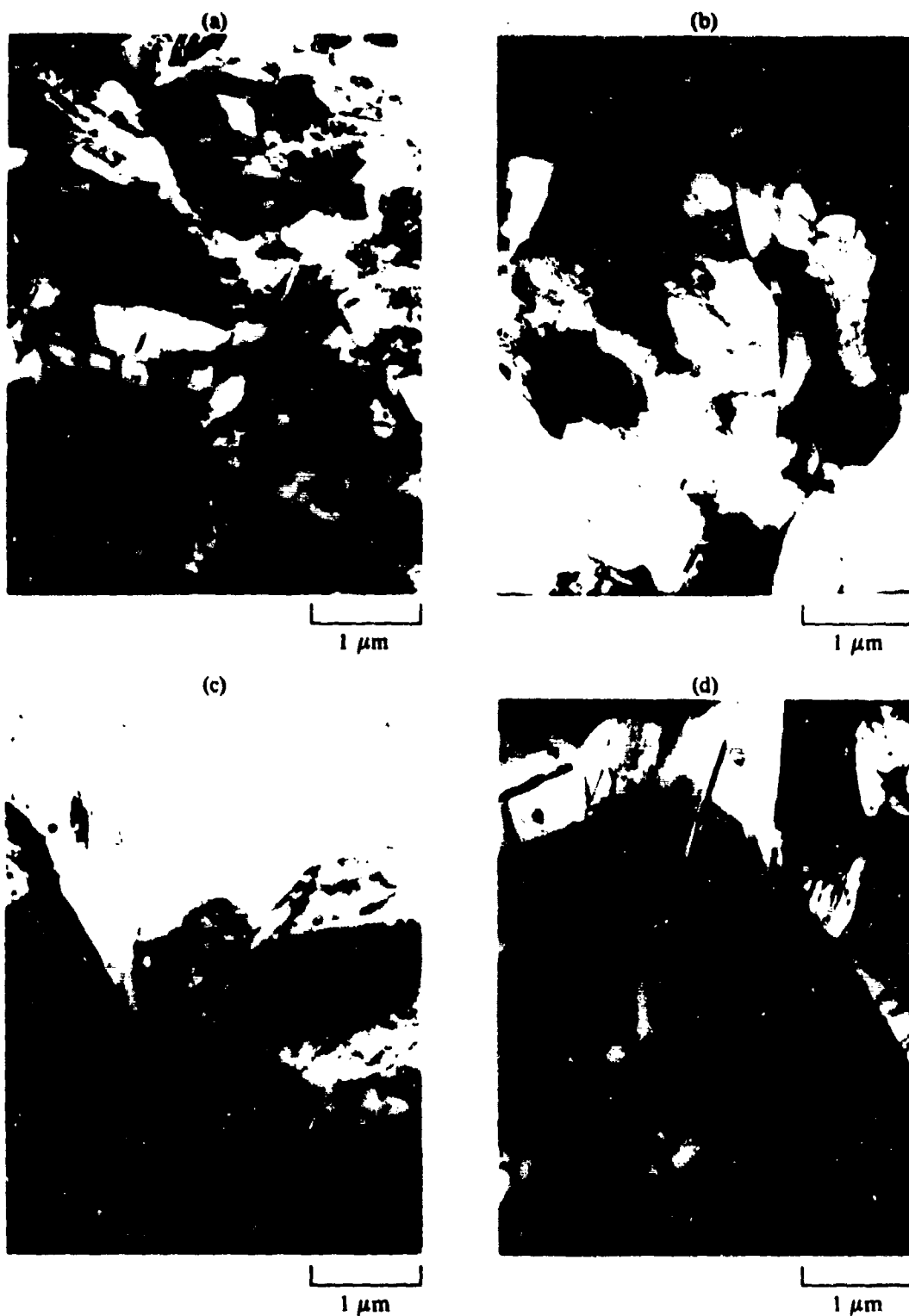


**Figure 16.** Effect of dehydrogenation temperature on substructure formation in Ti-6Al-4V-1.2H beta annealed at 870°C for 0.5 h, cooled to 595°C, transformed at 595°C for 4 h, and dehydrogenated at (a) 665°C for 20 h, (b) 682°C for 20 h, (c) 705°C for 6 h, and (d) 705°C for 20 h.

(1260°F) and conventionally processed specimens are listed in Table 5. Both sets of samples show significant strength increases and ductility losses. The hydrovac-processed specimens dehydrogenated at 660°C (1220°F) have the highest strength; however, in view of production temperature uncertainties and the anticipated brittleness arising from dehydrogenation temperatures of 660°C (1200°F) or less, 675°C (1245°F) was chosen for dehydrogenation.

Figures 17-19 are scanning electron micrographs of equiaxed- $\alpha$  Ti-6Al-4V, Widmanstätten Ti-6Al-4V, and Ti-6Al-2Sn-4Zr-2Mo showing the microstructural refinement caused by hydrovac processing. The equiaxed- $\alpha$  Ti-6Al-4V microstructure without hydrovac (Figure 17a) has an average grain diameter of 3  $\mu\text{m}$  and is considerably refined by hydrovac processing to an average grain diameter of 0.5  $\mu\text{m}$ . The Widmanstätten Ti-6Al-4V microstructure (Figure 18a) initially has colonies of alpha-beta with each colony having a single alpha orientation. Hydrovac processing results in considerable refinement of the alpha grains (Figure 18b). Figure 19a shows the fine, 2-4  $\mu\text{m}$  equiaxed-alpha + beta microstructure of the duplex-annealed Ti-6Al-2Sn-4Zr-2Mo. Figure 19b shows that hydrovac processing reduces the grain size to 0.5  $\mu\text{m}$ . Figures 20a-20c are higher magnification scanning electron micrographs of the three hydrovac-processed alloys.

**TABLE 5**  
**EFFECT OF DEHYDROGENATION TEMPERATURE ON MECHANICAL PROPERTIES**  
**OF HYDROVAC-PROCESSED EQUIAXED- $\alpha$  Ti-6Al-4V**

Dehydrogenation temperature (°C)	0.2% yield stress [MPa (ksi)]	Ultimate tensile stress [MPa (ksi)]	Total elongation (%)
700	1035 (150)	1090 (158)	8.3
700	1065 (154)	1095 (158)	7.2
660	1125 (163)	1155 (168)	4.3
660	1130 (164)	1153 (168)	5.3
Before hydrovac processing <sup>(a)</sup>	960 (139)	985 (143)	13.5

(a) Measurements were made by the alloy supplier.

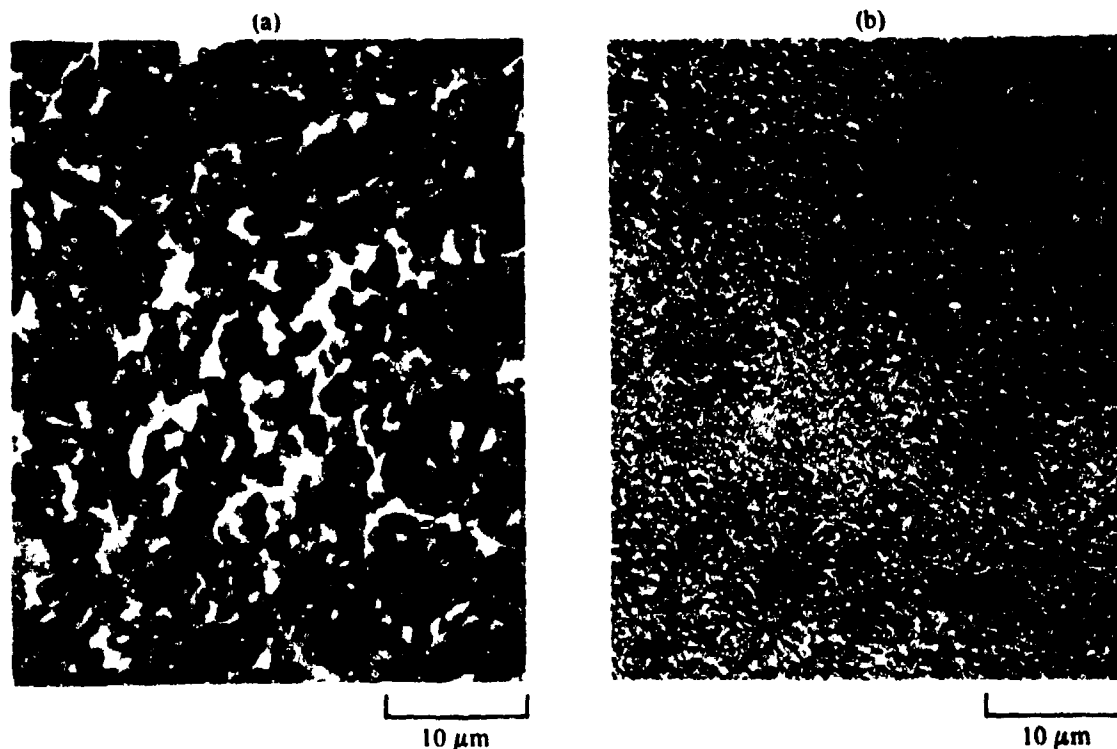
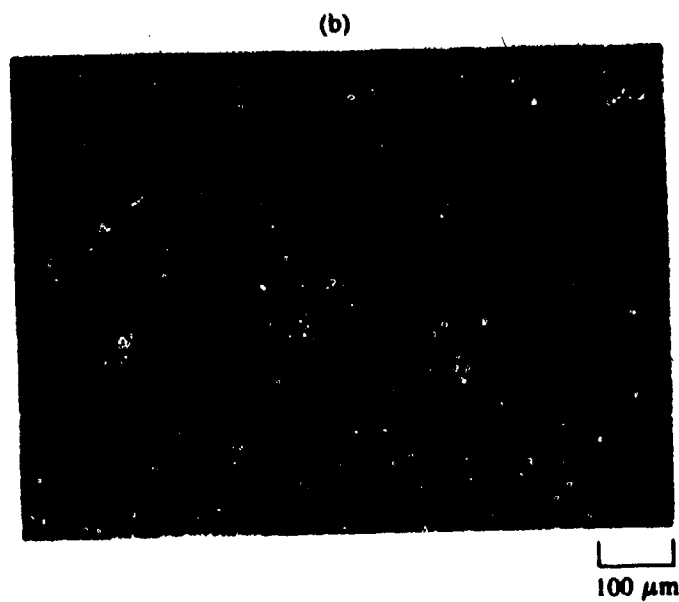
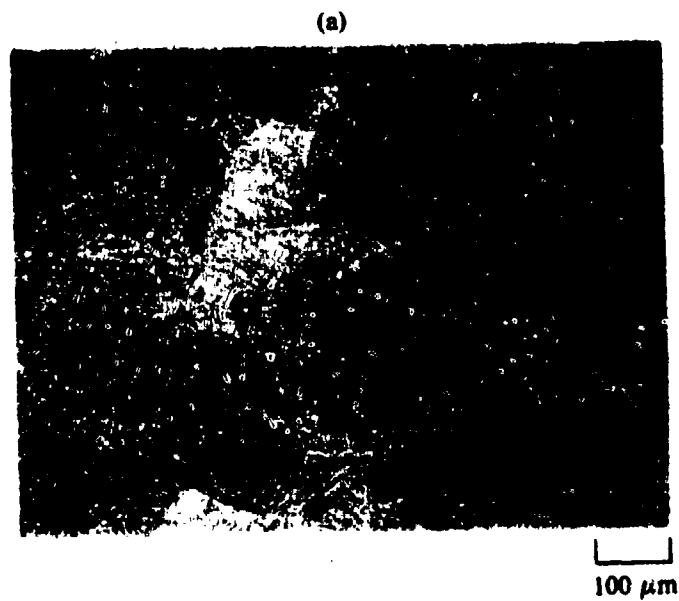
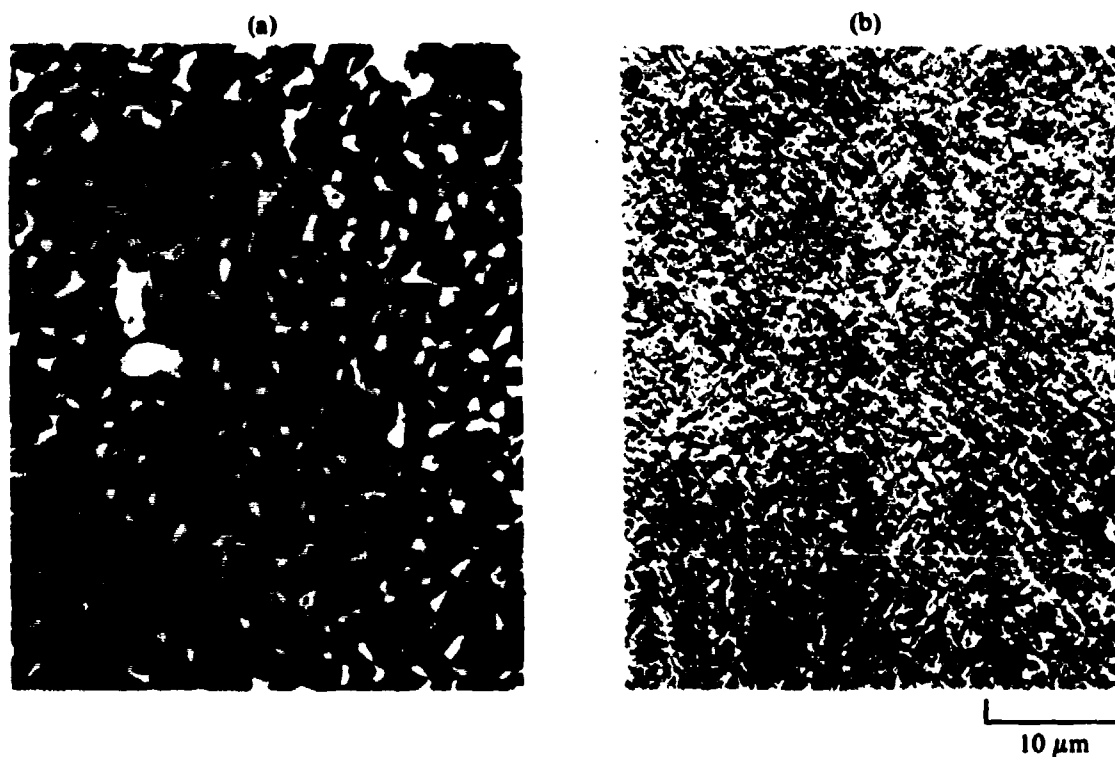


Figure 17. Scanning electron micrographs of equiaxed- $\alpha$  Ti-6Al-4V (a) before and (b) after hydrovac processing.

The crystallographic texture of the as-received and hydrovac-processed alloys was characterized by determining by x-ray pole-figure goniometry the basal and prism pole distributions. Equiaxed- $\alpha$  Ti-6Al-4V has a moderate degree of texture (texture sharpness of 7) with the basal poles of strong texture components tilted  $25-40^\circ$  from the sheet normal (Figure 21a). The hydrovac-processed alloy has the same moderate degree of texture with no tilting of the basal poles from the sheet normal (Figure 21c). The texture of Ti-6Al-2Sn-4Zr-2Mo (Figure 22) consists of one component with the  $[0001]$  direction tilted towards the transverse direction from the rolling plane normal by  $\sim 60^\circ$  and another component with the basal pole tilted towards the rolling direction from the sheet normal by  $\sim 30^\circ$ .



**Figure 18. Scanning electron micrographs of Widemanstätten Ti-6Al-4V (a) before and (b) after hydrovac processing.**



**Figure 19. Scanning electron micrographs of duplex-annealed Ti-6Al-2Sn-4Zr-2Mo (a) before and (b) after hydrovac processing.**

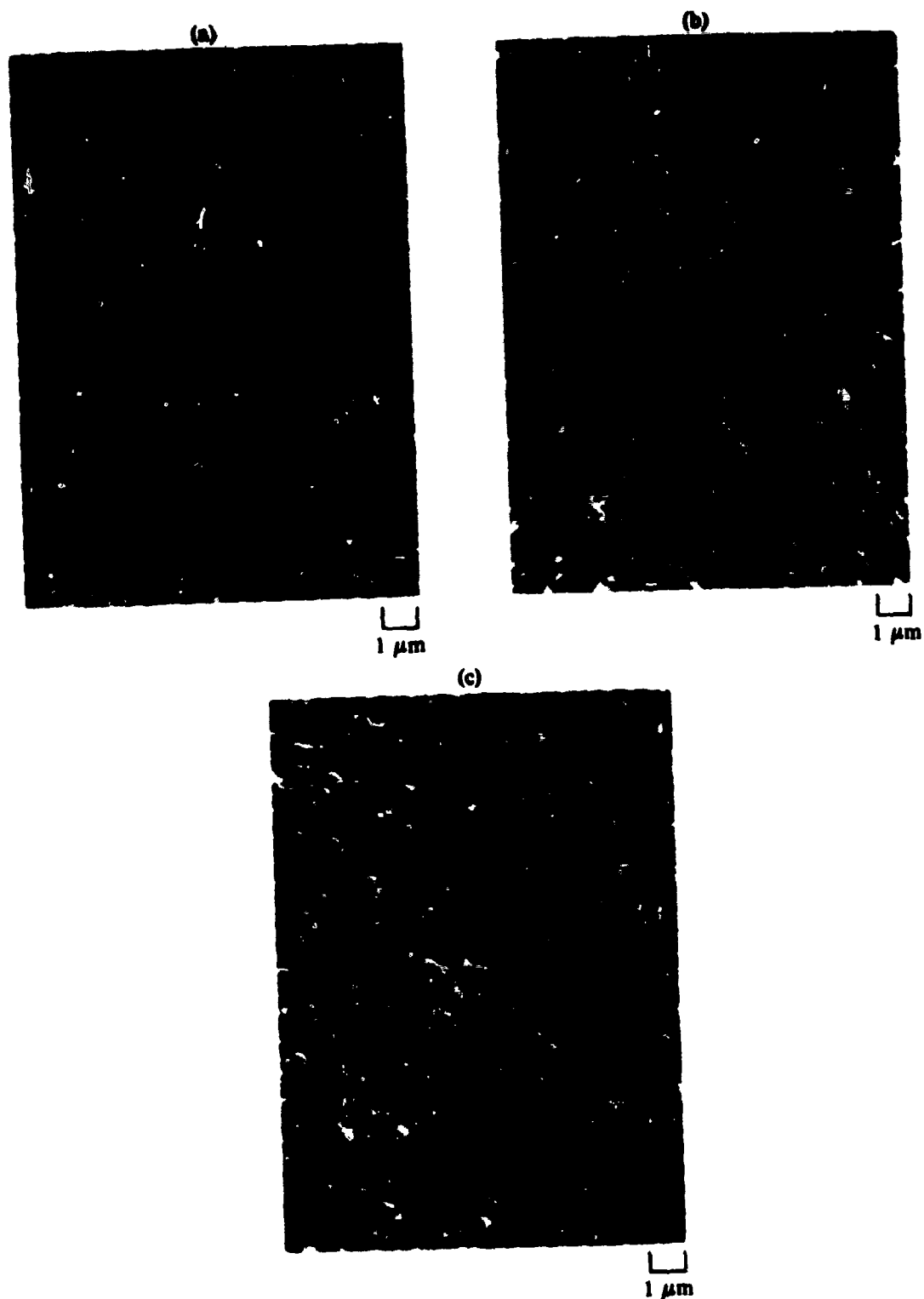


**Figure 20. High-magnification scanning electron micrographs of hydrovac-processed (a) Ti-6Al-4V, (b) Widmanstätten Ti-6Al-4V, and (c) duplex-annealed Ti-6Al-2Sn-4Zr-2Mo.**

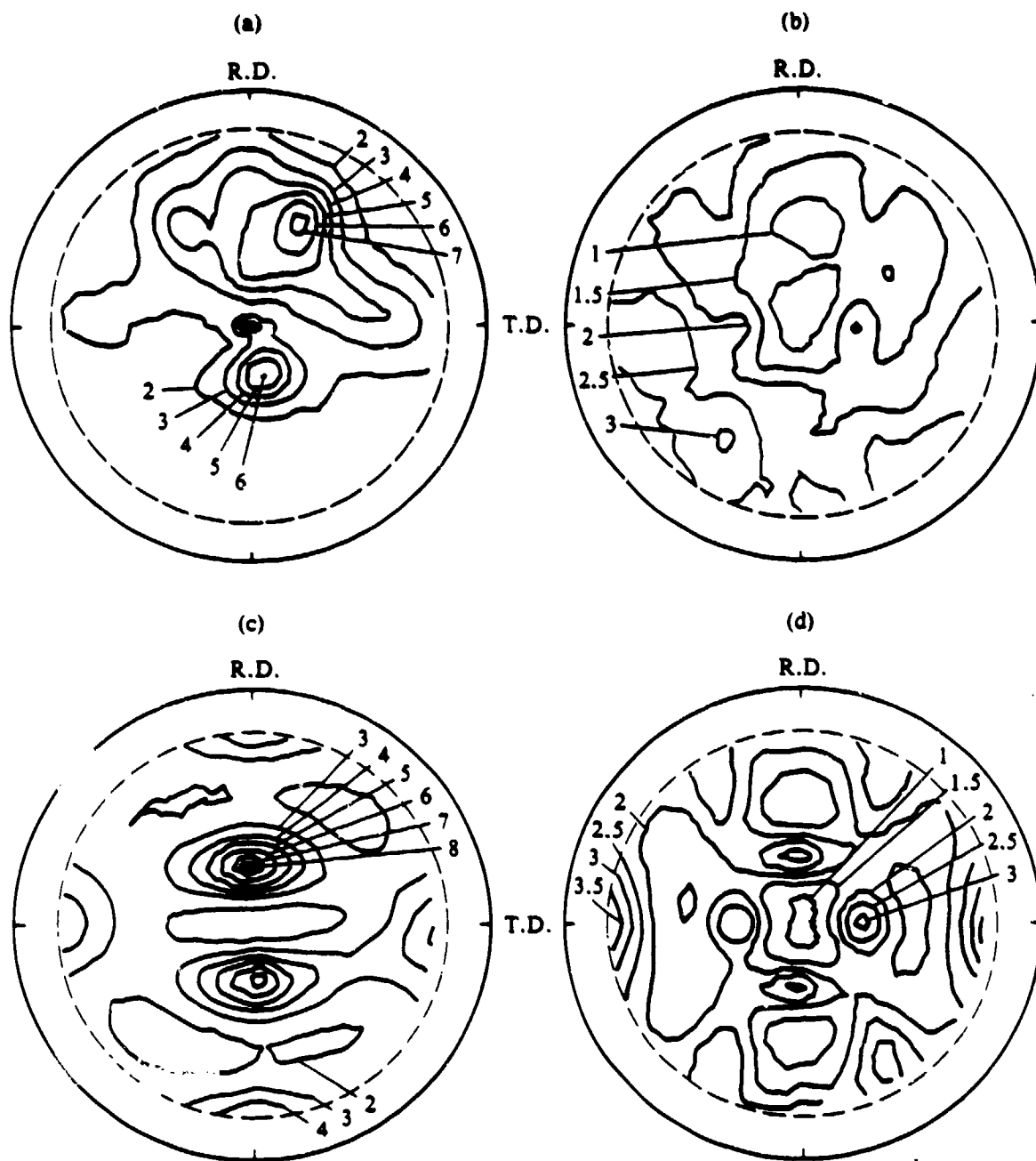


Figure 21. (a) (0002), (b) (1010) pole figures of equiaxed- $\alpha$  Ti-6Al-4V, and (c) (0002), (d) (1010) pole figures of hydrovac-processed Ti-6Al-4V.

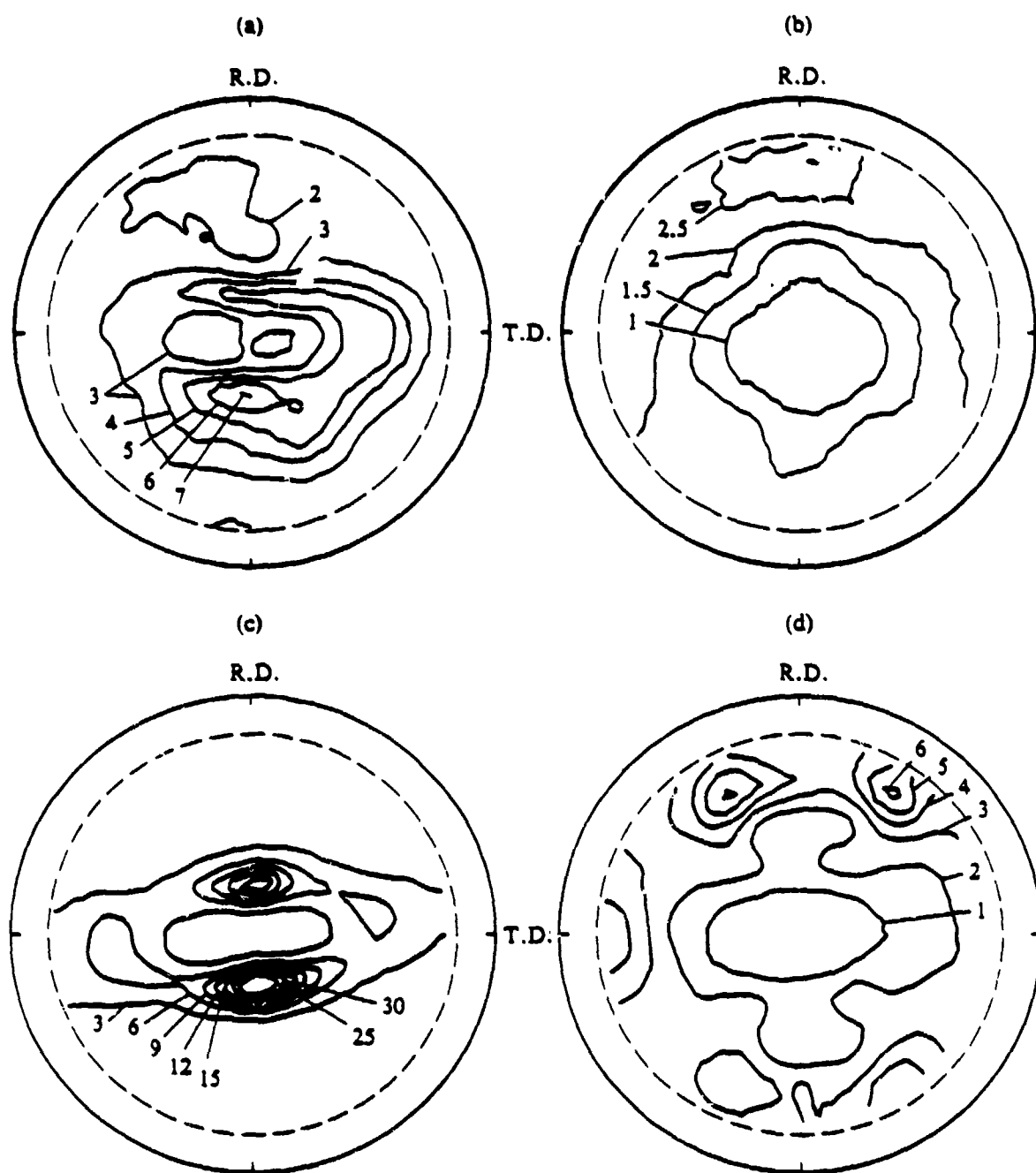


Figure 22. (a) (0002), (b) (1010) pole figures of duplex-annealed Ti-6Al-2Sn-4Zr-2Mo and (c) (0002), (d) (1010) pole figures of hydrovac-processed Ti-6Al-2Sn-4Zr-2Mo.

### 3. TENSILE AND CREEP PROPERTIES OF HYDROVAC-PROCESSED Ti-6Al-4V AND Ti-6Al-2Sn-4Zr-2Mo

Tensile and creep properties were determined for hydrovac-processed Ti-alloys using vacuum encapsulation for beta annealing and eutectoid transformation.

The mechanical properties of the as-received and hydrovac-processed alloys are listed in Tables 6 and 7. Hydrovac-processed Ti-6Al-2Sn-4Zr-2Mo was brittle at 25°C and fractured with negligible elongation. The optimum dehydrogenation temperature for hydrovac processing Ti-6Al-2Sn-4Zr-2Mo is slightly higher than that for Ti-6Al-4V. Figures 23-26 compare the temperature dependence of yield stress and ultimate tensile stress of as-received and hydrovac-processed samples. In general,

TABLE 6  
TENSILE PROPERTIES OF AS-RECEIVED ALLOYS

Alloy	Temperature [°C (°F)]	0.2% yield stress [MPa (ksi)]	Ultimate tensile stress [MPa (ksi)]	Total elongation (%)	
Equiaxed- $\alpha$ Ti-6Al-4V	21 (70)	959 (139)(a)	985 (143)(a)	13.5(a)	
		961 (139)	1000 (145)	12.8	
		964 (140)	1009 (146)	11.4	
	205 (400)	717 (104)	816 (118)	11.8	
		732 (106)	822 (119)	9.4	
	371 (700)	636 (92)	753 (109)	7.9	
		645 (93)	737 (107)	7.4	
		Widmanstätten Ti-6Al-4V	849 (123)	956 (139)	8.6
	849 (123)		956 (139)	8.2	
	205 (400)		616 (89)	745 (108)	8.7
658 (95)		763 (111)	7.8		
	371 (700)	506 (73)	622 (90)	7.7	
		544 (79)	641 (93)	8.6	
		550 (80)	633 (92)	7.8	
	Duplex-annealed Ti-6Al-2Sn-4Zr-2Mo	21 (70)	924 (134)(a)	1048 (152)(a)	13.0(a)
			936 (136)	1016 (147)	12.4
936 (136)			1017 (148)	12.6	
315 (600)		645 (93)	824 (119)	11.2	
		618 (90)	815 (118)	9.4	
482 (900)		589 (85)	774 (112)	14.0	
		622 (90)	779 (113)	16.0	

(a) Measurements were made by the alloy supplier.

**TABLE 7**  
**TENSILE PROPERTIES OF HYDROVAC-PROCESSED ALLOYS**

Alloy	Temperature [°C (°F)]	0.2% yield stress [MPa (ksi)]	Ultimate tensile stress [MPa (ksi)]	Total elongation (%)
Equiaxed- $\alpha$ Ti-6Al-4V	21 (70)	1065 (155)	1105 (161)	14.0
		1060 (154)	1110 (161)	8.4
	205 (400)	825 (119)	935 (135)	14.9
		835 (121)	920 (133)	15.6
	371 (700)	705 (102)	835 (121)	8.7
		770 (111)	865 (125)	12.7
Duplex-annealed Ti-6Al-2Sn-4Zr-2Mo	21 (70)	—	1140 (165)	—
		—	1020 (147)	—
	315 (600)	940 (136)	1025 (149)	9.0
		935 (135)	1035 (150)	10.8
	482 (900)	790 (115)	935 (136)	14.2
		—	—	—

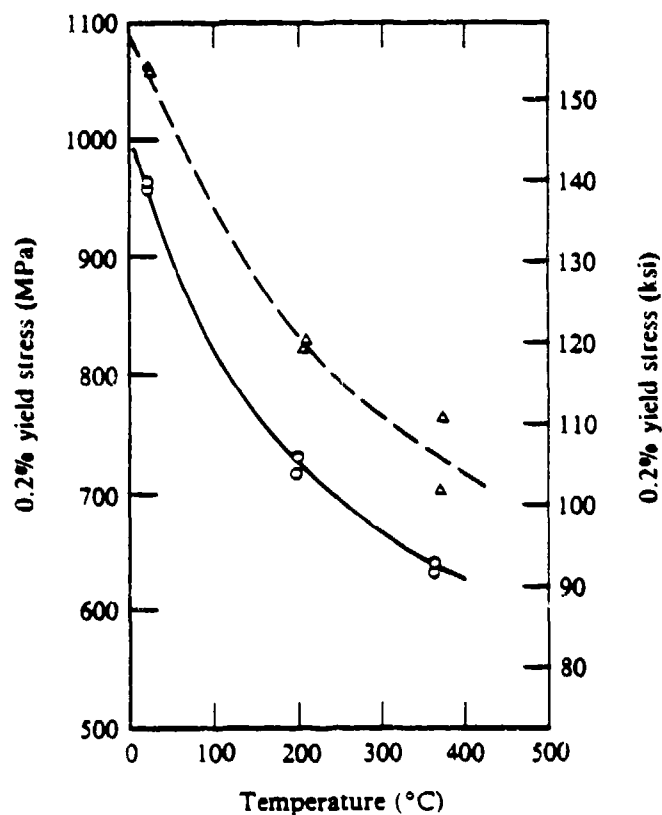


**Figure 23. Effect of temperature on the 0.2% yield stress of (○) as-received and (Δ) hydrovac-processed equiaxed- $\alpha$  Ti-6Al-4V.**

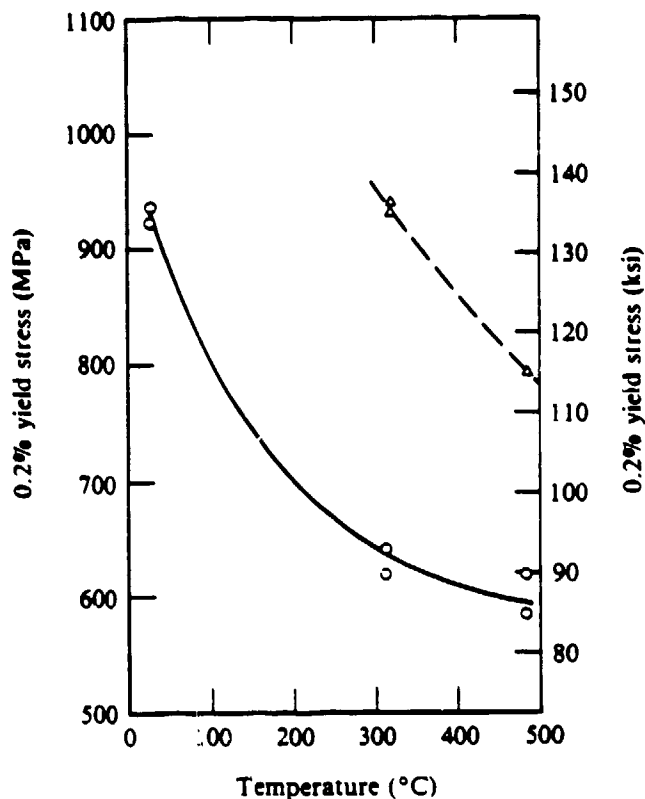


Figure 24. Effect of temperature on the 0.2% yield stress of (○) as-received and (△) hydrovac-processed duplex-annealed Ti-6Al-2Sn-4Zr-2Mo.

hydrovac processing increases the strengths by  $\approx 100$  MPa (15 ksi) for Ti-6Al-4V and by nearly 200 MPa (29 ksi) for Ti-6Al-2Sn-4Zr-2Mo with no loss in ductility. The strength increments are produced by fine sub-grain structure.

Figures 27 and 28 show the stress dependences of steady-state creep rates of conventionally-processed and hydrovac-processed Ti-6Al-4V and Ti-6Al-2Sn-4Zr-2Mo. Hydrovac processing reduces the creep rates by approximately an order-of-magnitude at 600°C (1110°F) and 520°C (970°F) and more than an order-of-magnitude at 435°C (815°F) and 350°C (660°F).

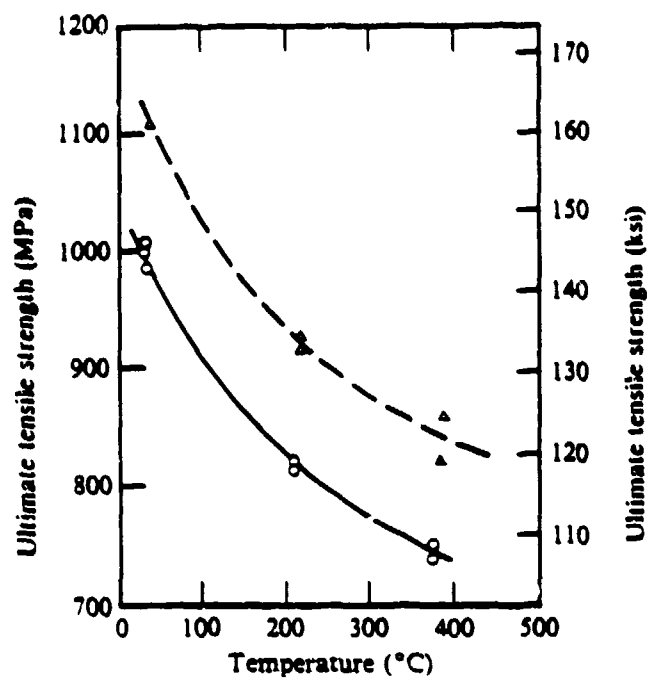


Figure 25. Effect of temperature on the ultimate tensile strength of (○) as-received and (Δ) hydrovac-processed equiaxed- $\alpha$  Ti-6Al-4V.

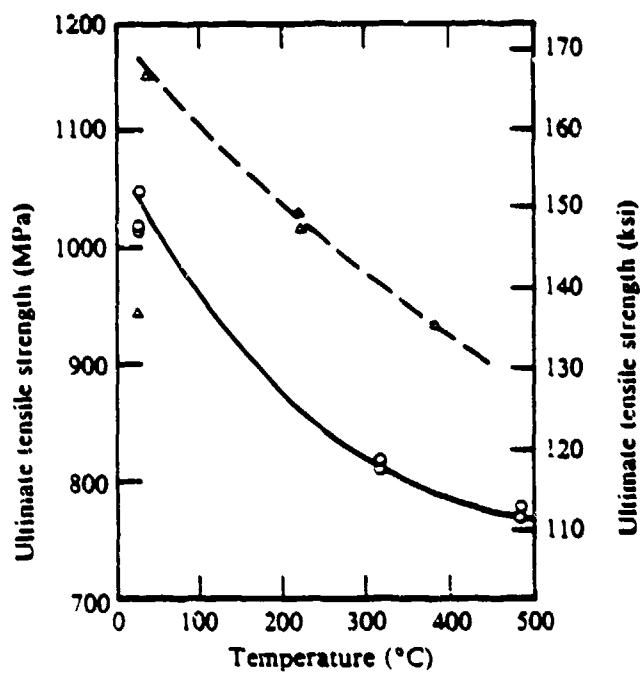


Figure 26. Effect of temperature on the ultimate tensile strength of (○) as-received and (Δ) hydrovac-processed duplex-annealed Ti-6Al-2Sn-4Zr-2Mo.

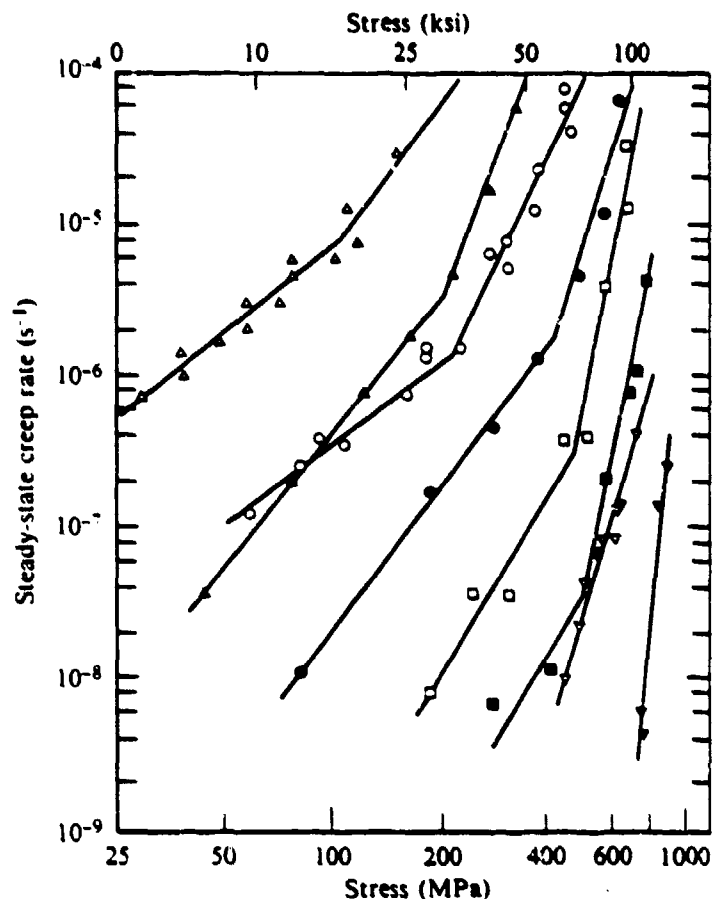


Figure 27. Stress dependence of steady-state creep rate for equiaxed- $\alpha$  Ti-6Al-4V in as-received condition (open symbols) and hydrovac condition (closed symbols) at ( $\Delta$ ,  $\blacktriangle$ ) 600°C, ( $\circ$ ,  $\bullet$ ) 520°C, ( $\square$ ,  $\blacksquare$ ) 435°C, and ( $\nabla$ ,  $\blacktriangledown$ ) 350°C.

#### 4. SUPERPLASTIC FORMING AND DIFFUSION BONDING OF HYDROVAC-PROCESSED Ti ALLOYS

The superplastic-forming and diffusion-bonding tests were conducted on Ti-6Al-4V and Ti-6Al-2Sn-4Zr-2Mo alloys hydrovac processed at Oregon Metallurgical Corporation using Formkote T50 coating and 810°C (1490°F) beta annealing. The microstructural refinements produced by this processing were similar to those produced by hydrovac processing of vacuum encapsulated and 870°C (1600°F) beta-annealed specimens. Oxygen concentrations in the alloys were  $\approx$  0.19 wt%, close to the specification limit of 0.2 wt%.

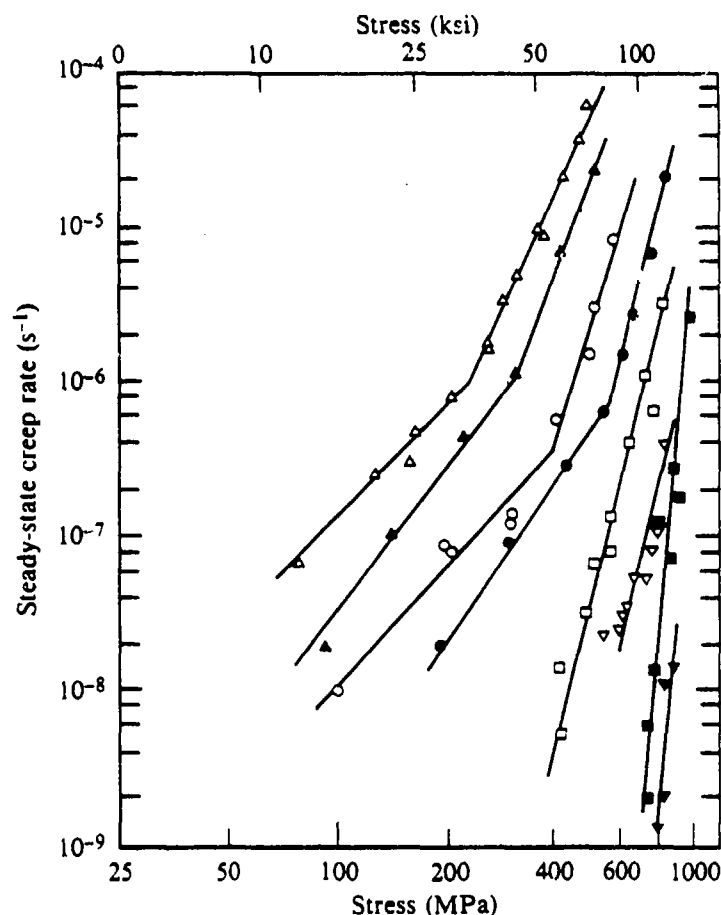


Figure 28. Stress dependence of steady-state creep rate for duplex-annealed Ti-6Al-2Sn-4Zr-2Mo in as-received condition (open symbols) and hydrovac condition (closed symbols) at ( $\Delta, \blacktriangle$ ) 600°C, ( $\circ, \bullet$ ) 520°C, ( $\square, \blacksquare$ ) 435°C and ( $\nabla, \blacktriangledown$ ) 350°C.

Conventionally-processed and hydrovac-processed alloys were superplastically formed using the cone-forming tester described in Section III.6. The matrix of test conditions used in this part of the study is shown in Table 8.

Figure 29 shows examples of equiaxed- $\alpha$  Ti-6Al-4V samples superplastically formed at 900°C (1650°F) at stresses of 3.2-18.8 MPa (0.47-2.72 ksi). Figure 30 shows cross sections of the equiaxed- $\alpha$  Ti-6Al-4V cones and a Widmanstätten Ti-6Al-4V cone formed at 900°C (1650°F) and 18.8 MPa (2.72 ksi). The equiaxed- $\alpha$  Ti-6Al-4V cones show uniform straining. The Widmanstätten alloy, which has poor SPF properties, has extensive non-uniform thinning.

**TABLE 8**  
**MATRIX OF SUPERPLASTIC-FORMING TESTS**

Stress [MPa (ksi)]	Temperature (°C)					
	900	830	800	780	760	720
18.8 (2.72)	$\alpha$ , W, D $\alpha$ H	$\alpha$ , W, D $\alpha$ H, WH, DH	$\alpha$ $\alpha$ H	$\alpha$ $\alpha$ H	$\alpha$ $\alpha$ H	$\alpha$ $\alpha$ H
9.7 (1.40)	$\alpha$ $\alpha$ H	$\alpha$ , D $\alpha$ H	—	—	—	—
6.6 (0.95)	$\alpha$ , W, D	—	—	—	—	—
3.2 (0.47)	$\alpha$	—	—	—	—	—

$\alpha$  — Equiaxed- $\alpha$  Ti-6Al-4V  
W — Widmanstätten Ti-6Al-4V  
D — Duplex-annealed Ti-6Al-2Sn-4Zr-2Mo  
 $\alpha$ H — Hydrovac equiaxed- $\alpha$  Ti-6Al-4V  
WH — Hydrovac Widmanstätten Ti-6Al-4V  
DH — Hydrovac duplex-annealed Ti-6Al-2Sn-4Zr-2Mo



**Figure 29. Ti-6Al-4V cones formed at 900°C and at various pressures.**

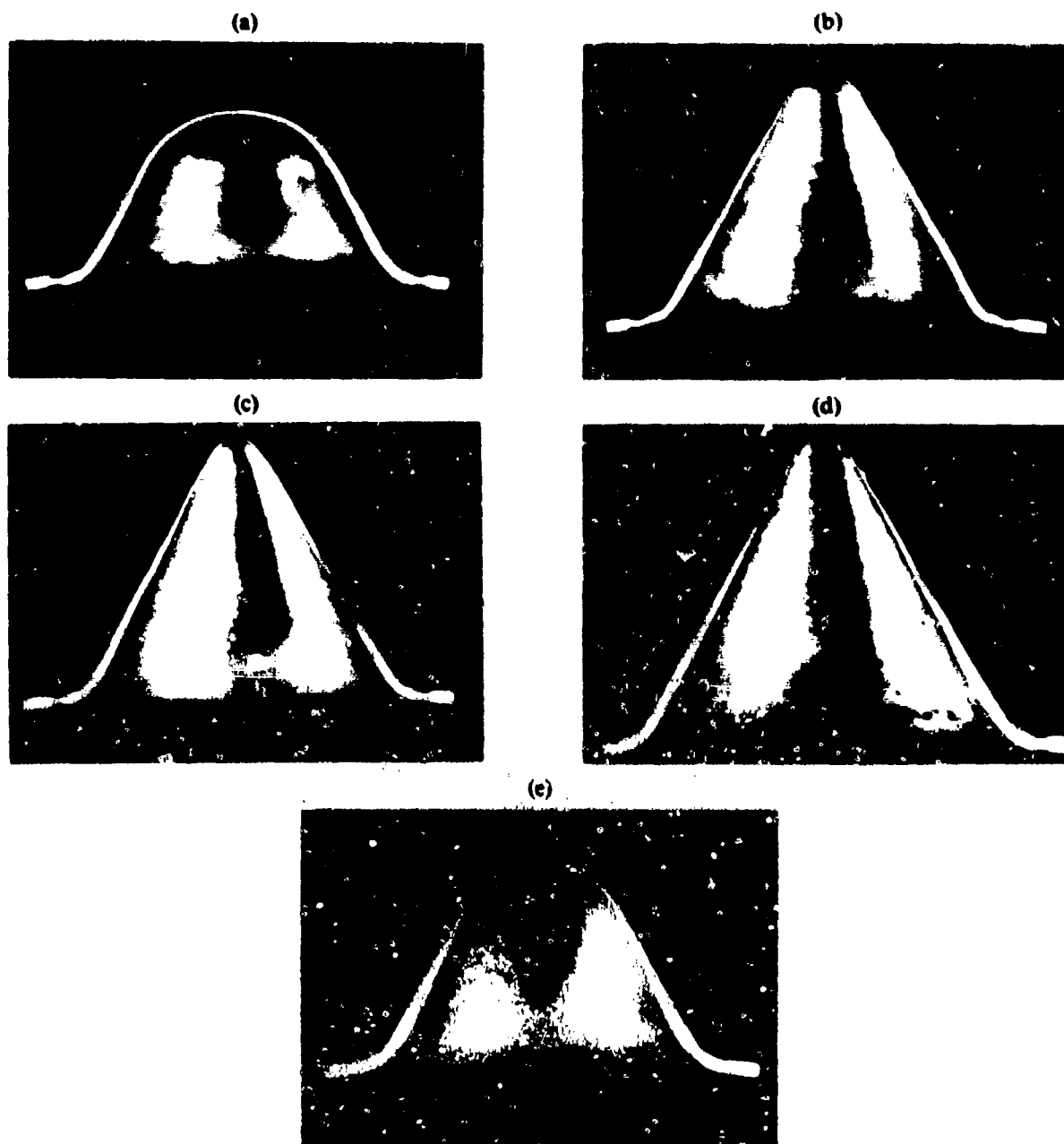


Figure 30. Photographs of cross sections of cones superplastically formed at 900°C; (a) Ti-6Al-4V at 3.2 MPa (0.47 ksi), (b) Ti-6Al-4V at 6.6 MPa (0.95 ksi), (c) Ti-6Al-4V at 9.7 MPa (1.40 ksi), (d) Ti-6Al-4V at 18.8 MPa (2.72 ksi), and (e) Widmanstätten Ti-6Al-4V at 18.8 MPa (2.72 ksi).

Figure 31 compares the superplastic forming strain rates of conventionally-processed and hydrovac-processed equiaxed- $\alpha$  Ti-6Al-4V. The hydrovac-processed Ti-6Al-4V has slightly superior superplastic formability properties above 800°C (1470°F). The microstructures of the formed cones shown in Figure 32 indicate that above 800°C (1470°F), grain growth in hydrovac-processed alloys is identical to that in the as-received alloys, and below 800°C (1470°F), the grain size is considerably smaller and grain growth is slower in hydrovac-processed alloys than in as-received Ti-6Al-4V. However, because grain-boundary sliding and diffusion processes conducive to SPF are less dominant below 800°C (1470°F), the fine-grain microstructure of hydrovac-processed Ti-6Al-4V does not improve the superplasticity below 800°C (1470°F). The slightly higher strain rate in hydrovac-processed Ti-6Al-4V above 800°C (1470°F) results from a higher amount of beta phase.

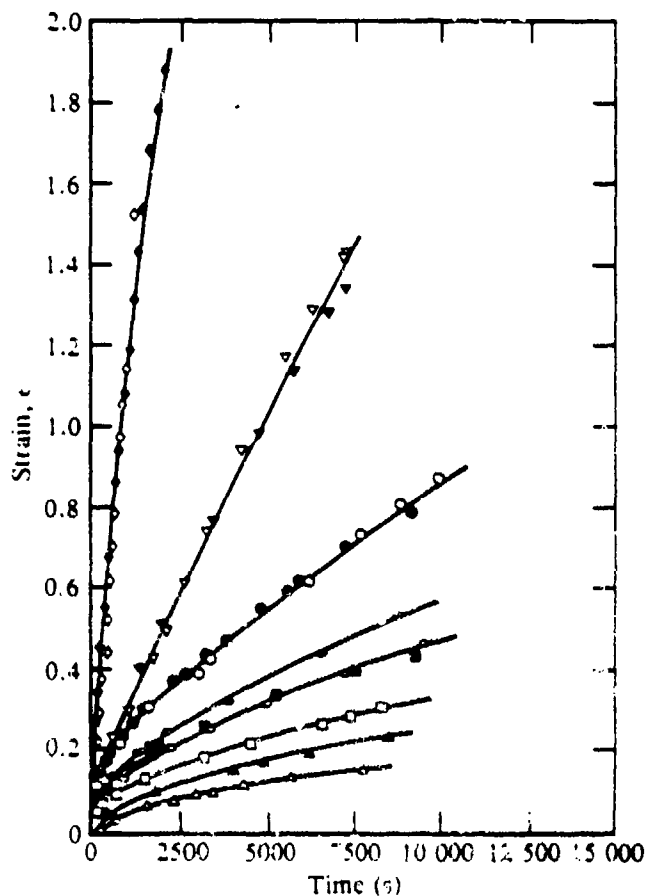
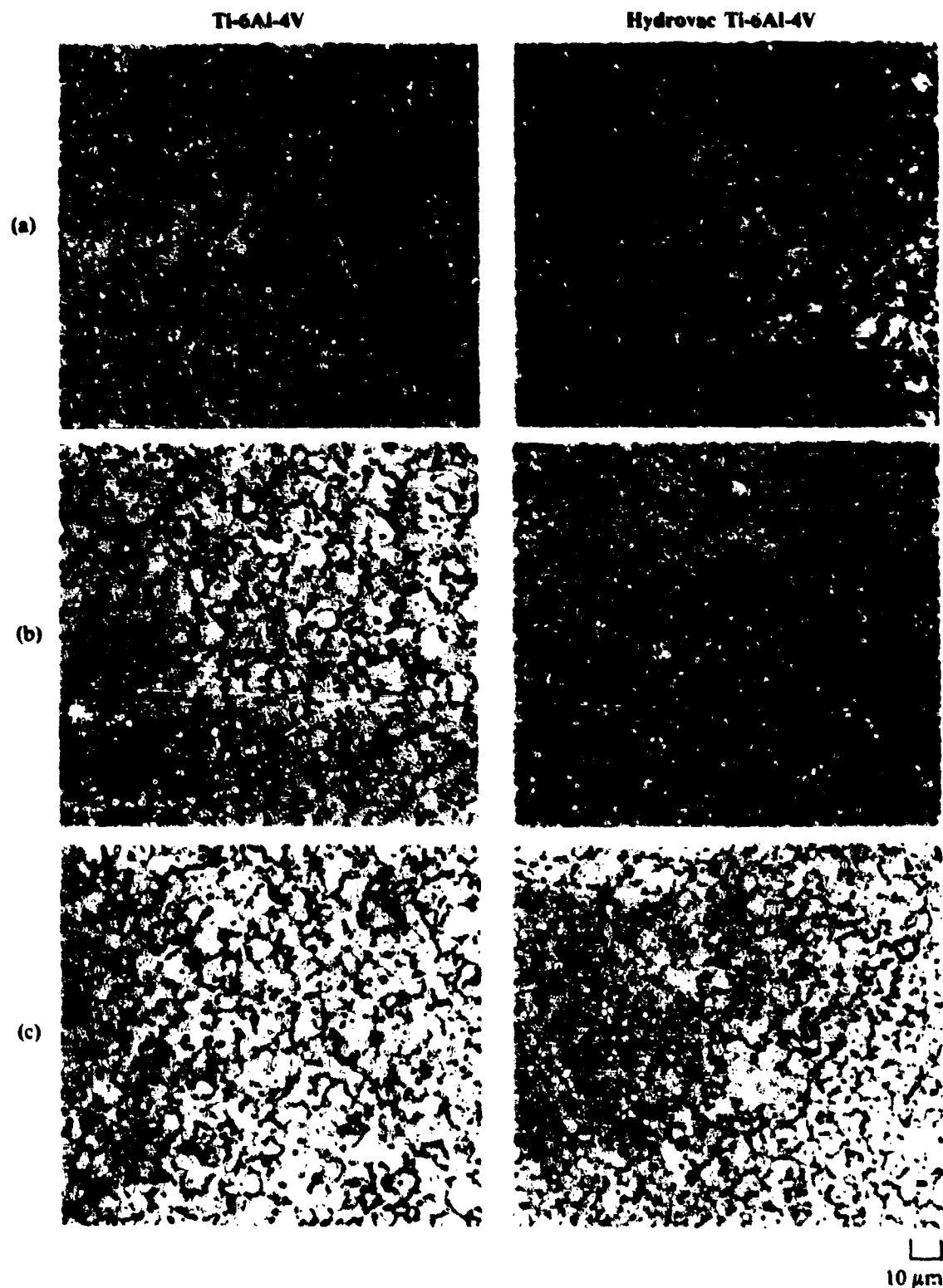


Figure 31. Time dependence of strain rate of equiaxed- $\alpha$  Ti-6Al-4V superplastically formed at 18.8 MPa (2.72 ksi) and (•, ○) 900°C, (▼, ▽) 830°C, (●, ○) 800°C, (◐, ◑) 780°C, (◒, ◓) 760°C, and (▲, △) 720°C. Closed symbols denote as-received condition while open symbols denote hydrovac processing.



**Figure 32.** Microstructures of equiaxed- $\alpha$  Ti-6Al-4V and hydrovac-processed equiaxed- $\alpha$  Ti-6Al-4V after cone forming at (a) 720°C, (b) 760°C, (c) 780°C, (d) 800°C, (e) 830°C, and (f) 900°C.

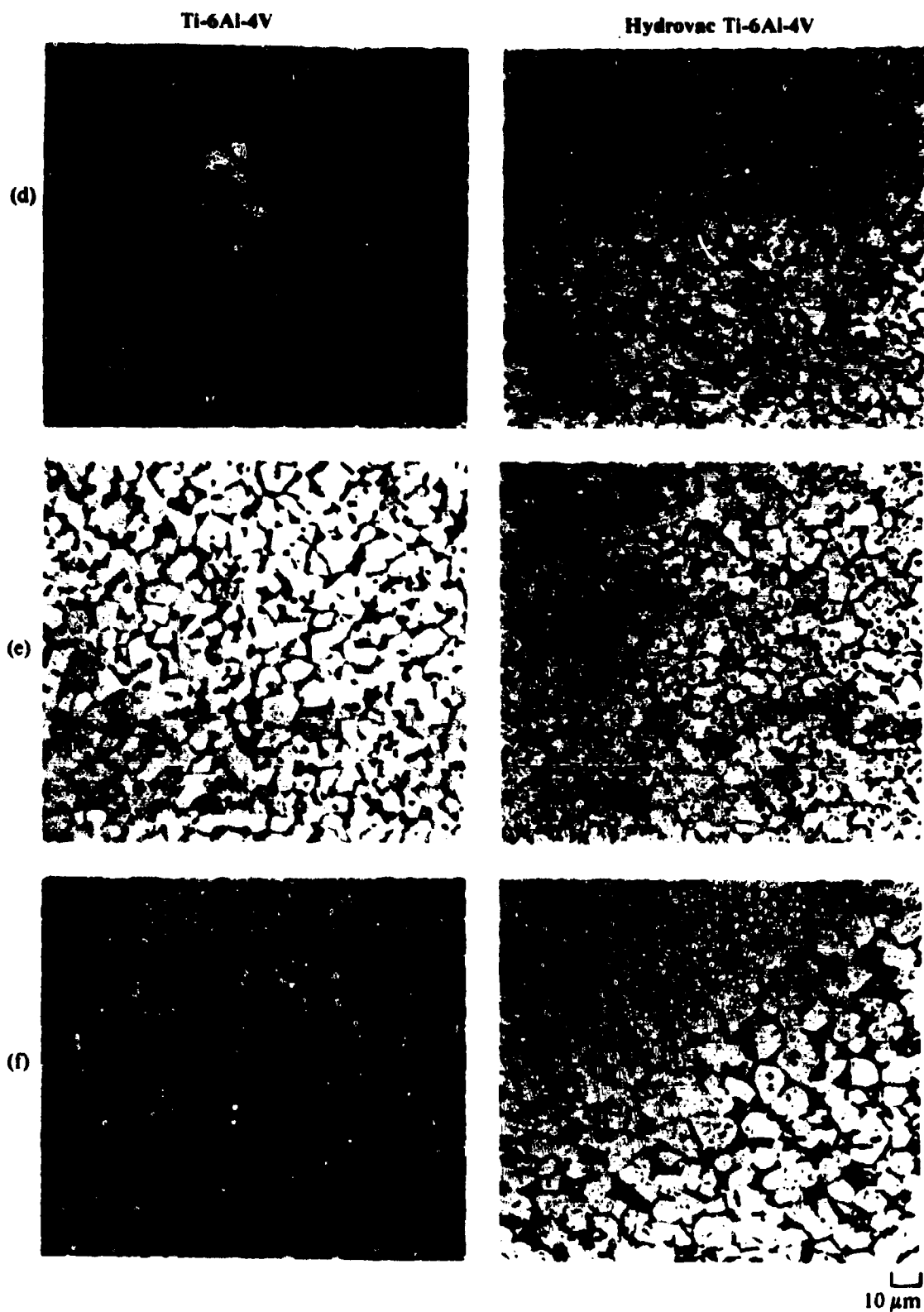


Figure 32. Concluded.

Hydrovac processing has no beneficial effect on the superplasticity at 830°C (1525°F) of Widmanstätten Ti-6Al-4V (Figure 33) and Ti-6Al-2Sn-4Zr-2Mo (Figure 34); the strain rates are too low for practical applications.

To simulate the effect of diffusion bonding preceding superplastic forming, equiaxed- $\alpha$  Ti-6Al-4V and hydrovac-processed Ti-6Al-4V were superplastically formed after exposure to 900°C (1650°F) for 4 h. The results, shown in Figure 35, indicate that the grain growth occurring during the soak time decreases the superplastic strain rates by the same amount for each alloy. The increase in strain rates for strains > 1 for the heat-treated alloys is attributed to thin-out, which does not occur in cones formed with no prior heat-treatment. The thin-out is caused by grain growth occurring during the 900°C (1650°F) anneal.

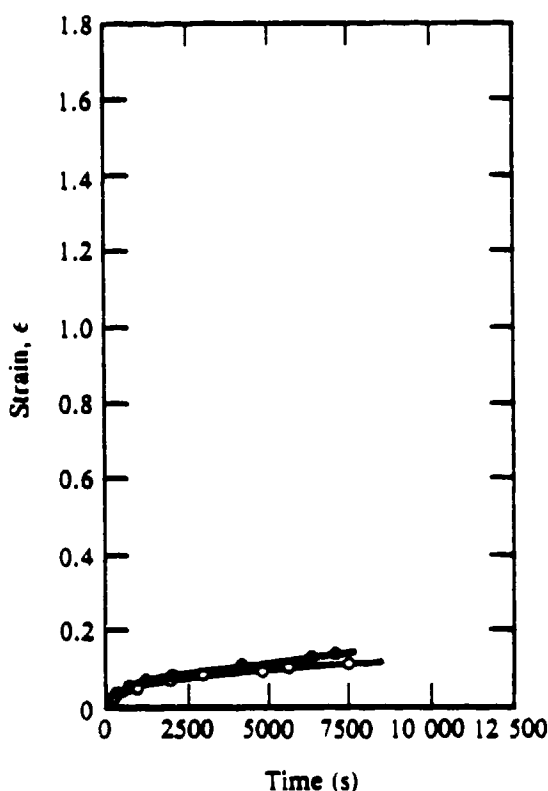


Figure 33. Time dependence of strain of (•) Widmanstätten and (○) hydrovac-processed Widmanstätten Ti-6Al-4V superplastically formed at 830°C and 18.8 MPa (2.72 ksi).

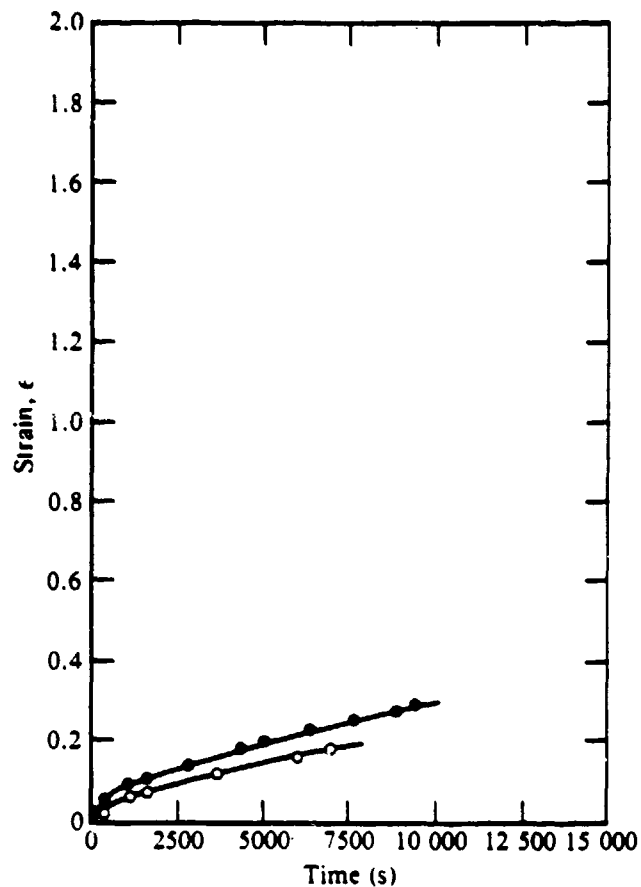


Figure 34. Time dependence of strain of (●) duplex-annealed and (○) hydrovac-processed Ti-6Al-2Sn-4Zr-2Mo superplastically formed at 830°C and 18.8 MPa (2.72 ksi).

Figures 36 and 37 are optical photomicrographs of interface regions of specimens diffusion-bonded at 1.0 MPa (150 psi) for 3 h at 850°C (1560°F) and at 1.3 MPa (200 psi) for 3 h at 900°C (1650°F). The as-received and hydrovac-processed equiaxed- $\alpha$  Ti-6Al-4V exhibit better bonding than the other alloys.

The effects on pore closure and grain growth of post-bonding heat treatments were determined by annealing at 900°C (1650°F) for 5 h the specimens that were diffusion-bonded at 850 and 900°C (1560 and 1650°F). The bonding of all alloys is improved by post-bonding heat treatment (Figures 38 and 39), although the post-bonding heat treatment does not result in closure of large pores formed due to high surface roughness of hydrovac-processed specimens.

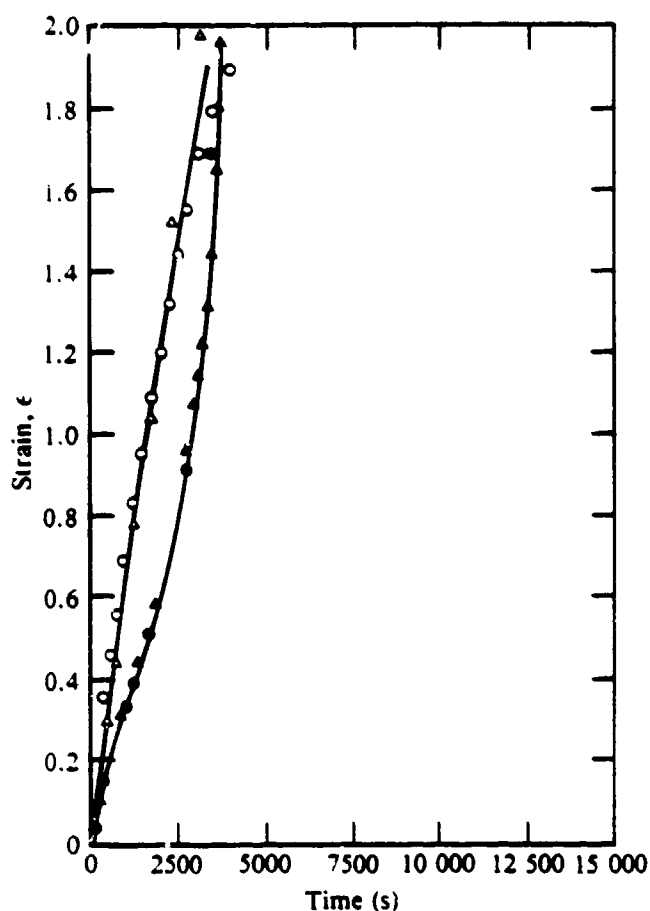
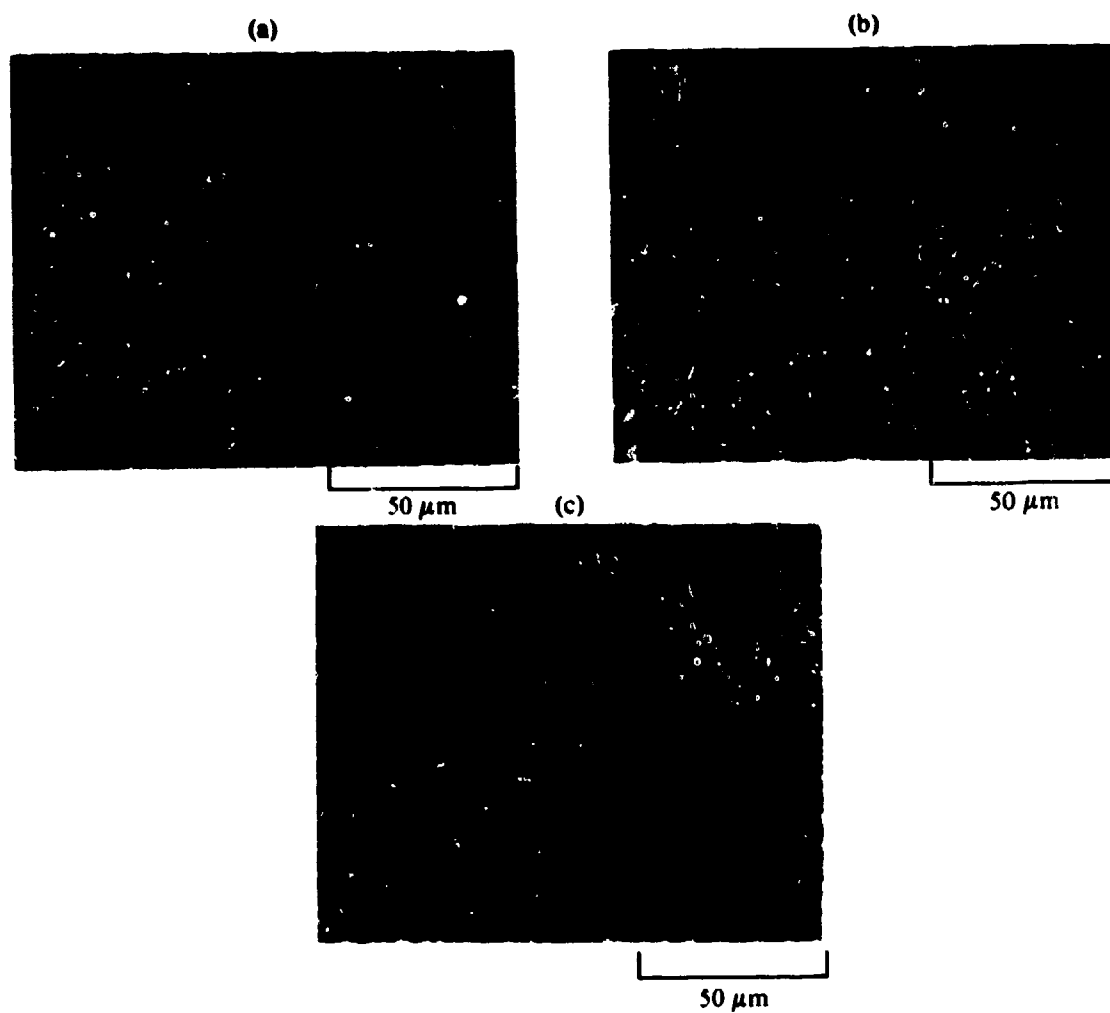
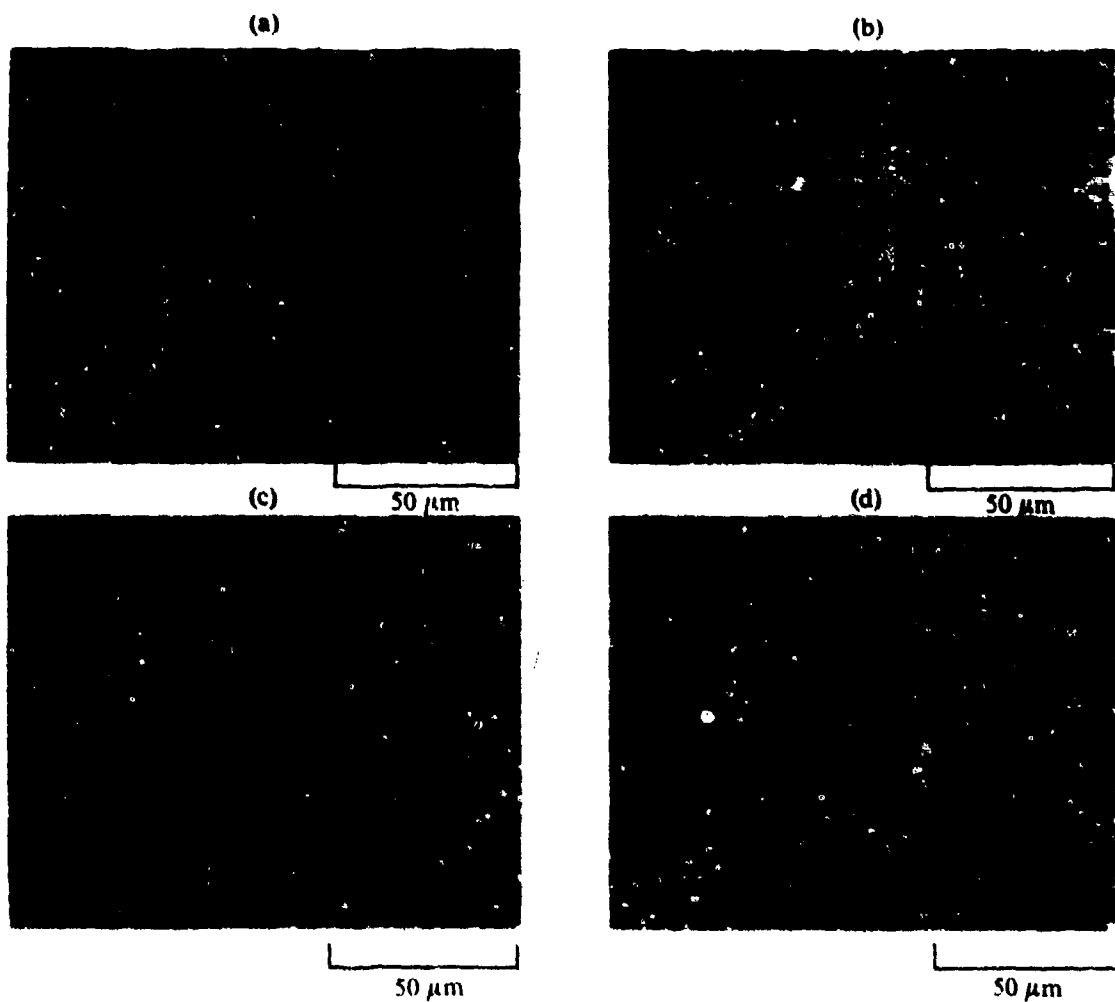


Figure 35. Time dependence of strain of (○, ●) equiaxed- $\alpha$  Ti-6Al-4V and (Δ, ▲) equiaxed- $\alpha$  hydrovac-processed Ti-6Al-4V superplastically formed at 900°C and 18.8 MPa (2.72 ksi) with no preheat-treatment (open symbols) and with a 900°C, 4 h, preheat-treatment (closed symbols).

The effect of surface roughness on bondability was also examined. Figures 40 and 41 are optical micrographs of the interface regions of specimens diffusion-bonded at 2.0 MPa (300 psi) for 3 h at 900°C (1650°F). The hydrovac-processed equiaxed- $\alpha$  Ti-6Al-4V had inferior bonding properties than the as-received alloy; this result is due entirely to surface roughness since the interface whose surface was polished (Figure 40c) bonded as well as the as-received alloy (Figure 40a). The Ti-6Al-2Sn-4Zr-2Mo alloy did not bond well. Hydrovac processing has no significant effect on the diffusion bondability of the alloys.



**Figure 36.** Photomicrographs of interface regions of specimens diffusion-bonded for 3 h at 850°C and 1.0 MPa (150 psi); (a) equiaxed- $\alpha$  Ti-6Al-4V, (b) hydrovac-processed Ti-6Al-4V, and (c) duplex-annealed Ti-6Al-2Sn-4Zr-2Mo.



**Figure 37. Photomicrographs of interface regions of specimens diffusion-bonded for 3 h at 900°C and 1.3 MPa (200 psi); (a) equiaxed- $\alpha$  Ti-6Al-4V, (b) hydrovac-processed Ti-6Al-4V, (c) duplex-annealed Ti-6Al-2Sn-4Zr-2Mo, and (d) hydrovac-processed Ti-6Al-2Sn-4Zr-2Mo.**

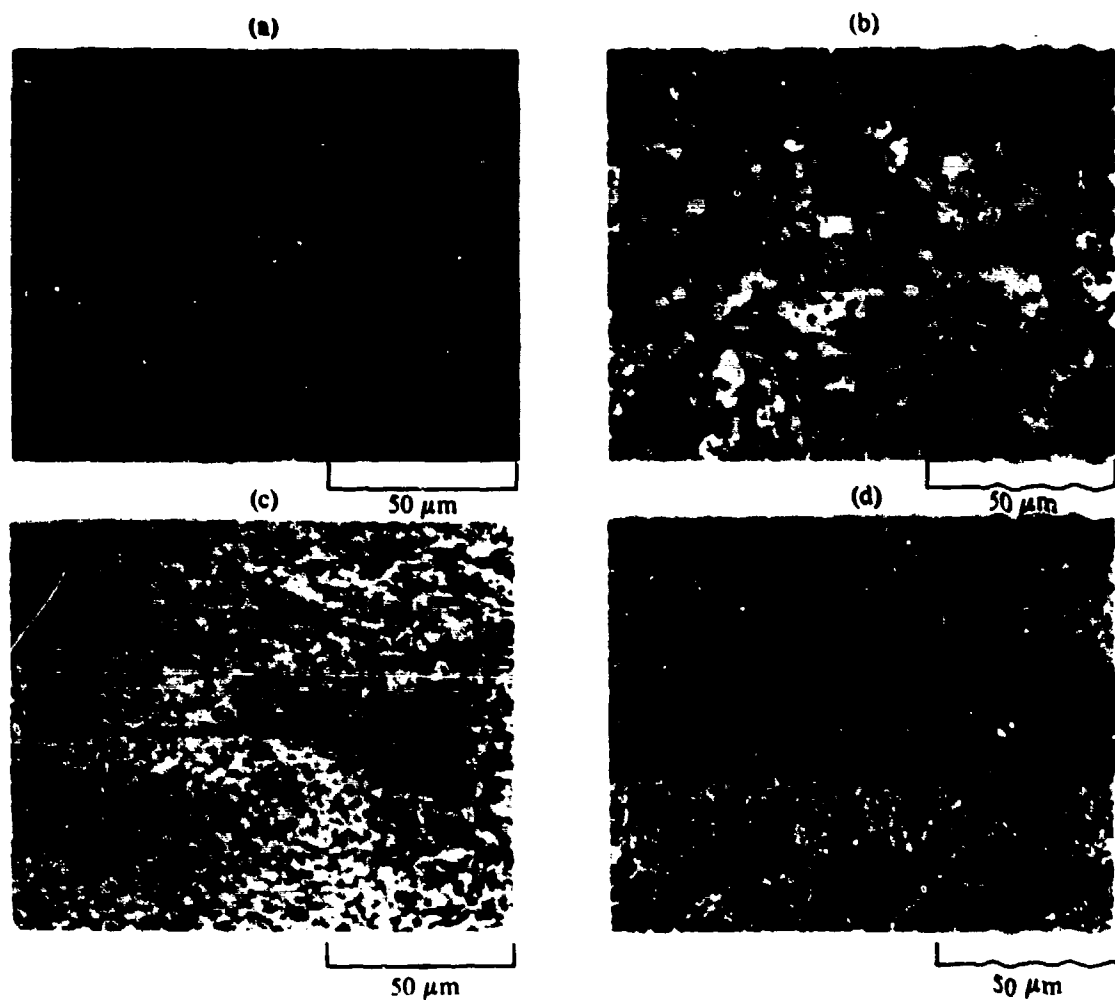


**Figure 38.** Photomicrographs of interface regions of specimens diffusion-bonded for 3 h at 850°C and 1.0 MPa (150 psi) and annealed at 900°C for 5 h; (a) equiaxed- $\alpha$  Ti-6Al-4V, (b) hydrovac-processed Ti-6Al-4V, (c) duplex-annealed Ti-6Al-2Sn-4Zr-2Mo, and (d) hydrovac-processed Ti-6Al-2Sn-4Zr-2Mo.

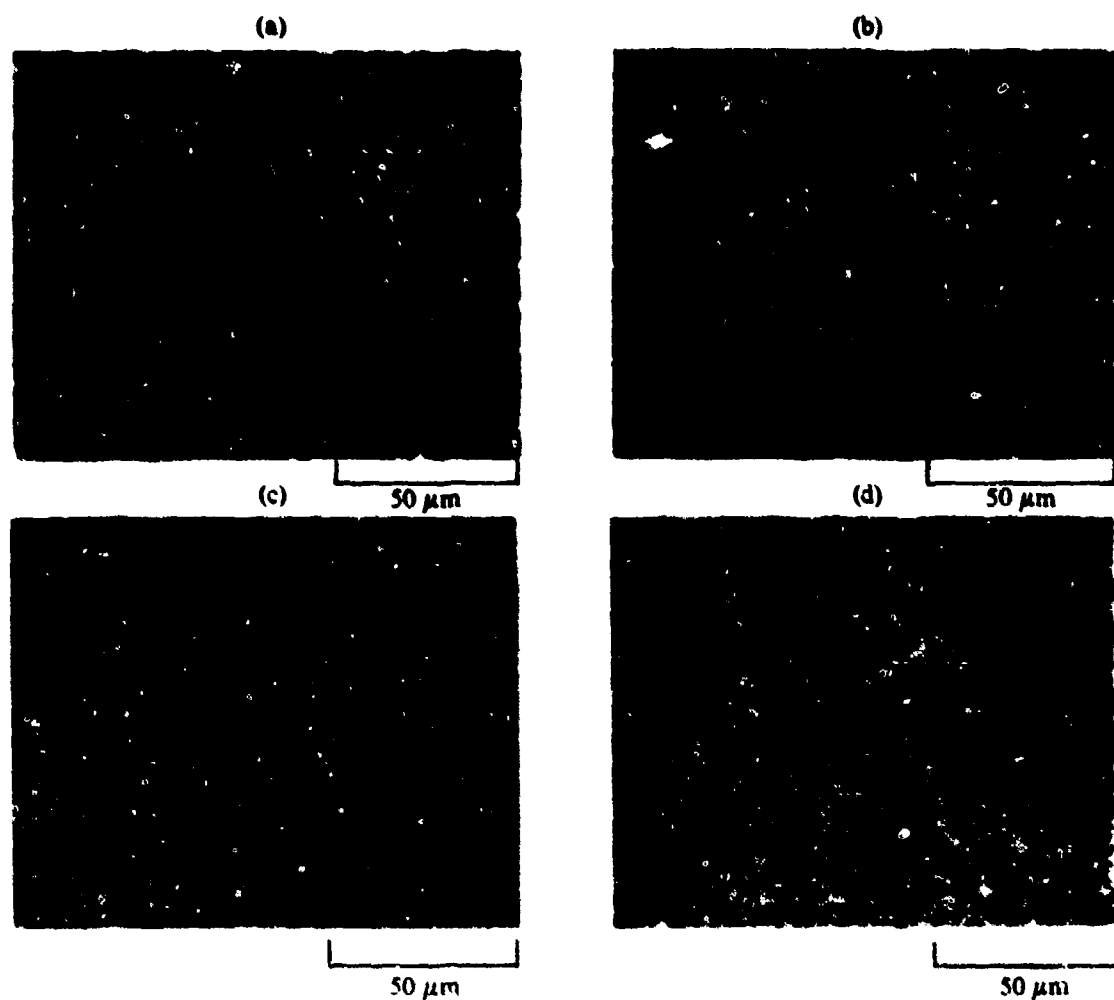


**Figure 39.** Photomicrographs of interface regions of specimens diffusion-bonded for 3 h at 900°C and 1.3 MPa (200 psi) and annealed at 900°C for 5 h; (a) equiaxed- $\alpha$  Ti-6Al-4V, (b) hydrovac-processed Ti-6Al-4V, (c) duplex-annealed Ti-6Al-2Sn-4Zr-2Mo, and (d) hydrovac-processed Ti-6Al-2Sn-4Zr-2Mo.

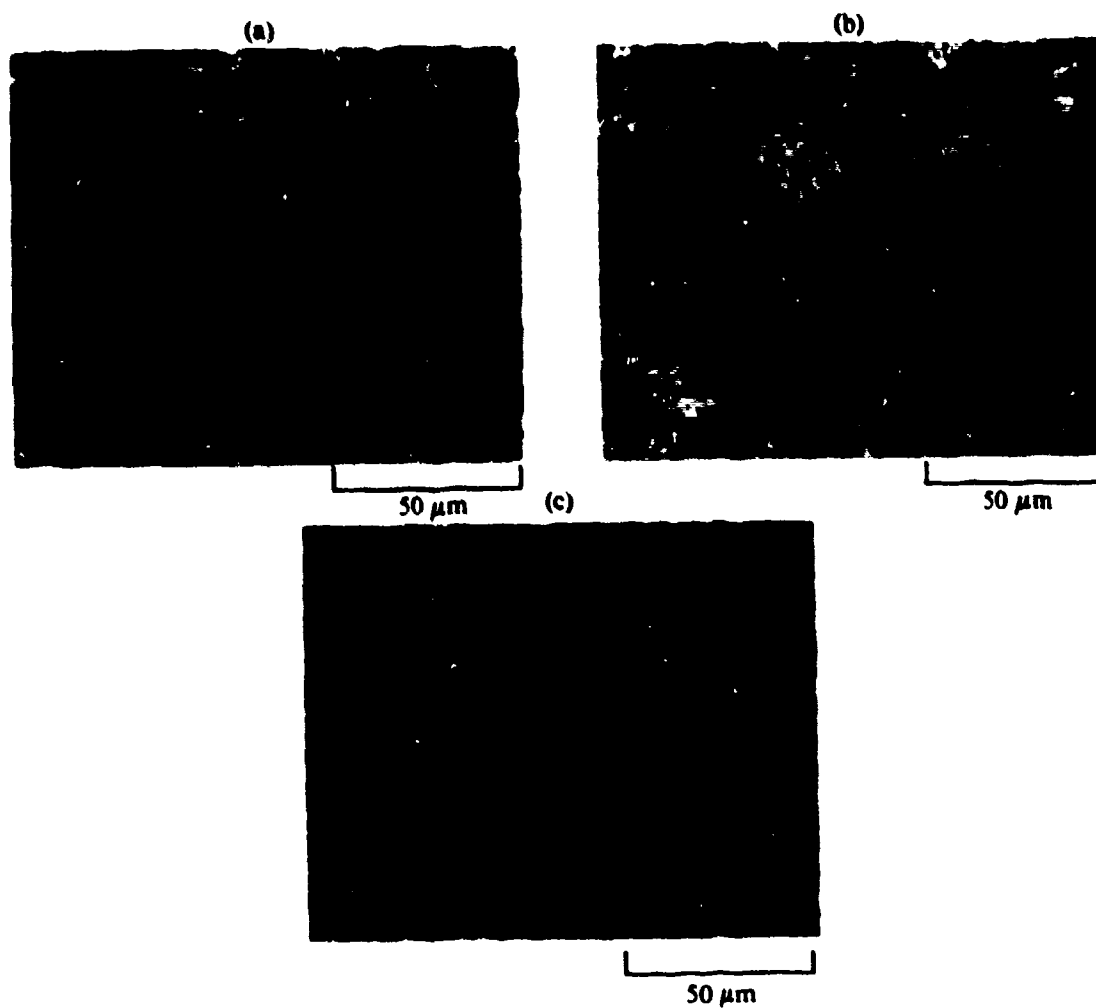


**Figure 40.** Photomicrographs of interface regions of specimens diffusion-bonded for 3 h at 900°C and 2.0 MPa (300 psi); (a) equiaxed- $\alpha$  Ti-6Al-4V, (b) hydrovac-processed Ti-6Al-4V, and (c) polished, hydrovac-processed Ti-6Al-4V.

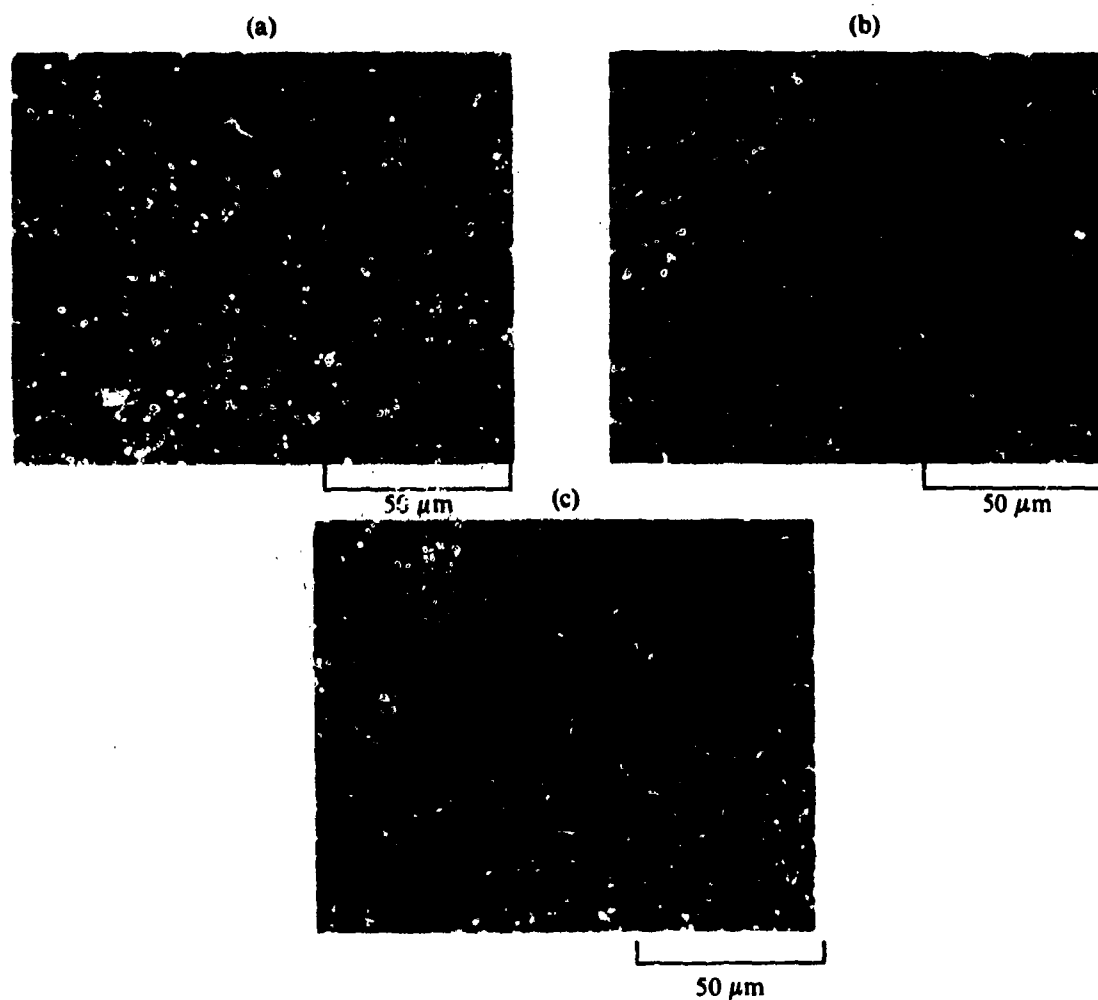


**Figure 41. Photomicrographs of interface regions of specimens diffusion-bonded for 3 h at 900°C and 2.0 MPa (300 psi); (a) duplex-annealed Ti-6Al-2Sn-4Zr-2Mo, (b) polished, duplex-annealed Ti-6Al-2Sn-4Zr-2Mo, and (c) polished, hydrovac-processed Ti-6Al-2Sn-4Zr-2Mo.**

SECTION V  
SUPERPLASTIC FORMING AND DIFFUSION BONDING OF Ti-ALLOYS  
CONTAINING INTERNAL HYDROGEN

1. EFFECTS OF INTERNAL HYDROGEN ON SPF/DB OF TITANIUM ALLOYS

The instrumented cone-forming test apparatus shown in Figure 12 was used to charge the specimens with hydrogen and determine the SPF properties of samples at different forming parameters.

In-situ hydrogen charging for cone-forming tests was accomplished by applying equal pressures of argon with 1-4 vol% hydrogen to both sides of the sample disk. The clamping force on the disk was monitored and adjusted to permit controlled amounts of gas to escape and thus ensure a fresh supply of hydrogen at each surface. Generally, the desired hydrogen concentration was obtained by heating at  $760^{\circ}\text{C}$  ( $1400^{\circ}\text{F}$ ) for 2.5 h at the appropriate hydrogen partial pressure [400-4000 Pa (3-30 Torr)]. For samples formed at temperatures less than  $760^{\circ}\text{C}$  ( $1400^{\circ}\text{F}$ ), charging was done at the test temperature, and the hydrogen partial pressure was changed accordingly. For tests where internal hydrogen was maintained, the pressure was released from one side of the sample, and the pressure on the other side was increased to the desired level for forming. The superplastic forming test then progressed as for uncharged specimens. Internal hydrogen concentrations were determined by measuring the change in weight of sections of formed samples upon vacuum annealing at  $950^{\circ}\text{C}$  ( $1740^{\circ}\text{F}$ ) for 4 h. Typical micrographs (Figure 42) of cross sections of water-quenched samples show the hydrides to be uniformly distributed throughout the bulk, thus indicating that the inner and outer surfaces of the cones have the same hydrogen concentrations.

Photographs of cross sections of cones formed for 2 h at  $760^{\circ}\text{C}$  ( $1400^{\circ}\text{F}$ ) shown in Figure 43 illustrate the dramatic improvement in forming caused by 0.11 wt% hydrogen. The time dependences of superplastic strain rates of equiaxed- $\alpha$  Ti-6Al-4V containing different amounts of hydrogen and tested at 860, 800, and  $760^{\circ}\text{C}$  (1580, 1470, and  $1400^{\circ}\text{F}$ ) are shown in Figures 44-46 respectively. At  $860^{\circ}\text{C}$  (1580 $^{\circ}\text{F}$ ), samples containing less than 0.38 wt% hydrogen formed at a faster rate than the as-received alloy. Similarly, at  $800^{\circ}\text{C}$  (1470 $^{\circ}\text{F}$ ), samples containing less

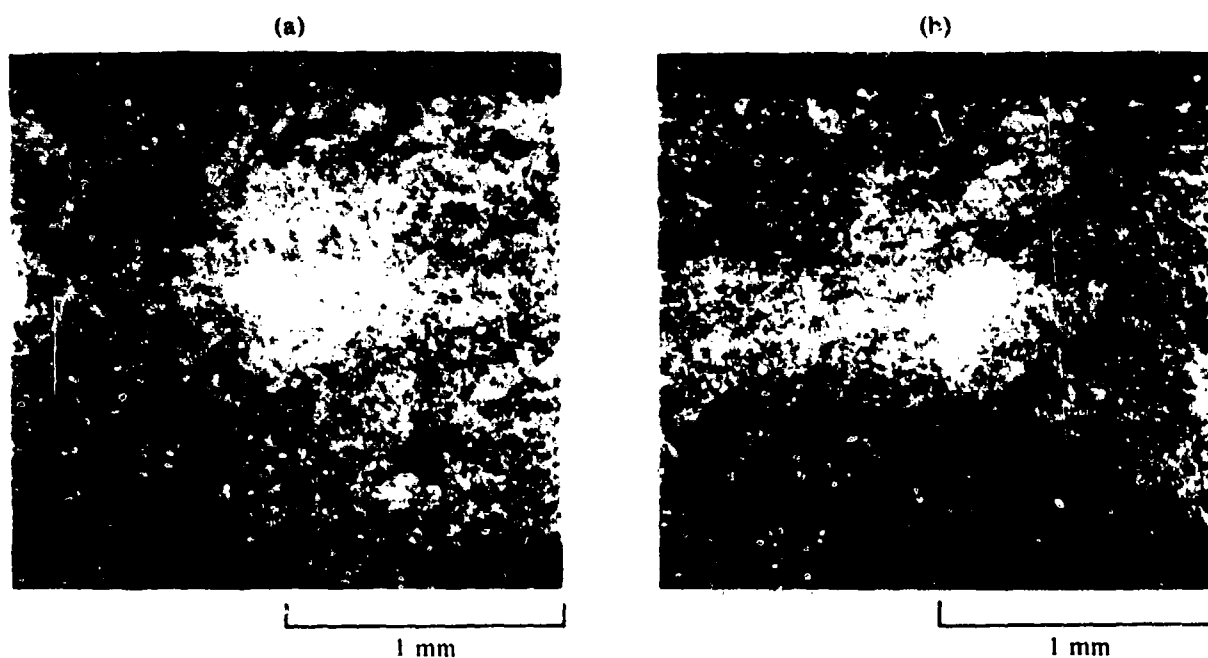


Figure 42. Cross sections of equiaxed- $\alpha$  Ti-6Al-4V cones containing (a) 0.34 and (b) 0.39 wt% hydrogen and superplastically formed at 800°C and 18.8 MPa (2.72 ksi).

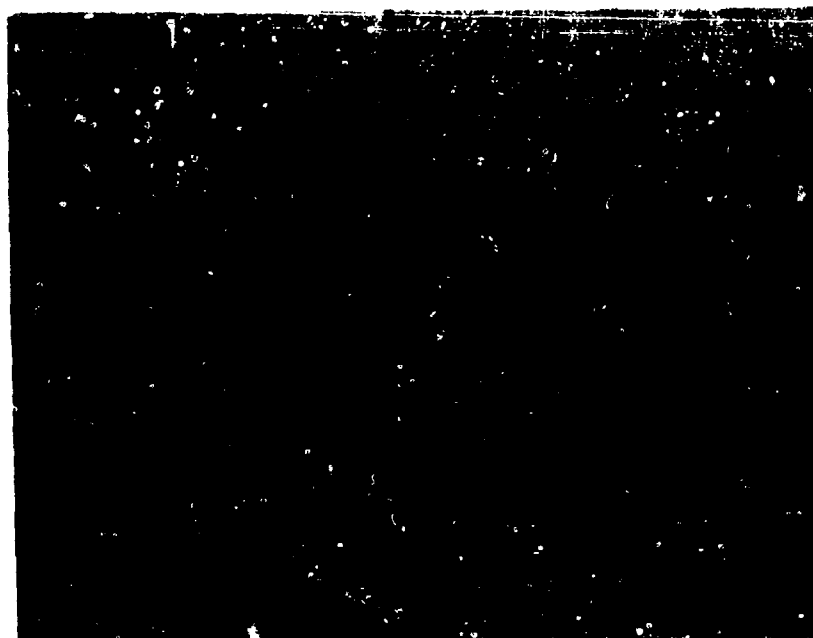


Figure 43. Cross sections of equiaxed- $\alpha$  Ti-6Al-4V cones superplastically formed at 760°C and 18.8 MPa (2.72 ksi) for 2 h (a) uncharged and (b) charged to 0.11 wt% hydrogen.

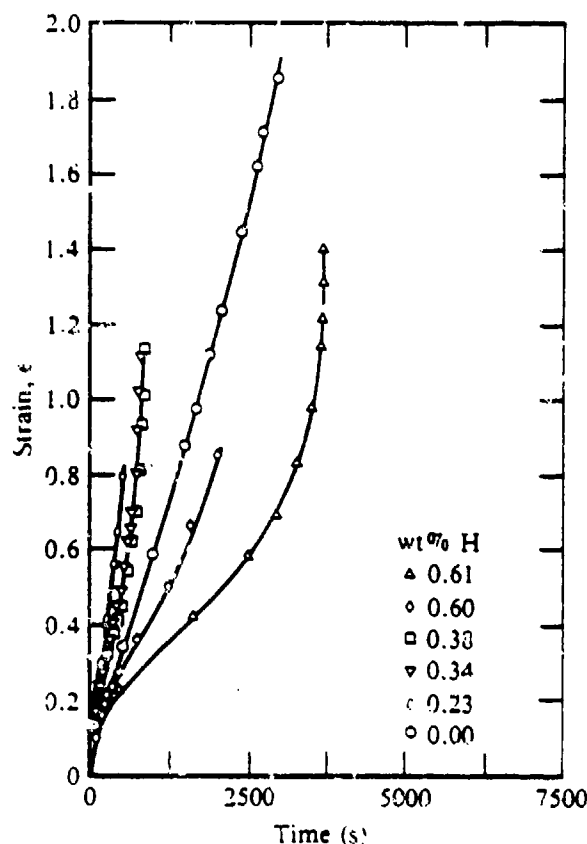


Figure 44. Effect of internal hydrogen of superplastic forming of equiaxed- $\alpha$  Ti-6Al-4V at 550°C and 13.8 MPa (2.72 ksi).

than 0.68 wt% hydrogen formed at faster rates than as-received materials. At 760°C (1400°F), samples containing hydrogen concentrations of 0.11 to 0.49 wt% formed faster than the as-received material. At the three temperatures, small amounts of hydrogen (usually < 0.15 wt%) result in the best forming properties.

Figure 47 shows the modification in microstructures and superplastic strain rates effected by hydrogen additions at 720-900°C (1330-1650°F). The number associated with each data point refers to the ratio of the strain rate at that concentration and temperature divided by the strain rate of an as-received sample at the same temperature. Strain rates were determined from the slope of the strain/time plots by neglecting the initial rapid strain-rate region (where stresses are higher because the sample has not yet made tangential contact with the die) and any

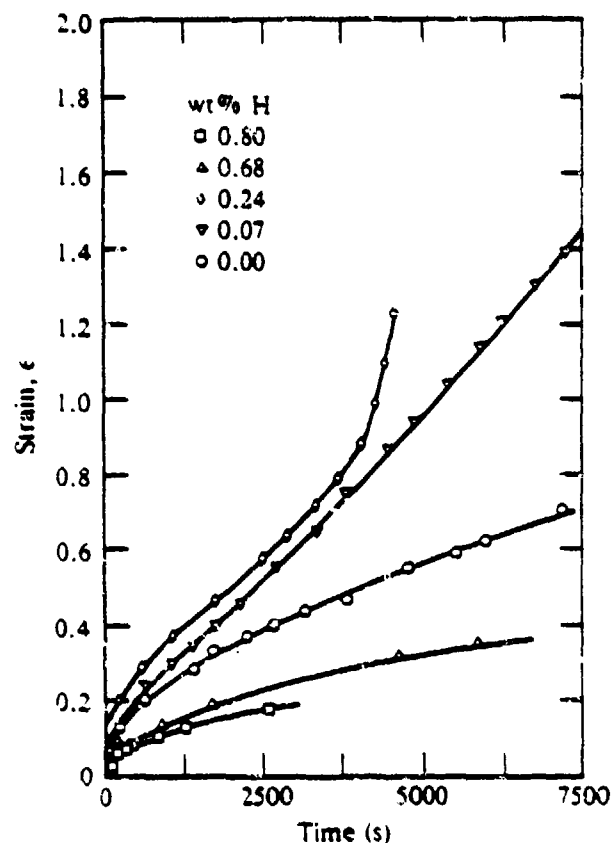
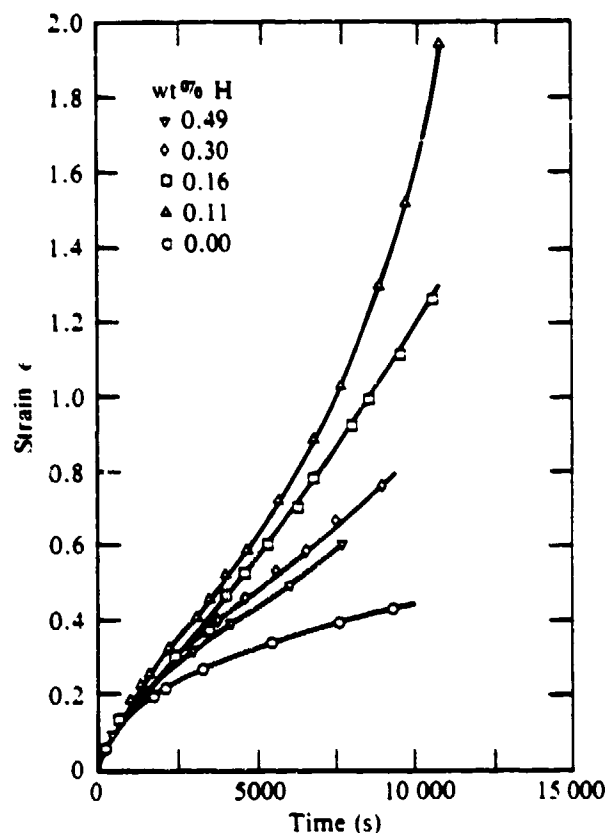


Figure 45. Effect of internal hydrogen on superplastic forming of equiaxed- $\alpha$  Ti-6Al-4V at 800°C and 18.8 MPa (2.72 ksi).

terminal increase in strain rate caused by thin-out of the sample. Samples in region A were formed in the  $\alpha$ - $\beta$  region, while region B is the  $\beta$  region. Microstructures of samples formed in region C are those of eutectoid decomposition products.

The results of Figures 44-46 can be explained using the diagram of Figure 47. All hydrogen-charged samples at 860°C (1580°F) (Figure 44) have a  $\beta$  microstructure during forming and failed at small strains ( $< 1.4$ ), whereas the uncharged  $\alpha$ - $\beta$  sample attained much larger strains. Samples barely in the  $\beta$  region (0.23 - 0.38 wt%  $H_2$ ) formed at a faster rate because of the lower flow stress of  $\beta$  phase and slower grain growth, but samples of higher hydrogen content formed slower because of excessive grain growth of the single phase relative to grain growth in  $\alpha + \beta$  phase field. Similarly at 800°C (1470°F) (Figure 45),



**Figure 46. Effect of internal hydrogen on superplastic forming of equiaxed- $\alpha$  Ti-6Al-4V at 760°C and 18.8 MPa (2.72 ksi).**

samples containing 0.07 and 0.24 wt% H formed faster with the latter sample failing at a lower strain because of its beta microstructure. Samples having greater amounts of hydrogen formed at slower rates because of the resistance to sliding of the larger grains. At 760°C (1400°F), hydrogen provides improvements, with the improvements being less when samples are out of the alpha-beta region.

The improvement in forming that can be obtained through hydrogen additions is depicted in Figure 48, which shows the forming time required to obtain a true strain of 1.25 for various temperature/hydrogen-concentration combinations. For example, an uncharged sample must be formed at 870°C (1600°F) to reach a strain of 1.25 in 30 min, while samples containing 0.2 wt% hydrogen will achieve the same strain in 30 min at 820°C (1510°F).

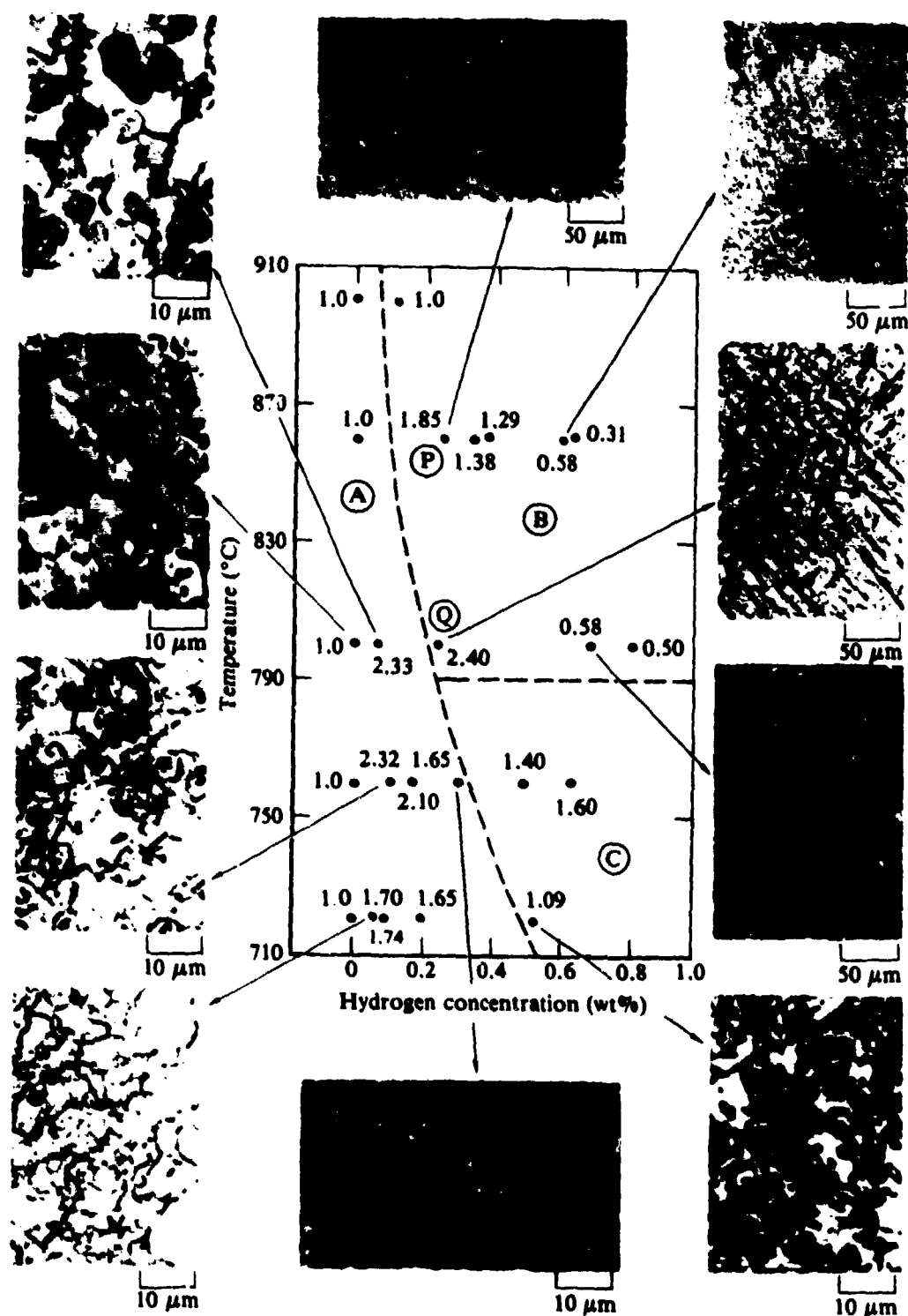
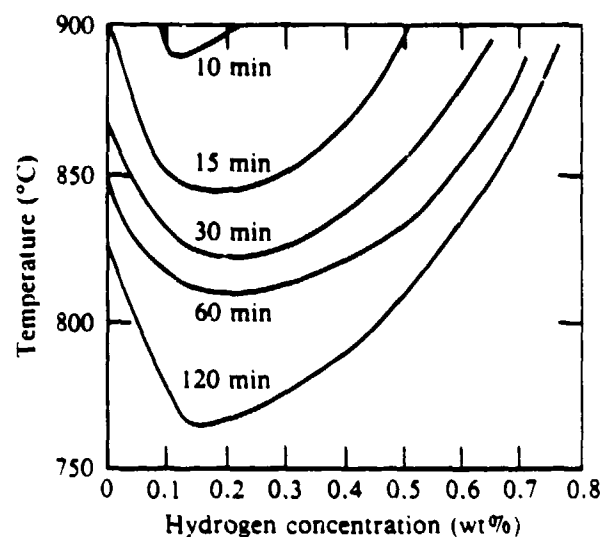


Figure 47. Effect of hydrogen concentration on the superplastic forming properties of Ti-6Al-4V at various temperatures. The number associated with each data point is the ratio of the strain rate at that hydrogen concentration divided by the strain rate of the uncharged sample at that temperature. Also shown are microstructures of selected formed parts.



**Figure 48.** Forming time required to achieve a true strain of 1.25 in equiaxed- $\alpha$  Ti-6Al-4V for temperature/hydrogen-concentration combinations.

The time dependence of superplastic strain rates of Ti-6Al-2Sn-4Zr-2Mo containing different amounts of hydrogen and tested at 900, 830, and 800°C (1650, 1525, and 1470°F) are shown in Figures 49-51, respectively. Improvements are more dramatic than for Ti-6Al-4V. For instance, at the lower temperature of 800°C (1470°F), strains that could not be approached for uncharged samples are easily achievable for low amounts of hydrogen. Figure 52 illustrates this improvement in formability. At 830°C (1525°F), the uncharged Ti-6Al-2Sn-4Zr-2Mo is not sufficiently formable for any practical applications, but the addition of 0.14 wt% hydrogen permits strains of 2 to be obtained in less than 2 h. Figure 53 summarizes the modifications in microstructures and SPF strain rates effected by hydrogen additions for Ti-6Al-2Sn-4Zr-2Mo. At 830°C (1525°F), for example, hydrogen concentrations of 0.06 and 0.14 wt% cause large increases in strain rate. The photomicrographs show the microstructure to be alpha-beta with little change in grain size but with a large increase in volume fraction of the beta phase, as expected from the decrease in the beta transus temperature. The sample containing 0.41 wt% hydrogen is all beta phase; however, the grain size is much larger, thus causing an overall decrease in strain rate. The dotted line in Figure 53 separates the alpha-beta (A) from the beta (B) regions.

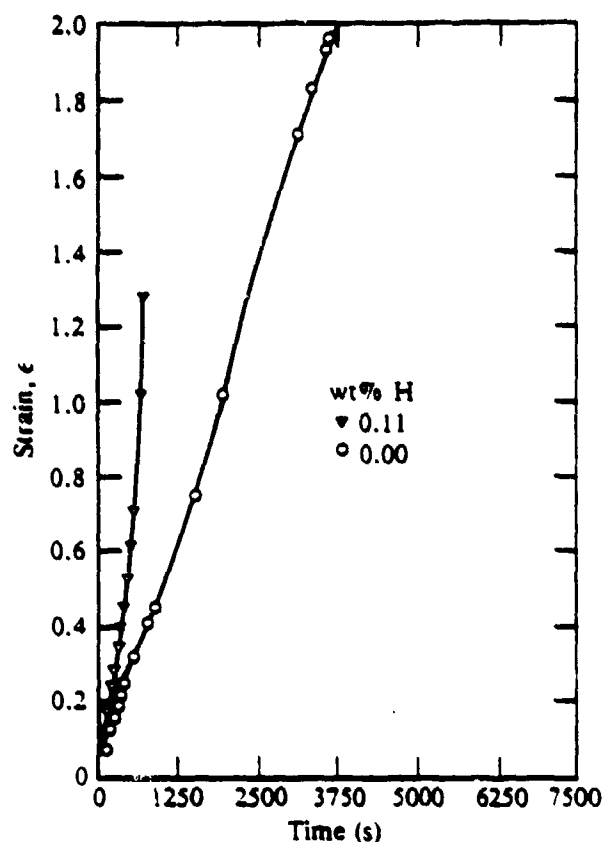


Figure 49. Effect of internal hydrogen on superplastic forming of duplex-annealed Ti-6Al-2Sn-4Zr-2Mo at 900°C and 18.8 MPa (2.72 ksi).

The beneficial effects of hydrogen additions on the superplastic deformation of titanium alloys arise from the production of superplastic-favorable alpha-beta proportions at lower temperatures by lowering the beta transus temperature. The beneficial effects on hot workability of lowering the beta transus temperature in hydrogen-modified titanium alloys were previously identified by Birla and DePeire (Reference 6), who demonstrated a 30-50% reduction in flow stress during isothermal forging at 730°C (1345°F) of Ti-6Al-2Sn-4Zr-2Mo-0.4H.

To model the high-temperature deformation of a two-phase alloy in terms of properties of the individual phases, the rule of mixtures given by the following equations is used (References 11 and 12):

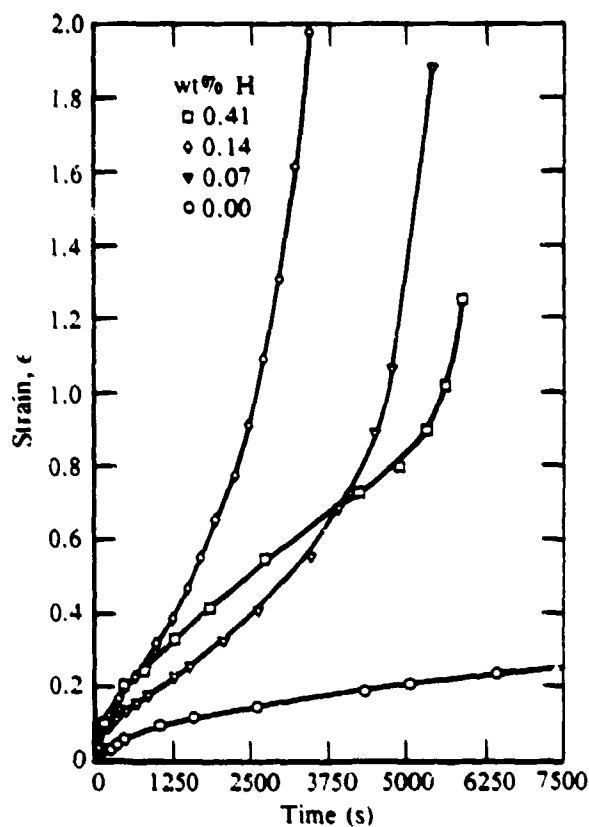


Figure 50. Effect of internal hydrogen on superplastic forming of duplex-annealed Ti-6Al-2Sn-4Zr-2Mo at 830°C and 18.8 MPa (2.72 ksi).

$$S = S_{\alpha} V_{\alpha} + S_{\beta} V_{\beta} \quad (3)$$

for isostress conditions, and

$$\epsilon = \epsilon_{\alpha} V_{\alpha} + \epsilon_{\beta} V_{\beta} \quad (4)$$

for isostrain conditions, where  $S$  and  $\epsilon$  are the overall flow stress and strain of the two phase alloys,  $V_{\alpha}$  and  $V_{\beta}$  are the volume fractions of alpha and beta phases,  $S_{\alpha}$  and  $S_{\beta}$  are the flow stresses of alpha and beta phases, and  $\epsilon_{\alpha}$  and  $\epsilon_{\beta}$  are the strains in alpha and beta phases. For a rigorous analysis of the superplastic behavior of two-phase Ti alloys in

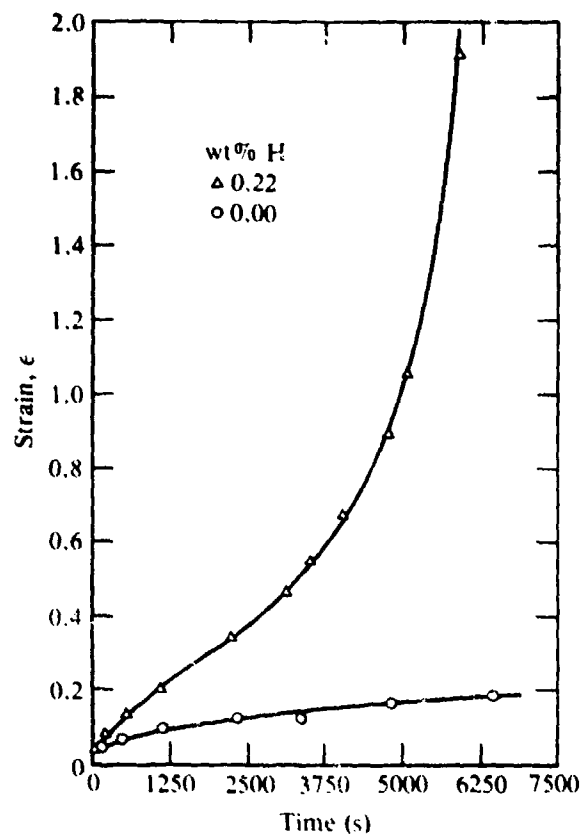


**Figure 51.** Effect of internal hydrogen on superplastic forming of duplex-annealed Ti-6Al-2Sn-4Zr-2Mo at 800°C and 18.8 MPa (2.72 ksi).

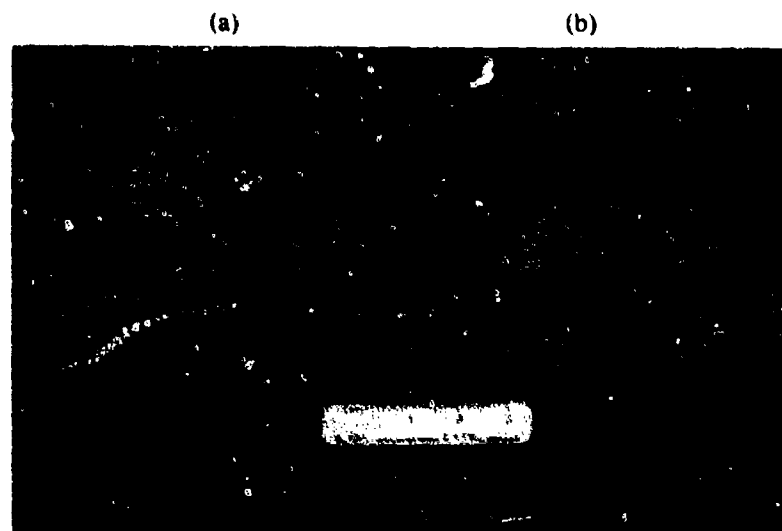


**Figure 52.** Cross sections of duplex-annealed Ti-6Al-2Sn-4Zr-2Mo cones superplastically formed at 830°C and 18.8 MPa (2.72 ksi) for 2 h (a) uncharged and (b) charged to 0.11 wt% hydrogen.

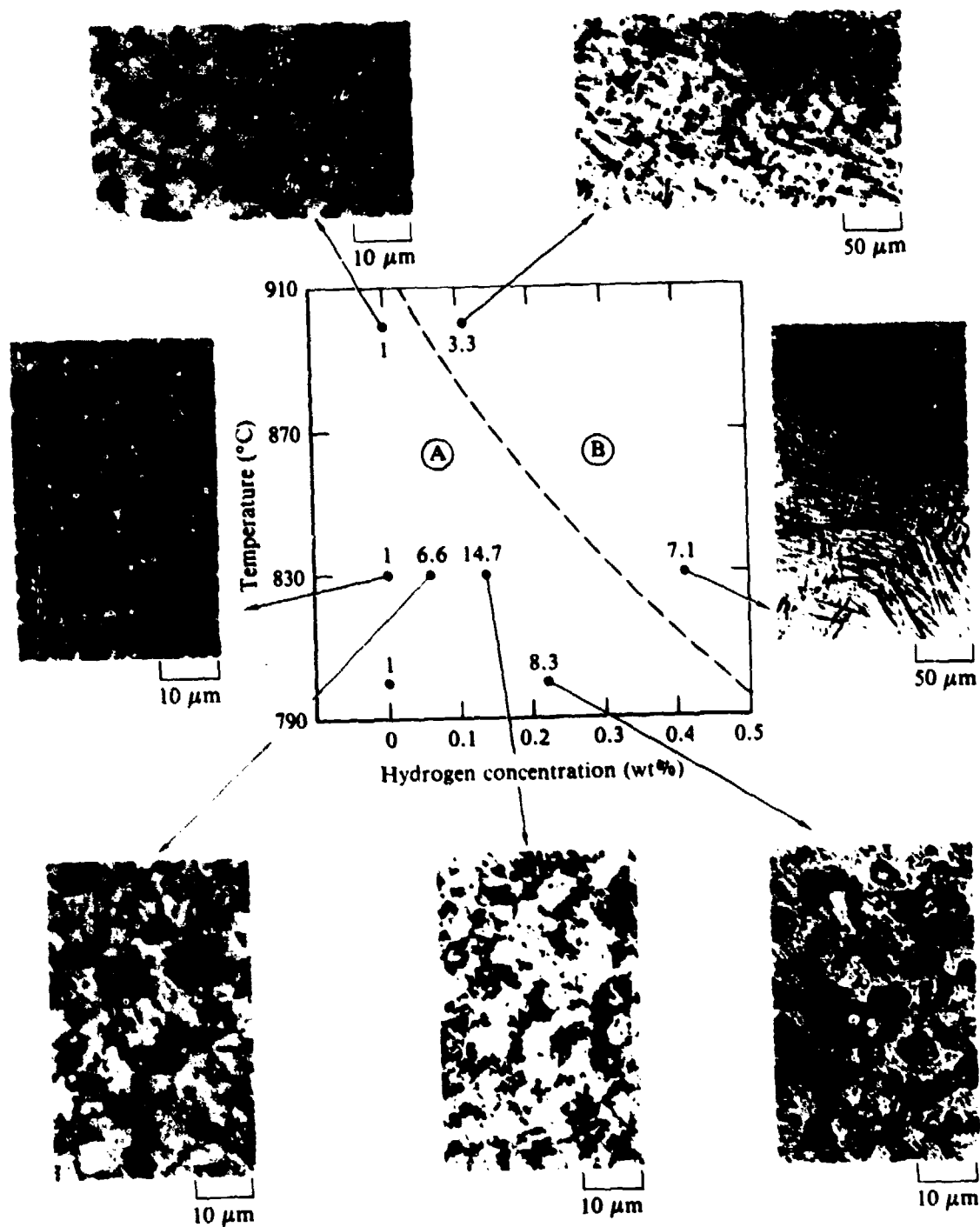


Figure 53. Effect of hydrogen concentration on the superplastic forming properties of duplex-annealed Ti-6Al-2Sn-4Zr-2Mo at various temperatures. The number associated with each data point is the ratio of the strain rate at that hydrogen concentration divided by the strain rate of the uncharged sample at that temperature. Also shown are microstructures of selected formed parts.

terms of Equations (3) and (4), the constitutive equations relating the alloys composition, grain size, and texture to the temperature, strain, and strain-rate dependence of flow stress must be known. The continuous changes in the alloy microstructure and phase composition with temperature and time should be given proper consideration in obtaining the constitutive equations. Because such detailed constitutive equations are not available, the observed effects of hydrogen additions will be qualitatively rationalized on the basis of the experimentally determined relation between metallurgical and process parameters for two-phase titanium alloys (References 1 and 13).

The increase in superplastic strain rate with increasing volume fraction of beta phase observed in the present investigation agrees with that predicted from Figure 8 when necessary corrections are made for the temperature effects on superplastic strain rates. At constant grain size and applied stress, the strain rate increases with increasing amounts of beta phase. Because diffusion processes are dominant in superplastic deformation, increasing amounts of beta phase result in an increased superplastic strain rate because of higher diffusivities in the beta phase (References 14 and 15). At high hydrogen concentrations where the alloy is single-phase beta, although diffusivities are considerably higher, the strain rates are not correspondingly higher because of extensive grain growth. Thus, a large amount of beta phase is required for higher strains, and a two-phase microstructure is required for obtaining stable, fine-grain microstructures. Thus, although the alloys P and Q in Figure 47 have higher initial strain rates, grain growth is rapid and failure occurs at small strains because these alloys are single phase (Figures 43 and 44).

The effect of hydrogen charging on the superplasticity of hydrovac-processed equiaxed- $\alpha$  Ti-6Al-4V was investigated. Figure 54 compares the forming rates of uncharged Ti-6Al-4V with hydrovac-processed Ti-6Al-4V and as-received Ti-6Al-4V specimens exposed to the same temperatures and times used in hydrogen charging. The properties of the hydrovac-processed Ti-6Al-4V are improved upon hydrogen additions, although to a lesser extent than in the hydrogen-charged, equiaxed- $\alpha$  Ti-6Al-4V.

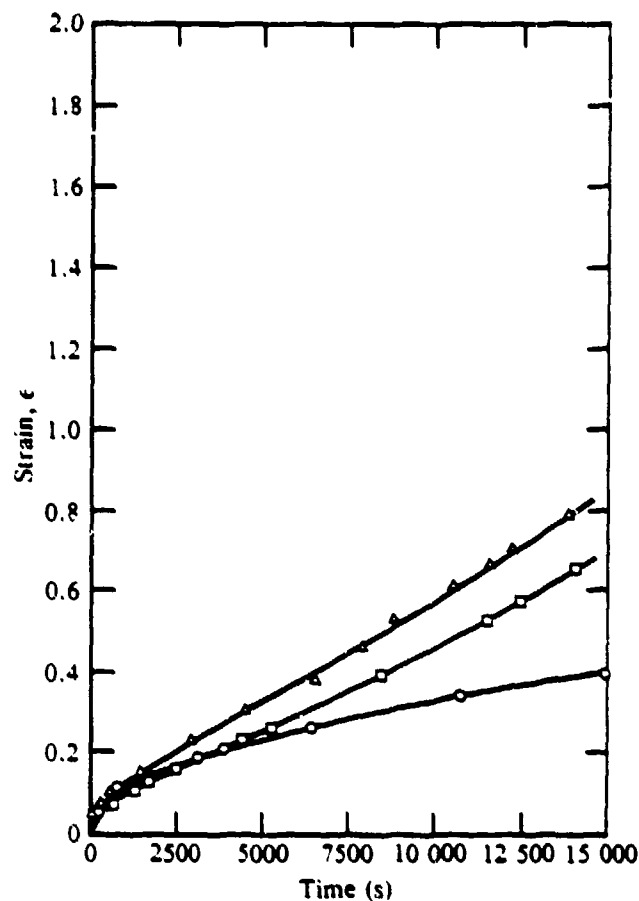


Figure 54. Time dependence of strain of (o) equiaxed- $\alpha$  Ti-6Al-4V, ( $\Delta$ ) hydrogen-charged Ti-6Al-4V, and ( $\square$ ) hydrogen-charged, hydrovac-processed Ti-6Al-4V superplastically formed at 760°C and 18.8 MPa (2.72 ksi).

The feasibility of improving diffusion bonding of Ti-alloys by hydrogen additions was investigated. 16 mm x 16 mm (0.6 x 0.6 in.) specimens charged with 0.06-0.9 wt% hydrogen were used. The diffusion-bonding procedure consisted of flushing the bonding chamber twice with the Ar + 4 wt% H<sub>2</sub> gas mixture, evacuating the chamber with no applied load on the samples to avoid entrapped gas, applying a load of 1.9 MPa (275 psi), heating to 450°C (840°F) in vacuum to degas the system while keeping the hydrogen in solution, bleeding in the Ar + 4 wt% H<sub>2</sub> gas mixture to atmospheric pressure, and heating to the bonding temperature which was maintained for 3.5 h.

The samples to be bonded were placed on top of each other, with each pair separated by a sheet of Mo to prevent diffusion from sample to

sample.  $10^5$  Pa (760 Torr) of Ar + 4 wt%  $H_2$  is in equilibrium with 0.29 wt%  $H_2$  in the sample. Hence it is expected that samples initially containing less than 0.29%  $H_2$  will pick-up hydrogen during the bonding, while samples initially containing > 0.29%  $H_2$  will lose some hydrogen. Table 9 shows that the changes in hydrogen concentration occurring during bonding for two typical bonding tests are negligible, and that the desired hydrogen levels are maintained during bonding.

**TABLE 9**  
**CHANGES IN INTERNAL HYDROGEN CONCENTRATIONS**  
**RESULTING FROM DIFFUSION BONDING TESTS**

Alloy-bonding temperature (°C)	Initial $H_2$ level (wt%)	Post-bonding $H_2$ level (wt%)
Equiaxed- $\alpha$	0	0.04
Ti-6Al-4V	0.17	0.13
800°C	0.31	0.31
	0.90	0.77
Duplex-annealed	0	0.03
Ti-6Al-2Sn-4Zr-2Mo	0.06	0.07
860°C	0.15	0.24
	0.25	0.23

Figure 55 indicates the effect of internal hydrogen on bondability of Ti-6Al-2Sn-4Zr-2Mo and equiaxed- $\alpha$  Ti-6Al-4V at various temperatures when a load of 1.9 MPa (275 psi) is applied for 3.5 h and hydrogen is maintained in solution. No noticeable improvement was observed.

## 2. EFFECTS OF HYDROGEN EVOLUTION ON SPF/DB OF TITANIUM ALLOYS

To investigate the possibility of utilizing the high density of lattice defects generated during hydrogen evolution for increasing superplastic forming rates, samples were charged with hydrogen and then superplastically formed as hydrogen evolved.

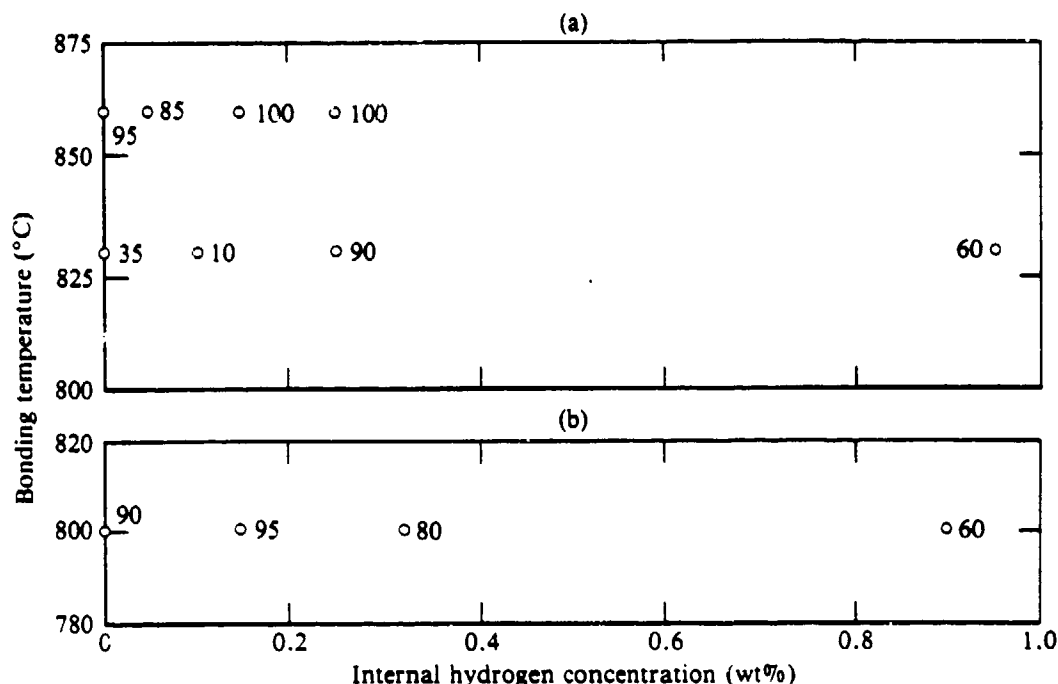
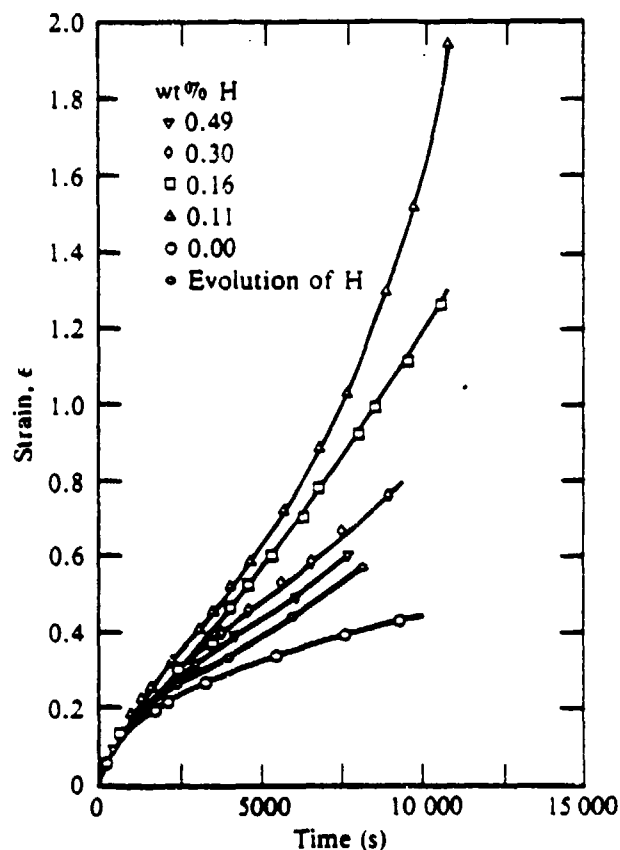


Figure 55. Percentage of bonded interface when (a) duplex-annealed Ti-6Al-2Sn-4Zr-2Mo and (b) equiaxed- $\alpha$  Ti-6Al-4V are exposed to a pressure of 1.9 MPa (275 psi) for 3.5 h and hydrogen is maintained in solution.

Samples of Ti-6Al-4V and Ti-6Al-2Sn-4Zr-2Mo were charged to 0.45 wt% hydrogen and then heated in a mechanically pumped chamber at 800°C (1470°F) for 2 h. The final hydrogen level was determined to be < 0.05 wt% H<sub>2</sub>, indicating that essentially all hydrogen evolved during the anneal. For cone-forming tests, samples were charged as described earlier and formed using a pure argon supply rather than the hydrogen-argon charging mixture to pressurize one side of the sample while evacuating the die side of the sample with a mechanical pump.

An equiaxed- $\alpha$  Ti-6Al-4V sample was charged to 0.15 wt% H<sub>2</sub> and then formed as internal hydrogen was allowed to evolve. The formed part had a hydrogen concentration of 0.05 wt%, which indicates that 0.10 wt% hydrogen evolved during forming. The forming rates of this sample are compared with those of other samples charged to various amounts of hydrogen in Figure 56. The formability of the sample evolving hydrogen is better than that of the uncharged specimen; however, the samples containing hydrogen have higher superplastic strain rates than the sample evolving hydrogen.



**Figure 56.** Effect of internal-hydrogen evolution on superplastic forming of equiaxed- $\alpha$  Ti-6Al-4V at 760°C and 18.8 MPa (2.72 ksi)

The effect of hydrogen evolution on bondability was investigated for two different situations: 1) hydrogen allowed to evolve while the samples are heated to the bonding temperature, and 2) hydrogen maintained in the sample until the bonding temperature is reached and then allowed to evolve. In both conditions, the sample preparation and initial bonding procedures were the same as those used in tests in which hydrogen was maintained in the sample during bonding. Hydrogen analysis of the bonded specimens revealed that complete hydrogen evolution occurred during the bonding operations.

Figures 57 and 58 indicate the effects of hydrogen evolution prior to bonding and during bonding, respectively. Neither procedure improves the bondability of the alloy.

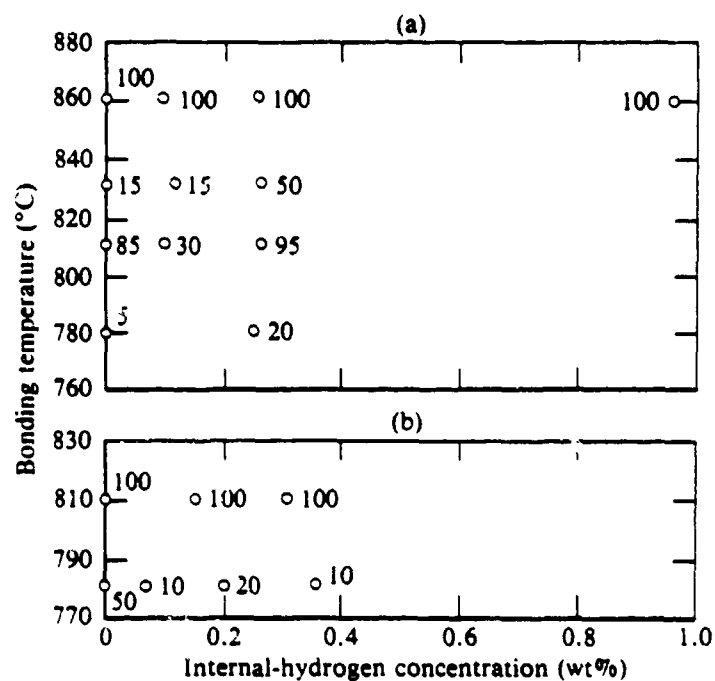


Figure 57. Percentage of bonded interface when (a) duplex-annealed Ti-6Al-2Sn-4Zr-2Mo and (b) equiaxed- $\alpha$  Ti-6Al-4V are exposed to a pressure of 1.9 MPa (275 psi) for 3.5 h and hydrogen is allowed to evolve as samples are heated to bonding temperatures.

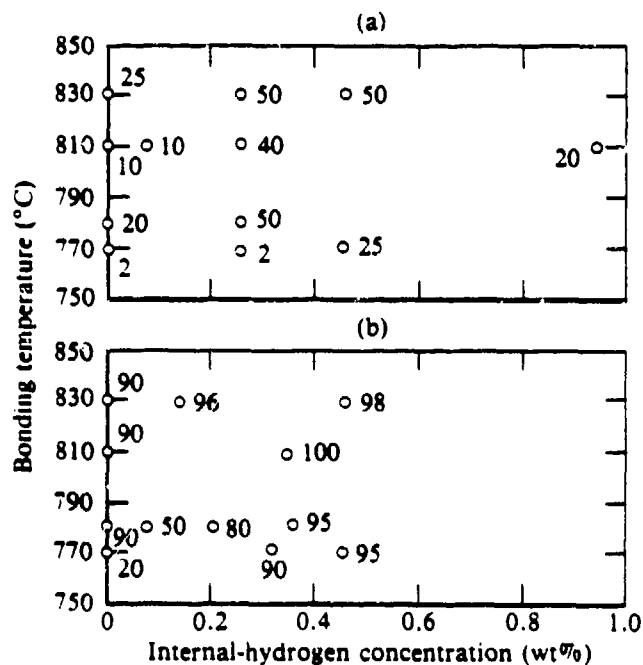


Figure 58. Percentage of bonded interface when (a) duplex-annealed Ti-6Al-2Sn-4Zr-2Mo and (b) equiaxed- $\alpha$  Ti-6Al-4V are exposed to a pressure of 1.9 MPa (275 psi) for 3.5 h and hydrogen is maintained in solution until the bonding temperature is reached and then allowed to evolve.

SECTION VI  
PROPERTIES OF SUPERPLASTICALLY FORMED Ti-ALLOY TROUGHS

Panels of Ti-6Al-4V and Ti-6Al-2Sn-4Zr-2Mo [400 x 400 mm (16 x 16 in.)) were hydrogen charged in-situ and superplastically formed into trough-shaped dies. Initially, equiaxed- $\alpha$  Ti-6Al-4V samples were charged with hydrogen using the conditions determined from the cone-forming tests. The samples were formed under constant pressure, and the preliminary tests were stopped prior to the panel touching the bottom of the die to enable the actual strain rate to be compared with that determined from cone-forming tests.

Hydrogen levels were determined by measuring weight loss caused by dehydrogenation of tabs cut from the formed parts. Table 10 lists the forming temperature, desired hydrogen level, predicted strain, actual hydrogen level, and actual strain for the first three tests.

Two troughs were formed in each test, thus accounting for the two values of actual strain. The good agreement between desired and actual strain for test 3 (uncharged) indicates the applicability of cone test data to actual forming conditions. The low actual strains for tests 1 and 2 are attributed to the low hydrogen levels achieved. The trough dies have a greater ratio of surface area to gas cavity volume than the cone tester, and this difference is believed to be the cause of the lower-than-expected amounts of internal hydrogen. Charging conditions were altered to increase the amounts of internal hydrogen in the suc-

TABLE 10  
FORMING PARAMETERS AND ACTUAL STRAINS OF PRELIMINARY  
TROUGH-FORMING TESTS ON EQUIAXED- $\alpha$  Ti-6Al-4V CONTAINING HYDROGEN

Test number	Forming temperature (°C)	Desired wt% hydrogen	Predicted strain, $\epsilon$	Actual wt% hydrogen	Actual strain, $\epsilon$
1	760	0.2	0.189	0.03	0.069, 0.067
2	800	0.1	0.163	0.01	0.069, 0.066
3	800	0	0.062	0	0.061, 0.059

ceeding panels. Table 11 lists the charging conditions and the resulting hydrogen concentrations and strains actually obtained.

The hydrogen levels attained in tests 7 and 8 were in the lower end of the acceptable range. Panel 9 was formed to completion using the charging parameters of panel 8. Panel 9 was formed with an applied stress of 26.2 MPa (3.8 ksi) until the sample made contact with the trough (expected strain-rate is  $3 \times 10^{-4}/s$ ), and the stress was decreased to 18.8 MPa (2.7 ksi) to fill in the corners (expected strain-rate is  $1 \times 10^{-4}/s$ ).

The equiaxed- $\alpha$  Ti-6Al-4V panel 9 formed to completion ( $\epsilon = 0.85$  at the corners) at  $800^{\circ}\text{C}$  ( $1470^{\circ}\text{F}$ ) and three views of the formed panel are shown in Figure 59. The hydrogen concentration was determined to be 0.17 wt%. From the final strain obtained and the duration of applied stress, the strain rate was determined to be at least 1.85 times faster than the expected strain rate for uncharged Ti-6Al-4V.

Ti-6Al-2Sn-4Zr-2Mo samples were charged with the conditions used in forming panel 9 in an attempt to achieve hydrogen levels of approximately 0.2 wt%. Table 12 lists the results of the first two charging and forming attempts. Panel 11 was stopped prematurely because of a leak. The attained hydrogen levels were less than the desired value.

TABLE 11  
HYDROGEN CONCENTRATIONS OBTAINED IN EQUIAXED- $\alpha$  Ti-6Al-4V  
PANELS UNDER DIFFERENT CHARGING CONDITIONS AND  
STRAIN ATTAINED WHEN FORMED INTO TROUGH.

Test Number	Charging temperature ( $^{\circ}\text{C}$ )	Charging time (h)	Charge pressure (kPa)	% Hydrogen in gas mixture	Hydrogen flow rate (L/h)	Actual wt% hydrogen	Trough-forming strain, $\epsilon$
1	760	2	1.03	1	140	0.03	0.068
2	760	2	0.34	1	140	0.01	0.068
3	No charging - merely a forming test of as-received specimen						0.060
4	760	2	0.34	5	140	0.05	0.054
5	720	2	1.38	5	140	0.05	0.052
6	720	2	1.38	5	140	0.04	0.061
7	640	4	1.38	5	140	0.10	0.089
8	640	4	1.38	5	140	0.09	0.081

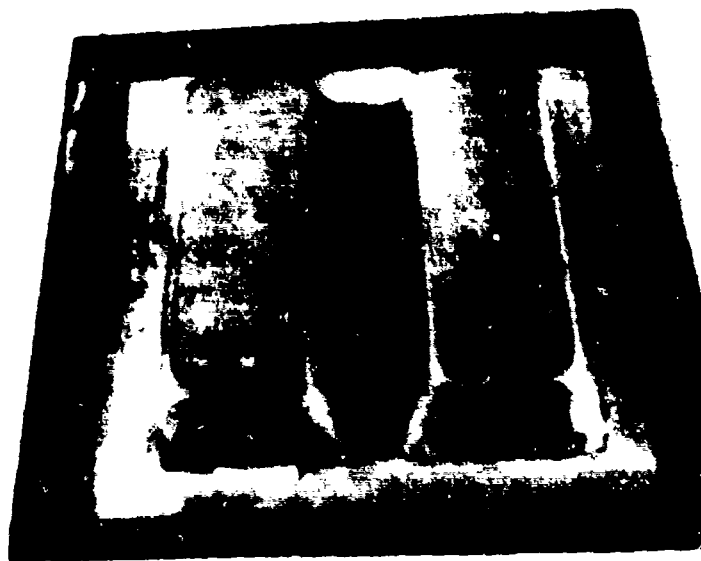


Figure 59. Three views of a hydrogen-charged Ti-6Al-4V panel (9) formed at 800°C.

Panel 12 was charged under the same conditions as panel 11 and then formed at a stress of 18.8 MPa (2.7 ksi) at a higher temperature of 875°C. This panel formed to near-completion attaining a strain of 0.80 at the corners with a two-fold increase in forming rate over the uncharged specimens. The hydrogen level was only 0.06 wt%, and a faster rate would be anticipated if a higher hydrogen level were attained. Figure 60 shows three views of the formed part. Sections of the through bottoms of panels 9 and 12 were dehydrogenated at 675°C (1245°F) for 4 h. Table 13 compares the tensile properties of these sections with those of the  $\alpha$ -fabricated alloys and with panels formed from uncharged alloys. The panels formed by hydrogen additions and dehydrogenated after forming have strengths equal to the as-fabricated material and slightly lower ductilities; however, the uniform elongations are comparable. Panels 9 and 12 have somewhat superior strengths than conventionally formed panels, although they were not as ductile.

Figure 61 shows the microstructures of as-received, hydrogen-charged and heated, and hydrogen-charged and superplastically formed Ti-6Al-2Sn-6Zr-2Mo. The formed parts have coarser grains, possibly accounting for the decreased ductility; grain growth appears to be strain rather than temperature induced. Figure 62 shows the grain growth caused by strain in superplastically formed, equiaxed- $\alpha$  Ti-6Al-4V.

**TABLE 12**  
**FORMING PARAMETERS FOR PRELIMINARY TROUGH-FORMING TESTS ON**  
**DUPLEX-ANNEALED Ti-6Al-2Sn-4Zr-2Mo CONTAINING HYDROGEN**

Panel number	Hydrogen (wt%)	Test temperature (°C)	Test stress [MPa (ksi)]	Strain, $\epsilon$	Strain rate, $\dot{\epsilon}$ (s <sup>-1</sup> )
10	0.08	830	26.2 (3.8)	0.21	$4.7 \times 10^{-5}$
11	0.06	830	34.5 (5)	0.19	$7.0 \times 10^{-5}$

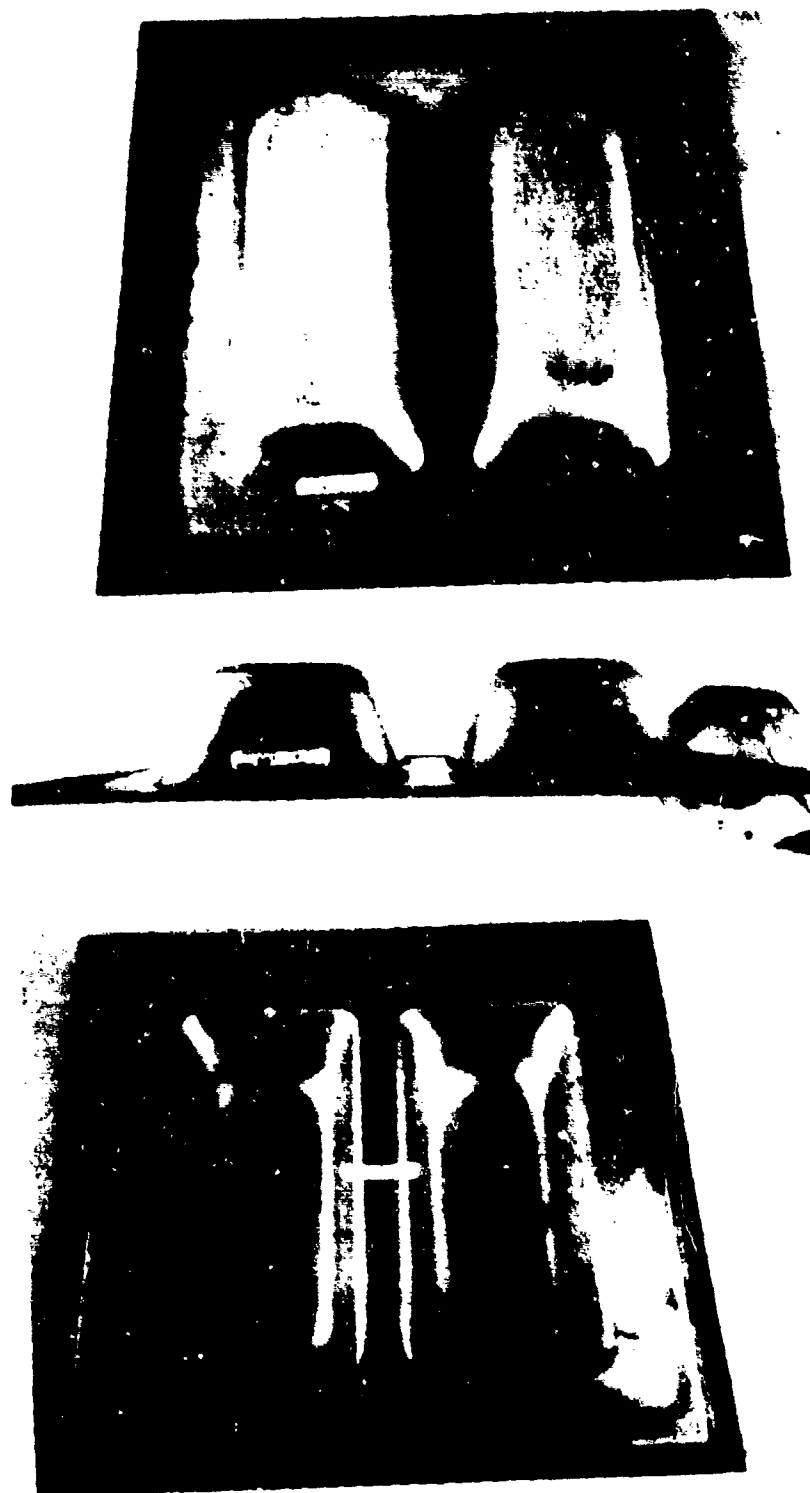
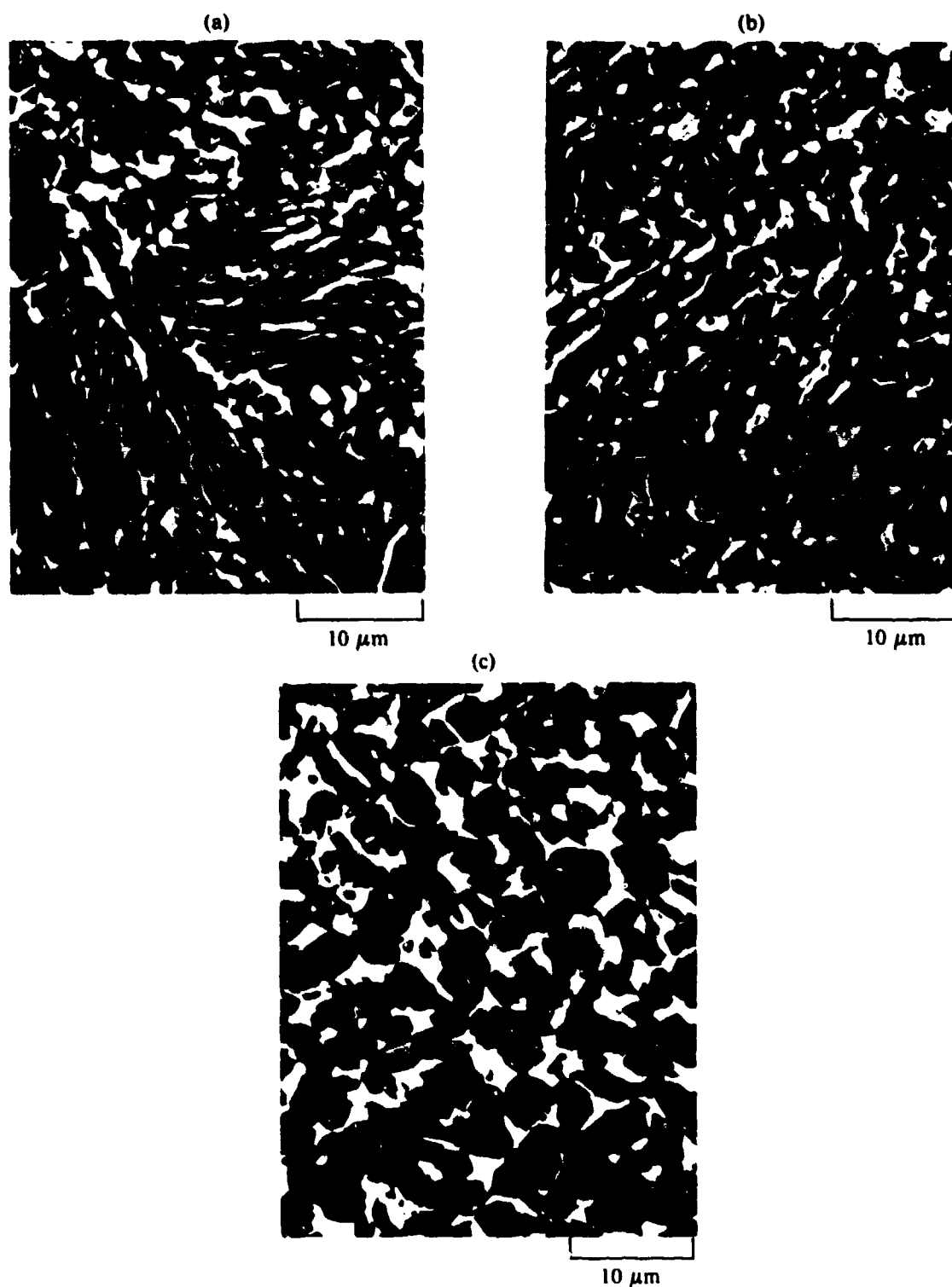


Figure 60. Three views of a hydrogen-charged Ti-6Al-2Sn-4Zr-2Mo panel (12) formed at 875°C.

**TABLE 13**  
**COMPARISON OF MECHANICAL PROPERTIES OF AS-RECEIVED PANELS,**  
**CONVENTIONALLY SUPERPLASTICALLY FORMED PANELS, AND**  
**SUPERPLASTICALLY FORMED PANELS WITH INTERNAL HYDROGEN.**

Alloy	Condition	0.2% yield stress [MPa (ksi)]	Ultimate tensile stress [MPa (ksi)]	Total elongation (%)	Uniform elongation (%)
Equiaxed- $\alpha$ Ti-6Al-4V	As-received	961 (139)	1000 (145)	12.8	7.8
		964 (140)	1009 (146)	11.4	7.6
	Conventional superplastic forming <sup>(a)</sup>	859 (125)	923 (134)	15.2	—
		872 (126)	910 (132)	12.5	—
	Superplastic forming with internal hydrogen	958 (139)	1005 (146)	7.0	5.9
		938 (136)	986 (143)	7.9	6.2
Duplex-annealed Ti-6Al-2Sn-4Zr-2Mo	As-received	936 (136)	1016 (147)	12.4	7.8
		936 (136)	1017 (148)	12.6	8.2
	Conventional superplastic forming <sup>(a)</sup>	925 (134)	987 (143)	12.5	—
		935 (136)	997 (145)	11.8	—
	Superplastic forming with internal hydrogen	958 (139)	1007 (146)	10.2	6.7
		936 (136)	986 (143)	7.3	4.6

(a) Reference 1.



**Figure 61.** Scanning electron micrographs of duplex-annealed Ti-6Al-2Sn-4Zr-2Mo used in the forming of panel 12: (a) as-received; (b) uncharged, heated, but unformed; and (c) hydrogen charged, heated, and formed to a true strain of 0.80.

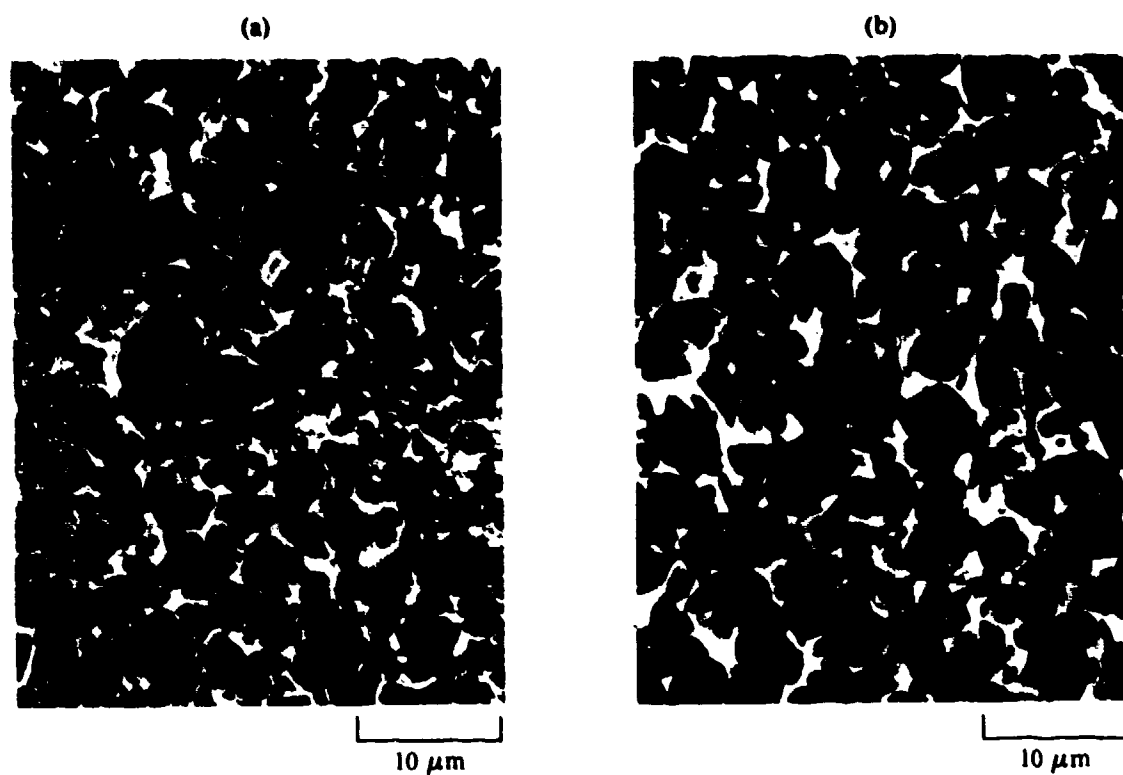


**Figure 62.** Scanning electron micrographs of equiaxed- $\alpha$  Ti-6Al-4V used in the forming of panel 9: (a) uncharged; heated, but unformed; and (b) hydrogen charged, heated, and formed to a true strain of 0.85.

## SECTION VII

### CONCLUSIONS

1. Uniquely fine microstructures can be obtained for laboratory-type specimens of Ti-6Al-4V and Ti-6Al-2Sn-4Zr-2Mo by hydrovac processing using vacuum encapsulation for beta annealing and subsequent transformation.
2. In order for production-size panels to be processed, a protective coating must be used to prevent oxygen pick-up during the beta anneal; the two coatings tested in this program, Formkote T50 and Daltaglaz 349 M, resulted in oxygen concentrations above the specification limits.
3. The temperature of the panels must be closely monitored because variations of  $\pm 15^{\circ}\text{C}$  during dehydrogenation are crucial; some care must be used in handling the panels before dehydrogenation, although they are not extremely brittle.
4. Correctly processed hydrovac materials exhibit increases in room- and elevated-temperature tensile strengths of over 100 MPa (15 ksi).
5. Hydrovac processed Ti-alloys exhibit decreases in creep rates of at least an order-of-magnitude; superplastic-forming and diffusion-bonding properties are not improved by hydrovac processing.
6. Small amounts of internal hydrogen decrease the beta transus temperature of the alloys, increase the percentage of beta phase at the superplastic forming temperature, and increase the superplastic strain rates.
7. Optimum amounts of hydrogen ( $\sim 0.1$  wt%) enable alloys to be formed at lower temperatures and Ti-6Al-2Sn-4Zr-2Mo to be formed into shapes not possible at any temperature using conventional forming methods.
8. Large troughs having good mechanical integrity can be formed in panels containing internal hydrogen.

9. Evolution of internal hydrogen during the forming cycle decreases formability by raising the beta transus temperature; however, formability is still better than for the as-received alloy.

10. The presence of internal hydrogen and the evolution of internal hydrogen do not improve diffusion bondability.

## SECTION VIII

### RECOMMENDATIONS

1. This investigation demonstrated that vacuum encapsulation of samples enables fine hydrovac microstructures to be obtained without oxygen contamination. The feasibility and cost effectiveness of hydrovac processing of large panels in evacuated metal jackets should be determined.
2. A systematic evaluation of different surface coatings should be conducted with the objective of identifying a coating that is an effective barrier for oxygen diffusion into the specimens at the beta-annealing temperature.
3. A thermodynamic investigation of the synergistic effects of internal hydrogen and coating chemistry is recommended for determining the conditions under which oxygen pick-up is minimal.
4. This investigation demonstrated that large parts can be superplastically formed at lower temperatures and in shorter times using an argon-hydrogen gas mixture with modifications to existing production setups. A logical extension of this study would be to scale-up the process and optimize the process parameters for the production by SPF/DB of large parts on a routine basis.

SECTION IX  
REPORTS AND PUBLICATIONS RESULTING FROM THIS CONTRACT

1. R. J. Lederich, J. E. O'Neal, and S. M. L. Sastry, Optimum Microstructures for Superplastic Forming Using Hydrovac, McDonnell Douglas Report MDC Q0736 (15 March 1981), Interim Report, AFWAL Contract No. F33615-80-C-5118.
2. R. J. Lederich, S. M. L. Sastry, and J. E. O'Neal, Optimum Microstructures for Superplastic Forming Using Hydrovac, McDonnell Douglas Report MDC Q0753 (15 September 1982), Interim Report, AFWAL Contract No. F33615-80-C-5118.
3. R. J. Lederich, S. M. L. Sastry, J. E. O'Neal, and W. R. Kerr, Influence of Hydrogen Additions on High-Temperature Superplasticity of Titanium Alloys, in **Advanced Processing Methods for Titanium**, ed. by D. F. Hasson and C. F. Hamilton (Metallurgical Society of AIME, Warrendale, PA, 1982), pp. 115-128.
4. R. J. Lederich, S. M. L. Sastry, J. E. O'Neal, and W. R. Kerr, Effects of Minor Alloying Additions on Superplastic Formability of Titanium Alloys, in **Superplastic Forming of Structural Alloys**, ed. by N. E. Paton and C. H. Hamilton (Metallurgical Society of AIME, Warrendale, PA, 1982), p. 356.

## APPENDIX A. PRACTICAL ASPECTS OF HYDROVAC PROCESSING ON A PRODUCTION SCALE

OREMET hydrovac processed 93 titanium alloy panels, which were divided into five lots. The hydrogen levels obtained in each of the panels are shown in Figures A-1 - A-5. Although the initial results were characterized by uneven hydrogen distributions, the last two lots show that with experience, the desired hydrogen concentrations can be obtained routinely.

As described in Section IV, the two coatings studied (Formakote T50 and Deltaglaze 349M) permitted excessive oxygen absorption to occur during the beta anneal. Considering the inherent temperature uncertainties and gradients present in production to be  $\pm 20^{\circ}\text{C}$  ( $35^{\circ}\text{F}$ ), a coating protective to  $840^{\circ}\text{C}$  ( $1545^{\circ}\text{F}$ ) must be found.

The dehydrogenation temperature is extremely critical. Since desirable tensile properties are obtained from  $660$  to  $700^{\circ}\text{C}$  ( $1200$  to  $1290^{\circ}\text{F}$ ), successful processing can occur if the uncertainties and gradients in temperature are less than  $\pm 20^{\circ}\text{C}$  ( $35^{\circ}\text{F}$ ).

OREMET reports that the hydrogen-charged samples are not unduly brittle and that only minor precautions are necessary to prevent panel breakage. In fact, no panels were broken after the first lot. All panels experienced slight warpage, which occurred because the panels stood on a short edge. Hanging the panels should alleviate this problem.

In summary, correctly processed panels can be produced if temperature gradients and uncertainties are less than  $\pm 20^{\circ}\text{C}$  ( $35^{\circ}\text{F}$ ) and if an adequate protective coating can be found.

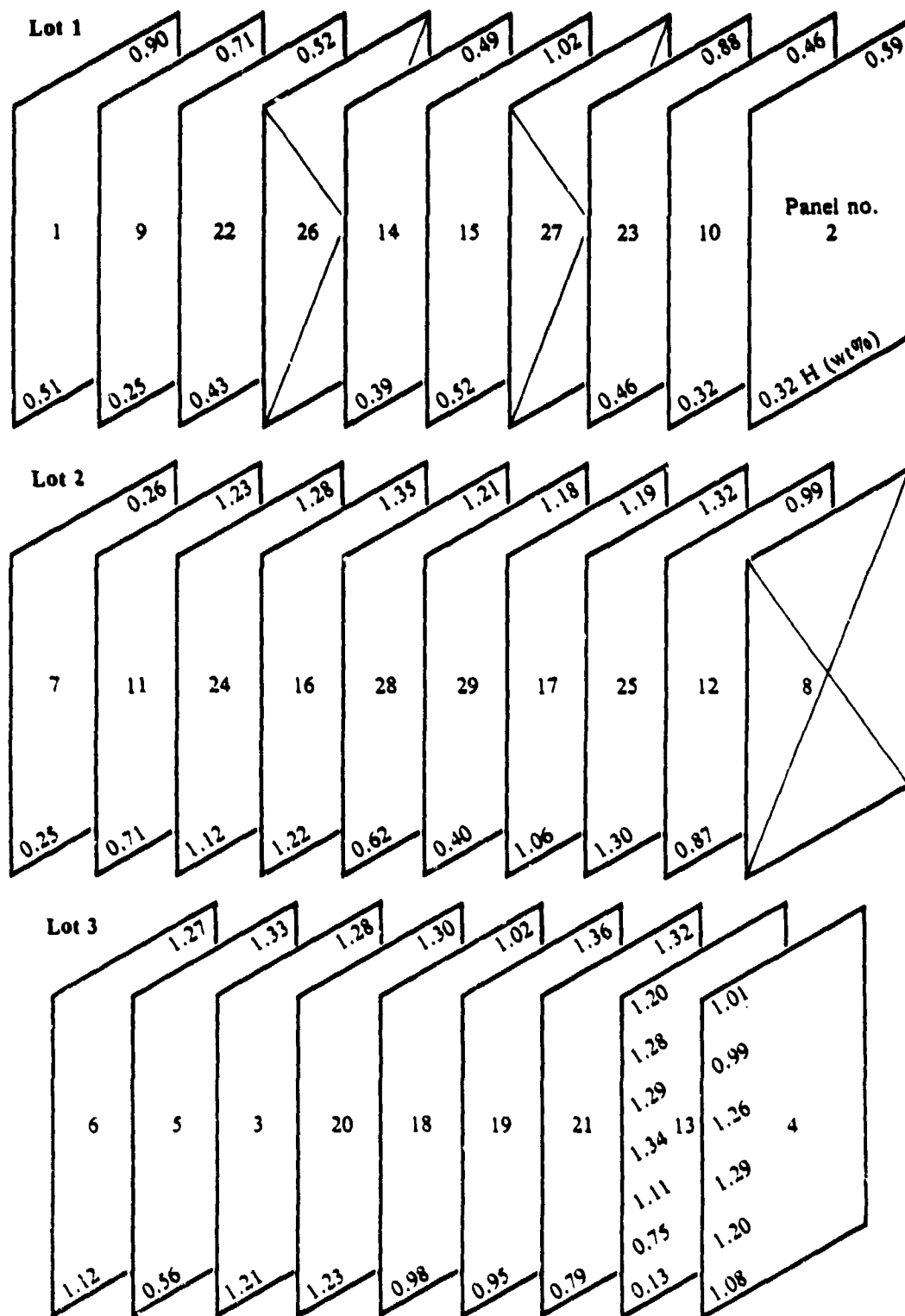
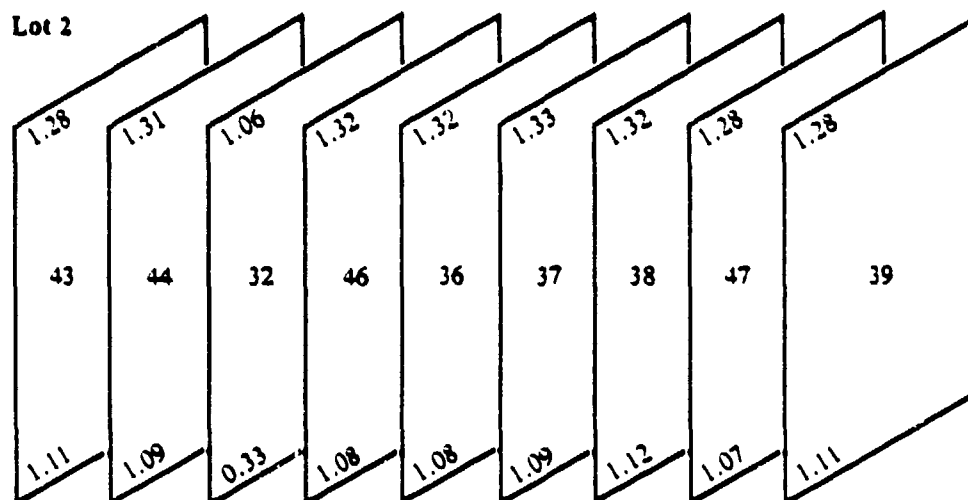
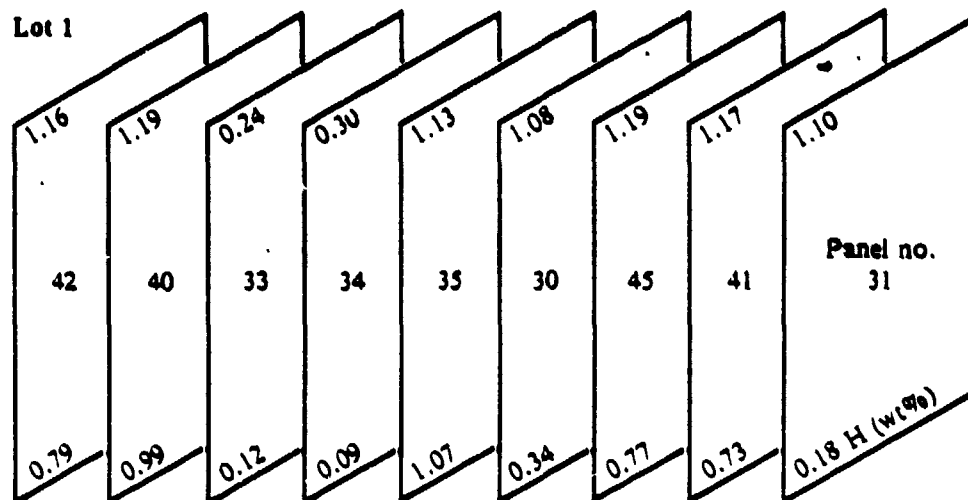
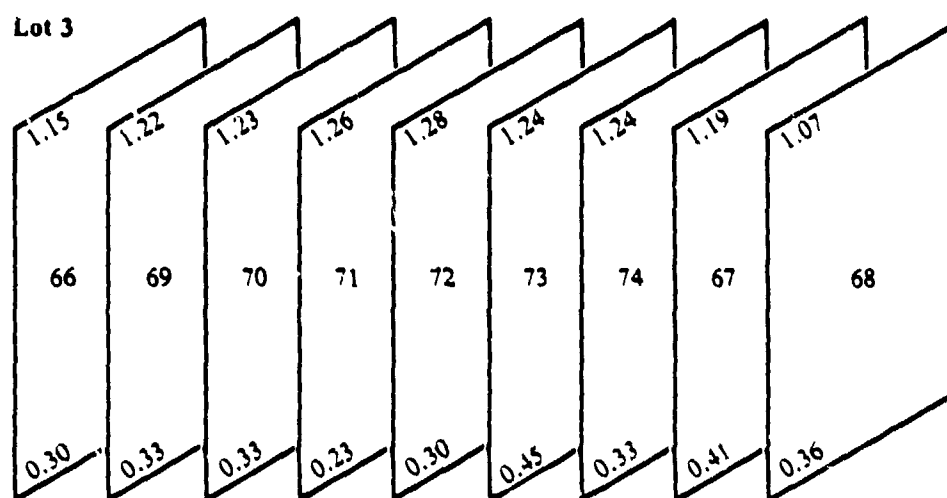
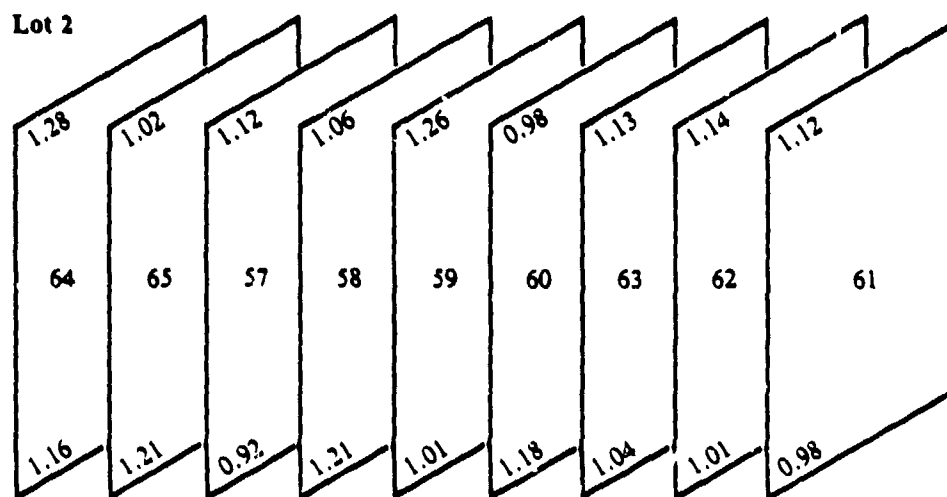
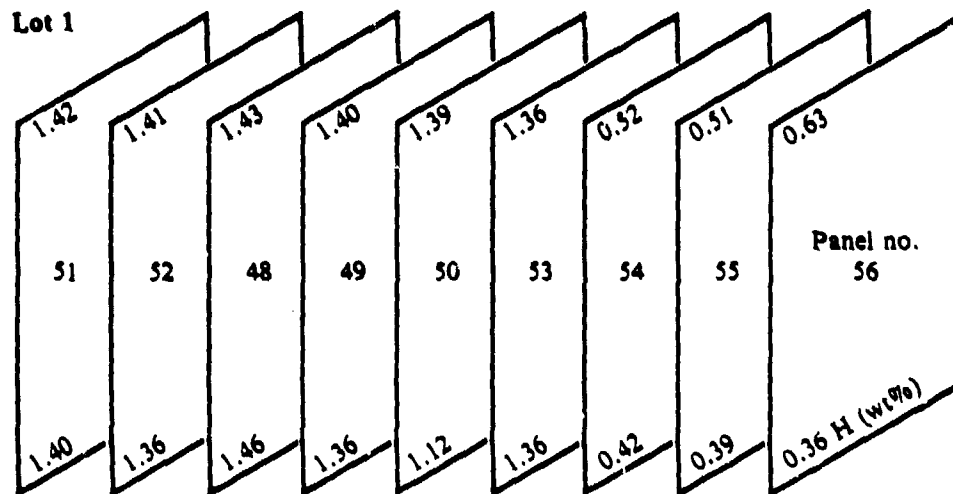


Figure A-1. Relative positions and final hydrogen concentrations of batch-1 panels after hydrogenation by OREMET.



**Figure A-2. Relative positions and final hydrogen concentrations of batch-2 panels after hydrogenation by OREMET.**



**Figure A-3. Relative positions and final hydrogen concentrations of batch-3 panels after hydrogenation by OREMET.**

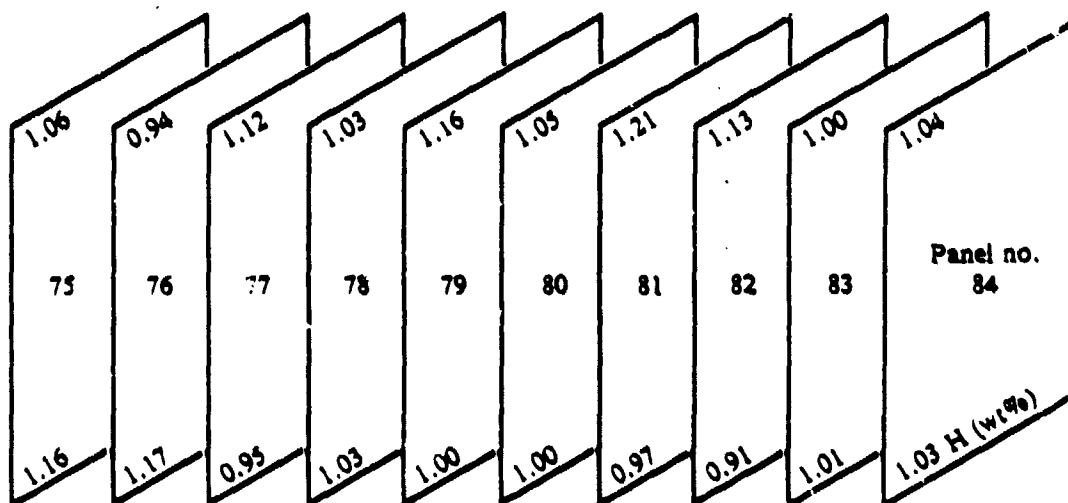


Figure A-4. Relative positions and final hydrogen concentrations of batch-4 panels after hydrogenation by OREMET.

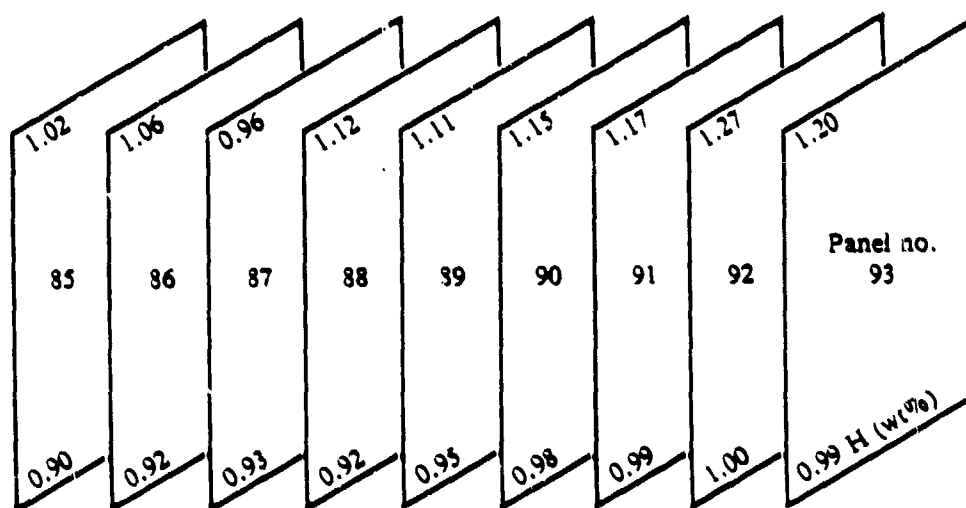


Figure A-5. Relative positions and final hydrogen concentrations of batch-5 panels after hydrogenation by OREMET.

# APPENDIX 8. ANALYSES OF BIAXIAL-STRESS CONE FORMING

As described in Section III.6, the cone-forming tester (Figure 12) enables the instantaneous cone height to be monitored as the sample forms under constant-stress conditions. Throughout the forming operations, the part of the sample not in contact with the die has a hemispherical configuration. The biaxial stress,  $\sigma(r)$ , of a thick-walled sphere subjected to an internal pressure  $P$  is

$$\sigma(r) = \frac{Pa^3(b^3 + 3r^3)}{2r^3(b^3 - a^3)} \quad (B-1)$$

where  $a$  is the inner radius,  $b$  is the outer radius, and  $r$  is the radius at the location of the stress. Thus the biaxial stress varies with radius, ranging from a minimum at the inner radius,

$$\sigma(a) = \frac{P}{2} \frac{(b^3 + 3a^3)}{(b^3 - a^3)} \quad (B-2)$$

to a maximum at the outer radius,

$$\sigma(b) = \frac{P}{2} \frac{(4a^3)}{(b^3 - a^3)} \quad (B-3)$$

For superplastic forming evaluations, it is desirable to use a thin-wall approximation, which yields a stress between  $\sigma(a)$  and  $\sigma(b)$ .

For the cone geometry employed in this testing (see Figure B-1), the cone radius,  $R$ , is 27.4 mm (1.078 in.) and the cone angle,  $\alpha$ , is  $58^\circ$ . The area of the spherical segment at point of first contact is  $2\pi xd$ ; hence constancy of volume yields the relation

$$\pi R^2 t_1 = t_2 2\pi x(x - h) \quad (B-4)$$

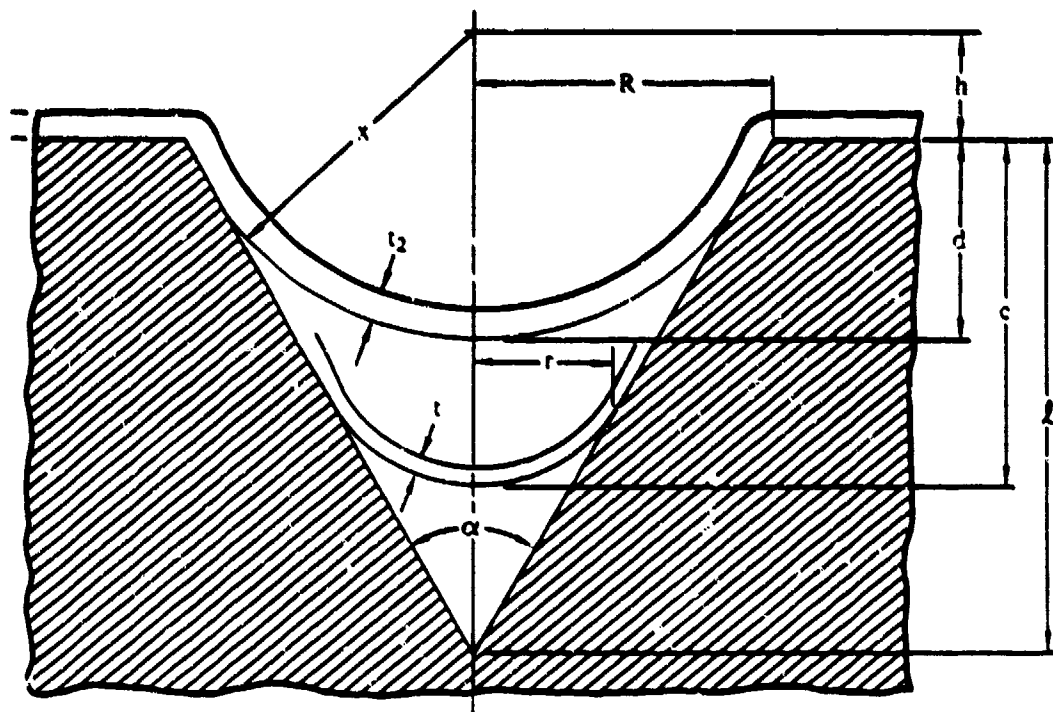


Figure B-1. Schematic cross-section of conical die.

From the cone geometry,

$$x = \frac{R}{\cos \alpha/2} \quad (B-5)$$

and

$$h = R \tan \alpha/2 \quad (B-6)$$

Therefore,

$$\frac{1}{t_2} = 2 \left\{ \frac{1}{\cos \alpha/2} \left[ \frac{1}{\cos \alpha/2} - \tan \alpha/2 \right] \right\} \quad (B-7)$$

$$\frac{t_1}{t_2} = \frac{2}{\cos^2 \alpha/2} [1 - \sin \alpha/2], \quad (8-8)$$

and

$$\frac{t_1}{t_2} = \frac{2}{1 + \sin \alpha/2} \quad (8-9)$$

Hence for  $\alpha/2 = 29^\circ$ ,

$$\frac{t_1}{t_2} = 1.347 \quad (8-10)$$

For most samples of this study,  $t_1 = 2.54$  mm (0.100 in.); therefore  $t_2 = 1.88$  mm (0.074 in.). Additionally,  $b = x = R/\cos \alpha/2$ ; therefore, at first contact with the conical die wall,  $b = 31.22$  mm (1.229 in.) and  $a = b - t_2 = 29.34$  mm (1.155 in.). Hence, the stress is  $\sigma = 7.84$  P at the inner radius and 7.34 P at the outer radius stress.

The thin-wall approximation,

$$\sigma = \frac{Pr}{2t_z} \quad (8-11)$$

utilizing the die radius of 27.4 mm (1.078 in.) yields  $\sigma = 8.30$  P, an unrealistically high value. If the membrane inner radius is used in Equation (8-11), the calculated stress is  $\sigma = 7.78$  P, a value within the stress range calculated from the thick-wall relation, Equation (8-1).

Therefore, for a general sample thickness,  $t_0$ , the thin-wall stress equation was used in the form

$$\sigma = \frac{Pr}{2t} \quad (8-12)$$

where

$$t = t_0/1.347 \quad (B-13)$$

and

$$x = 1.232 - \frac{t_0}{1.347} \quad (B-14)$$

The strain is given by

$$\epsilon = \ln(t/t_0) \quad (B-15)$$

The decrease in thickness is the sum of that occurring before and after the sheet makes contact with the die. From Equation (B-10), at moment of contact,  $t = t_0/1.347$ ; therefore,  $\epsilon_1 = 0.30$  at that point. Thereafter,  $t/r$  is a constant, as was demonstrated by Mackay et al. (Reference 1). Hence

$$\frac{dt}{t} = \frac{dr}{r} \quad (B-16)$$

From Figure B-1,  $r = (l - c) \tan \alpha/2$ ; therefore,

$$\frac{dr}{r} = - \frac{dc}{l - c} \quad (B-17)$$

and

$$\epsilon_2 = - \int_{q_1}^{q_2} \frac{dc}{l - c} = - \ln \left( \frac{l - q_2}{l - q_1} \right) \quad (B-18)$$

where  $q_2$  is the cone depth and  $q_1$  is the cone depth when contact is first made with the die.

The total strain is the sum of the two components:

$$\epsilon = \epsilon_1 + \epsilon_2 = 0.30 - \ln \left( \frac{l - q_2}{l - q_1} \right) \quad (\text{B-19})$$

Figure B-2 shows the strain rates at 900°C of equiaxed- $\alpha$  Ti-6Al-4V as a function of time for different stress levels. The decrease in strain rate as a function of time is attributed to grain growth.

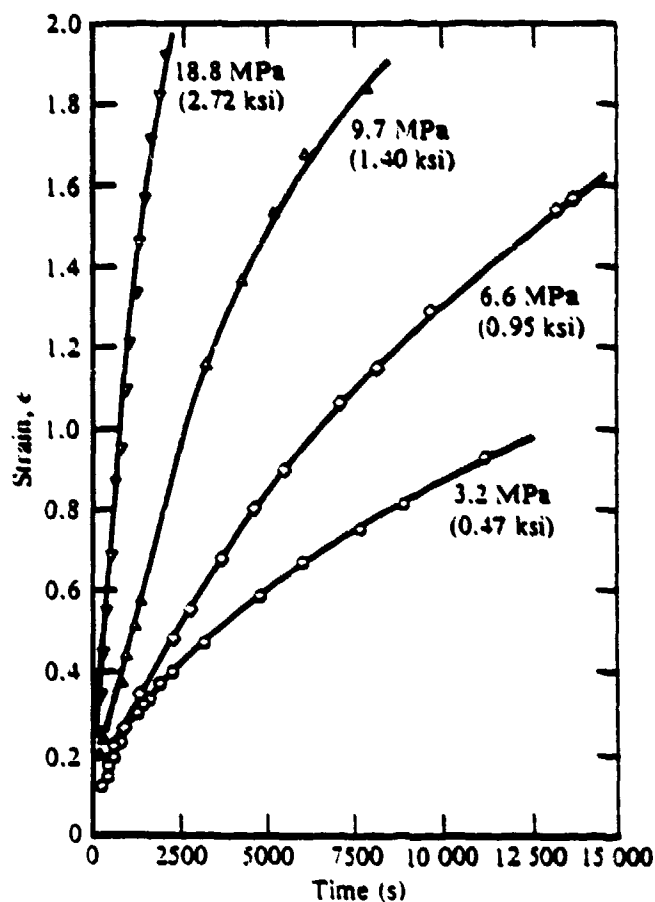


Figure B-2. Time dependence of strain of equiaxed- $\alpha$  Ti-6Al-4V superplastically formed at 900°C at the indicated stresses.

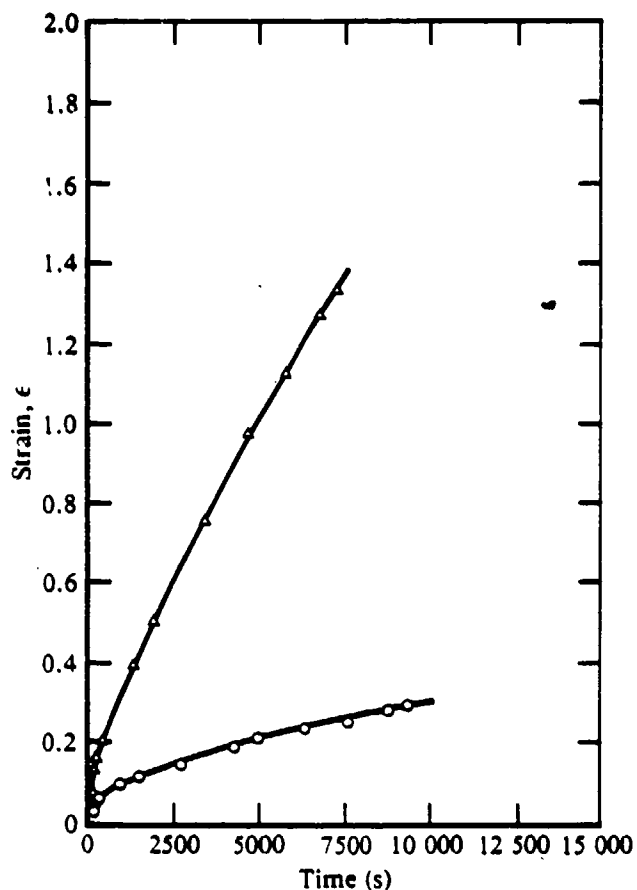


Figure B-3. Time dependence of strain of ( $\Delta$ ) equiaxed- $\alpha$  Ti-6Al-4V and ( $\circ$ ) duplex-annealed Ti-6Al-2Sn-4Zr-2Mo superplastically formed at 830°C and 18.8 MPa (2.72 ksi).

Figures B-3, B-4, and B-5 show the strain rates of the three as-received alloys at three different combinations of stress and temperature. Ti-6Al-2Sn-4Zr-2Mo has lower strain rates than equiaxed- $\alpha$  Ti-6Al-4V.

Constant-stress tests using tensile specimens were conducted at various temperature/stress combinations, and the results were compared with those obtained from the cone-forming tests. Figures B-6 and B-7 demonstrate that the agreement is good between the data obtained from the two tests at both 900 and 830°C (1650 and 1525°F). The differences in the time dependences of strain rate at large strains between the tensile specimens and cone specimens are caused by the extension of tensile specimen gauge length beyond the uniform-temperature hot zone of the furnace.

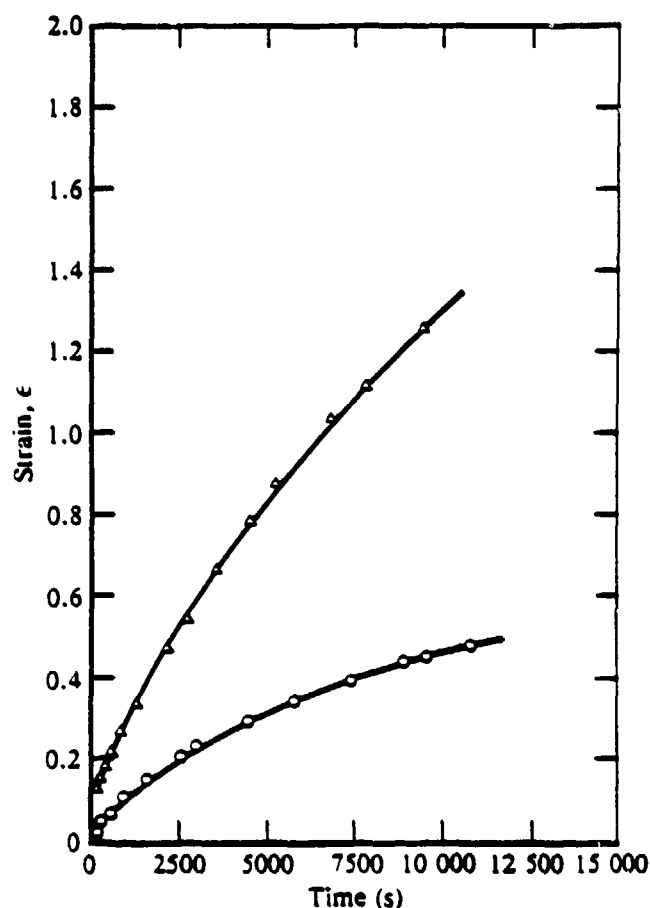
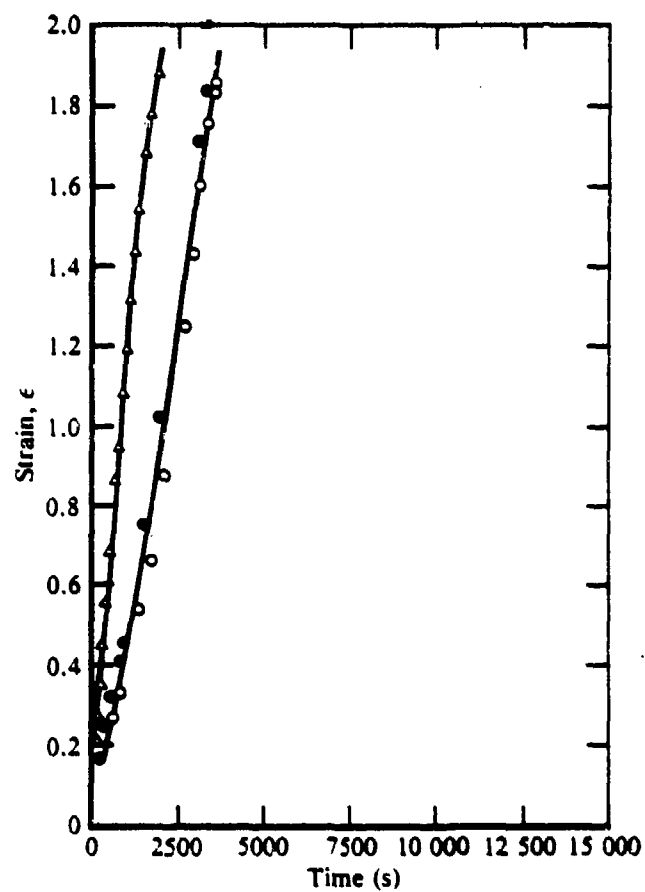


Figure B-4. Time dependence strain of (○) equiaxed- $\alpha$  Ti-6Al-4V and (Δ) duplex-annealed Ti-6Al-2Sn-4Zr-2Mo superplastically formed at 900°C and 9.7 MPa (1.40 ksi).

Constant-strain-rate tests were also conducted at 830°C (1525°F) using tensile specimens. As the specimens elongated, the crosshead speed was increased incrementally so that the instantaneous strain-rate was always within 2% of the nominal values. Figure B-8 shows true-stress/true-strain plots of specimens tested at five different strain rates. Also included in Figure B-8 are values obtained from the constant-stress tests..



**Figure B-5.** Time dependence strain of (▲) equiaxed- $\alpha$  Ti-6Al-4V and (●, ○) duplex-annealed Ti-6Al-2Sn-4Zr-2Mo superplastically formed at 900°C and 18.8 MPa (2.72 ksi).

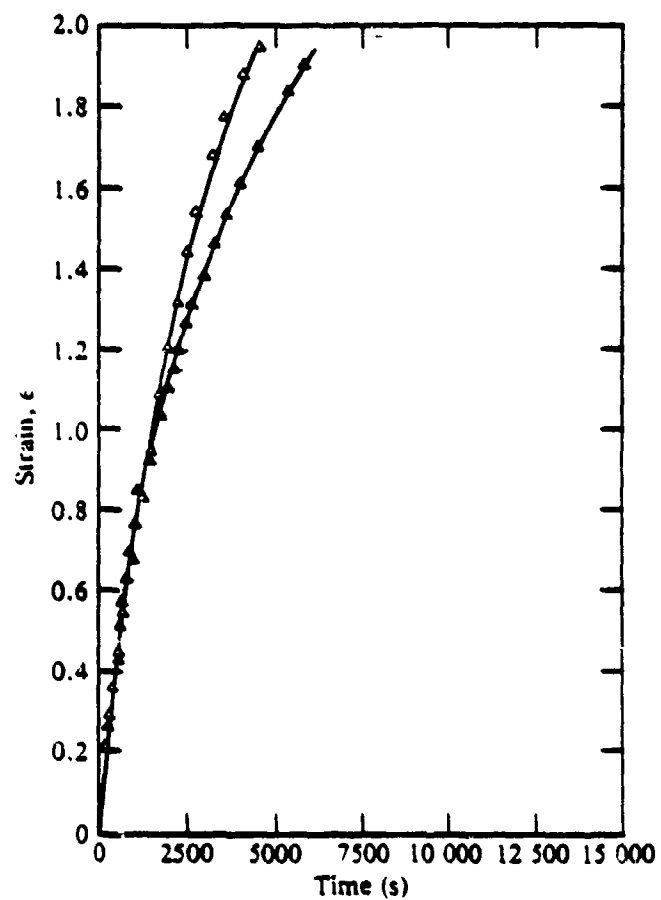


Figure B-6. Time dependence of strain of equiaxed- $\alpha$  Ti-6Al-4V superplastically formed at 900°C and 18.8 MPa (2.72 ksi) as determined by ( $\Delta$ ) tensile tests and ( $\blacktriangle$ ) cone-forming tests.

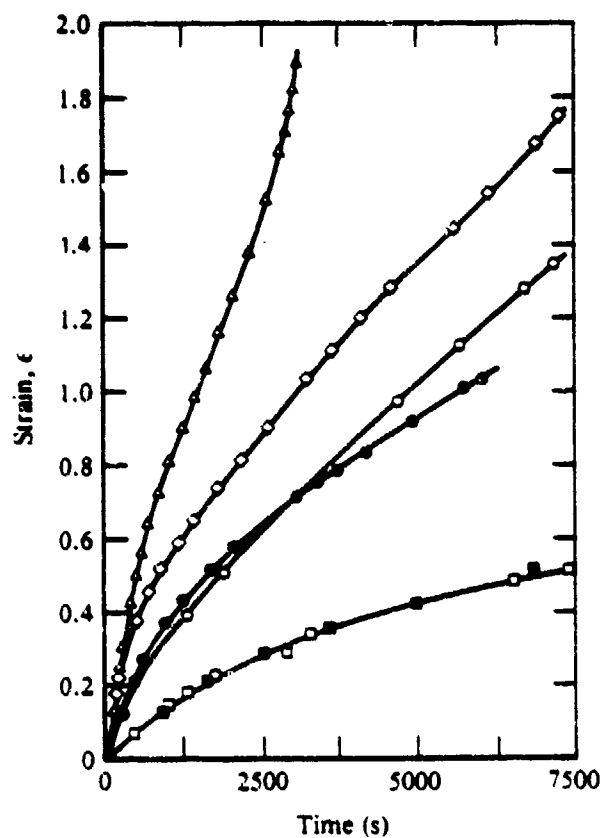


Figure B-7. Time dependence of strain of equiaxed- $\alpha$  Ti-6Al-4V superplastically formed at 830°C and (  $\Delta$  ) 31 MPa (4.5 ksi), (  $\diamond$  ) 25 MPa (3.6 ksi), (  $\bullet$  ,  $\circ$  ) 19 MPa (2.7 ksi), and (  $\blacksquare$  ,  $\square$  ) 10 MPa (1.4 ksi). Open symbols denote cone-forming measurements and closed symbols denote tensile-test measurements.

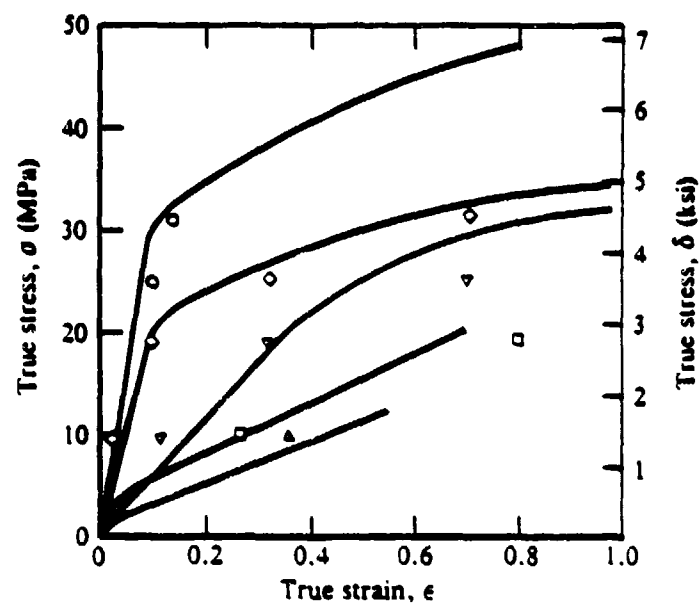


Figure B-8. True-stress/true-strain relation of equiaxed- $\alpha$  Ti-6Al-4V at 830°C as determined from tensile specimens deformed at a constant strain rate. The data points were obtained from tensile specimens deformed under constant-stress conditions and correspond to the following strain rates: ( $\circ$ )  $10^{-3}/s$ , ( $\diamond$ )  $5 \times 10^{-4}/s$ , ( $\nabla$ )  $2 \times 10^{-4}/s$ , ( $\square$ )  $10^{-4}/s$ , and ( $\triangle$ )  $5 \times 10^{-5}/s$ .

APPENDIX C. MECHANICAL PROPERTIES OF ALLOYS HYDROVAC-PROCESSED  
BY OREMET USING FORMKOTE T50 COATING AND 810°C (1490°F)  
BETA-ANNEALING TREATMENT

The tensile properties of the batch-1 improperly hydrovac-processed alloys were determined in the longitudinal orientation at room and elevated temperatures. Important mechanical properties are listed in Table C-1 for the hydrovac-processed alloys. These improperly hydrovac-processed alloys had less than the desired microstructural refinement and had oxygen concentrations of 0.19 wt% (a value significantly higher than in the mill-processed alloys). Therefore the properties of these alloys are not representative of optimally processed alloys. Figures C-1 - C-4 compare the temperature dependences of yield stress and ultimate tensile stress of as-received and hydrovac-processed samples. Both properties are improved slightly, by about 25 MPa (4 ksi), for Ti-6Al-4V; however, these properties are degraded for the hydrovac-processed Ti-6Al-2Sn-4Zr-2Mo, particularly at higher temperatures. Some of the low values for Ti-6Al-2Sn-4Zr-2Mo, as shown in Table C-1, were for samples that failed at extremely low strains.

TABLE C-1  
TENSILE PROPERTIES OF OREMET BATCH-1 HYDROVAC-PROCESSED ALLOYS

Alloy	Temperature [°C (°F)]	0.2% yield stress [MPa (ksi)]	Ultimate tensile stress [MPa (ksi)]	Total elongation (%)
Equiaxed- $\alpha$ Ti-6Al-4V	21 (70)	972 (141)	1020 (14.8)	11.3
	21 (70)	986 (143)	1048 (152)	7.4
	205 (400)	758 (110)	848 (123)	11.5
	205 (400)	752 (109)	841 (122)	9.5
	371 (700)	625 (90.6)	724 (105)	9.6
	371 (700)	671 (97.3)	779 (113)	9.2
Duplex-annealed Ti-6Al-2Sn-4Zr-2Mo	21 (70)	903 (131)	945 (137)	0.8
	21 (70)	945 (137)	1062 (154)	11.5
	315 (600)	690 (100)	779 (113)	3.5
	315 (600)	669 (97)	827 (120)	12.2
	982 (900)	569 (82.5)	717 (104)	18.0
	482 (900)	555 (80.5)	710 (103)	10.2

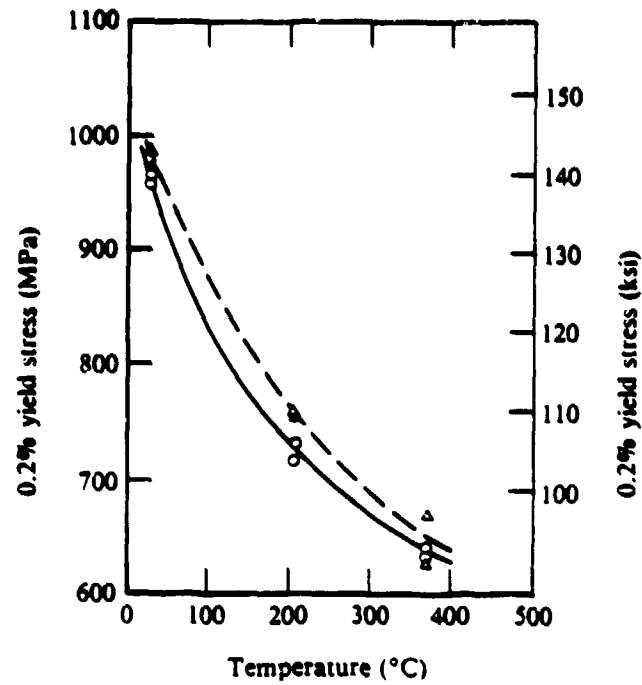


Figure C-1. Effect of temperature on the 0.2% yield stress of (○) as-received and (△) OREMET batch-1, hydrovac-processed, equiaxed- $\alpha$  Ti-6Al-4V.

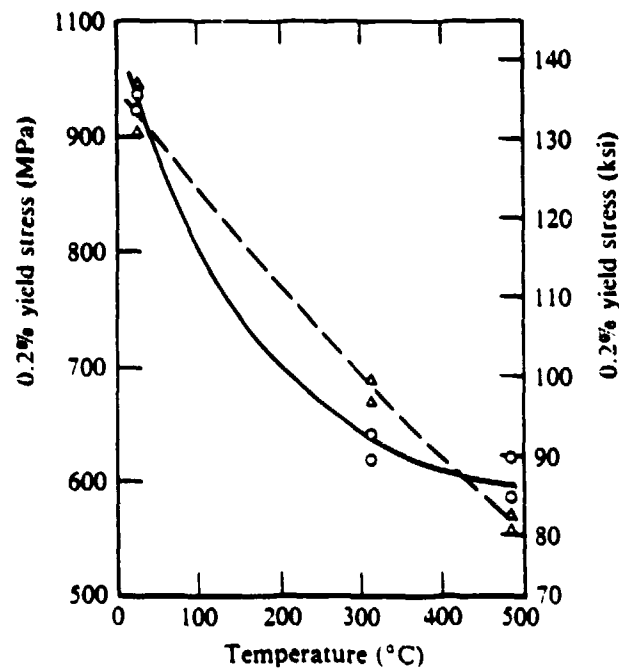


Figure C-2. Effect of temperature on the 0.2% yield stress of (○) as-received and (△) OREMET batch-1, hydrovac-processed Ti-6Al-2Sn-4Zr-2Mo.

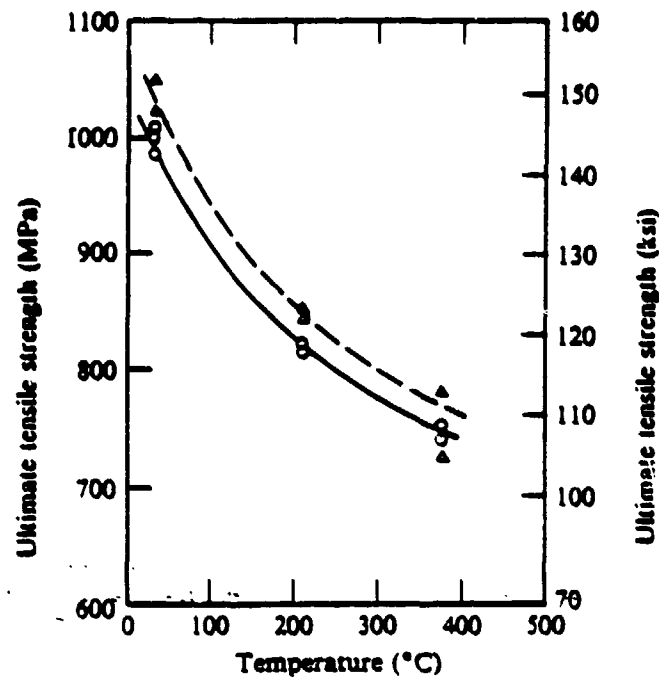


Figure C-3. Effect of temperature on the ultimate tensile strength of (○) as-received and (△) OREMET batch-1, hydrovac-processed, equiaxed- $\alpha$  Ti-6Al-4V.

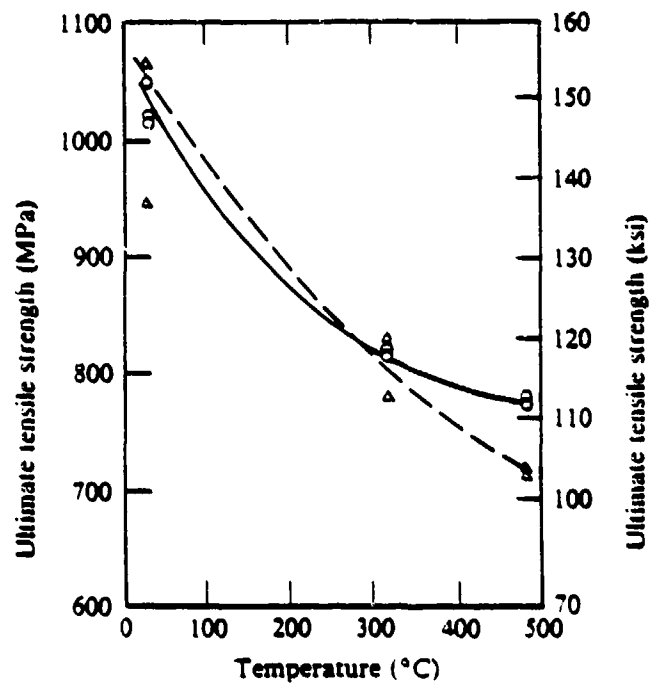


Figure C-4. Effect of temperature on the ultimate tensile strength of (○) as-received and (△) OREMET batch-1, hydrovac-processed Ti-6Al-2Sn-4Zr-2Mo.

# 1. CREEP MEASUREMENTS

Creep tests at 350, 435, 520, and 600°C (660, 815, 970, and 1110°F) were performed on duplicate samples of improperly hydrovac-processed, equiaxed- $\alpha$ Ti-6Al-4V and Ti-6Al-2Sn-4Zr-2Mo. Figures C-5 and C-6 show the effects of hydrovac processing on the steady-state creep rates of the alloys. The creep rate of Ti-6Al-4V is reduced by one-third upon hydrovac processing, but hydrovac processing does not improve the creep resistance of Ti-6Al-2Sn-4Zr-2Mo.

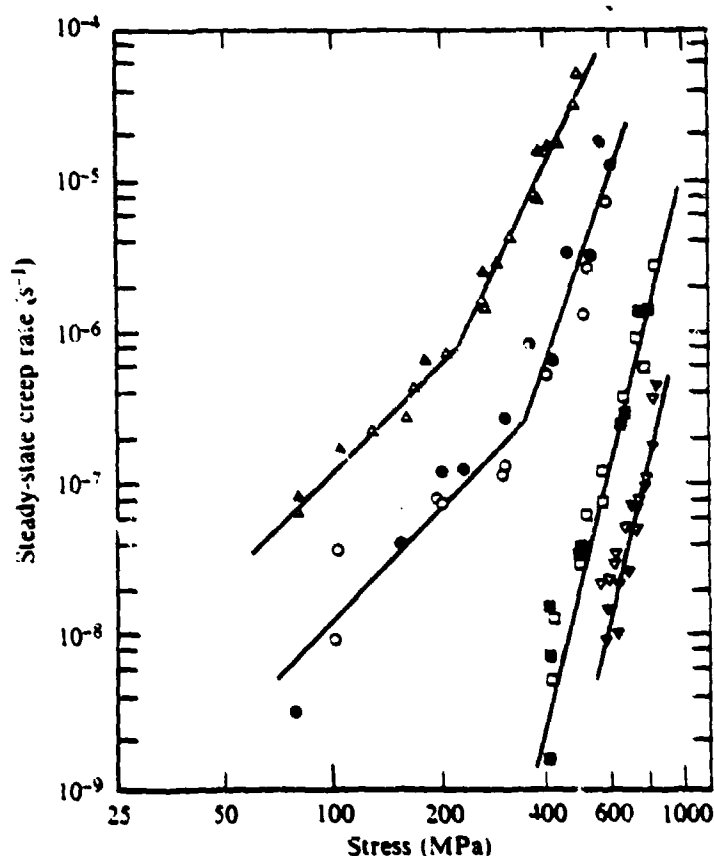


Figure C-5. Stress dependence of steady-state creep rate for equiaxed- $\alpha$  Ti-6Al-4V in as-received condition (open symbols) and OREMET batch-1 hydrovac condition (closed symbols) at ( $\Delta$ ,  $\blacktriangle$ ) 600°C, ( $\circ$ ,  $\bullet$ ) 520°C, ( $\square$ ,  $\blacksquare$ ) 435°C, and ( $\nabla$ ,  $\blacktriangledown$ ) 350°C.

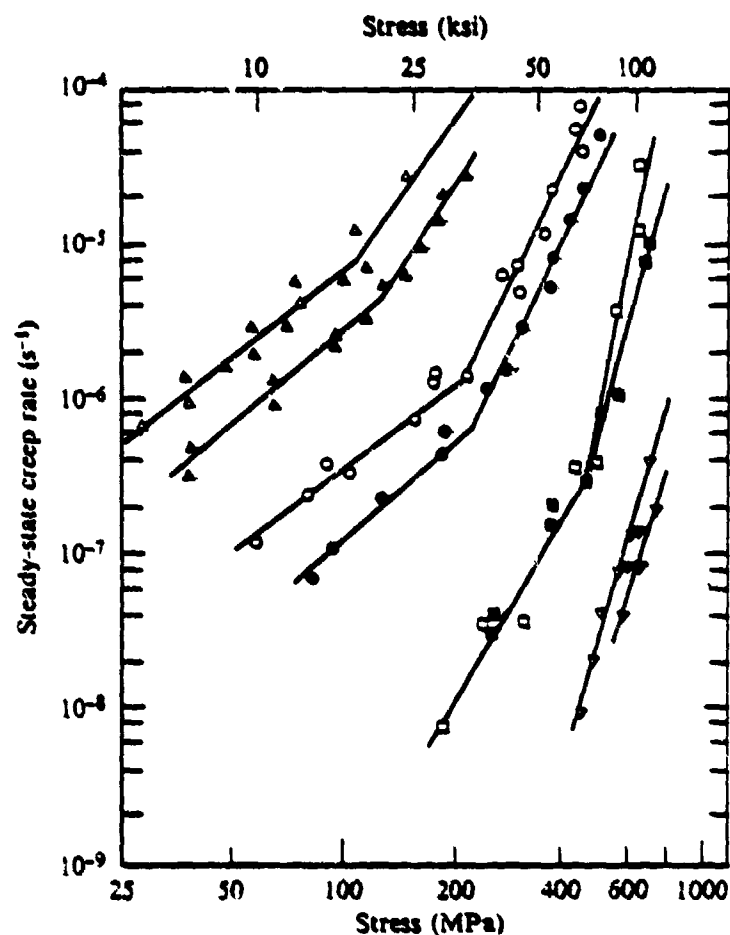


Figure C-6. Stress dependence of steady-state creep rate for duplex-annealed Ti-6Al-2Sn-4Zr-2Mo in as-received condition (open symbols) and OREMET batch-1 hydrovac condition (closed symbols) at ( $\Delta$ ,  $\blacktriangle$ ) 600°C, ( $\circ$ ,  $\bullet$ ) 520°C, ( $\square$ ,  $\blacksquare$ ) 435°C, and ( $\nabla$ ,  $\blacktriangledown$ ) 350°C.

## 2. FATIGUE CRACK-GROWTH-RATE MEASUREMENTS

Fatigue crack-growth rates of as-received and improperly hydrovac-processed equiaxed- $\alpha$  Ti-6Al-4V and Ti-6Al-2Sn-4Zr-2Mo alloys were determined using compact-tension specimens oriented in the long-transverse direction. Specimen geometry and test procedures conformed to ASTM Standard E647.

The fatigue crack-growth rates of duplicate and triplicate samples of the alloys shown in Figures C-7 - C-10 indicate a good reproducibility of data.

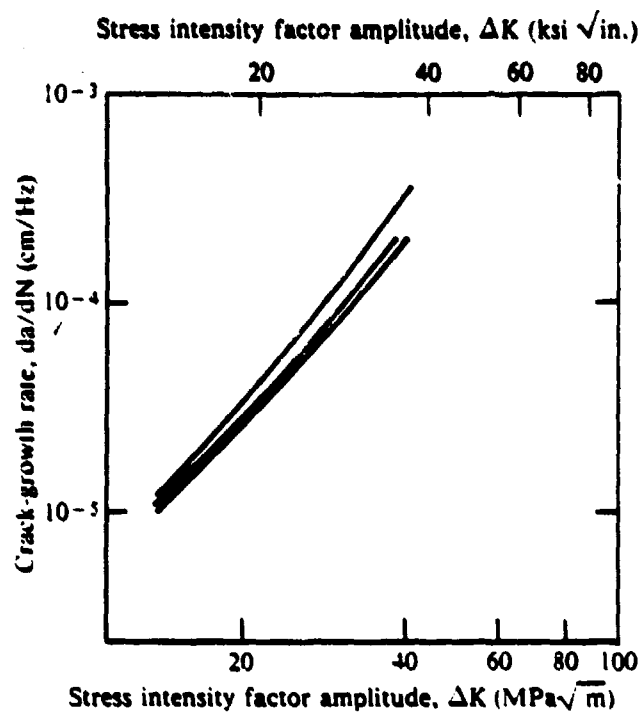


Figure C-7. Fatigue-crack-growth rate of equiaxed- $\alpha$  Ti-6Al-4V at room temperature in ambient air as determined by triplicate tests.

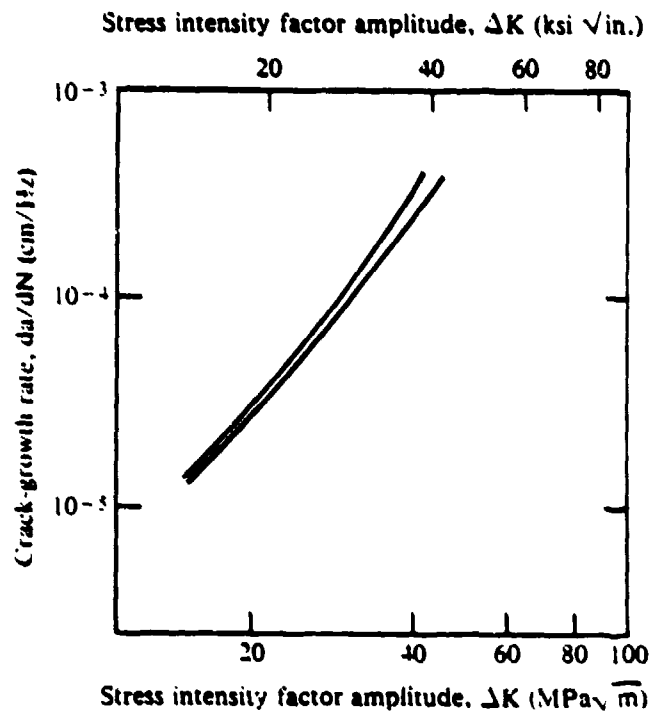


Figure C-8. Fatigue-crack-growth rate of duplex-annealed Ti-6Al-2Sn-4Zr-2Mo at room temperature in ambient air as determined by duplicate tests.

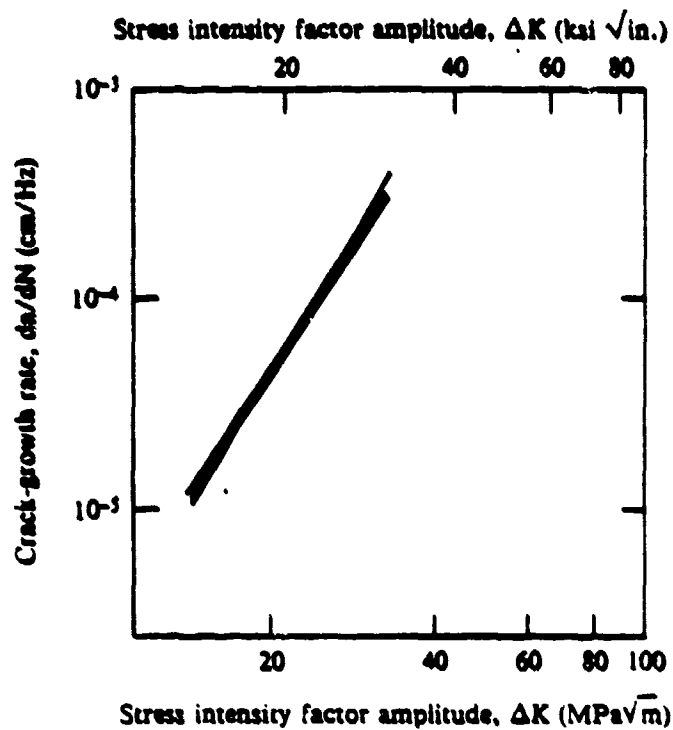


Figure C-9. Fatigue-crack-growth rate of hydrovac-processed, equiaxed- $\alpha$  Ti-6Al-4V at room temperature in ambient air as determined by triplicate tests.

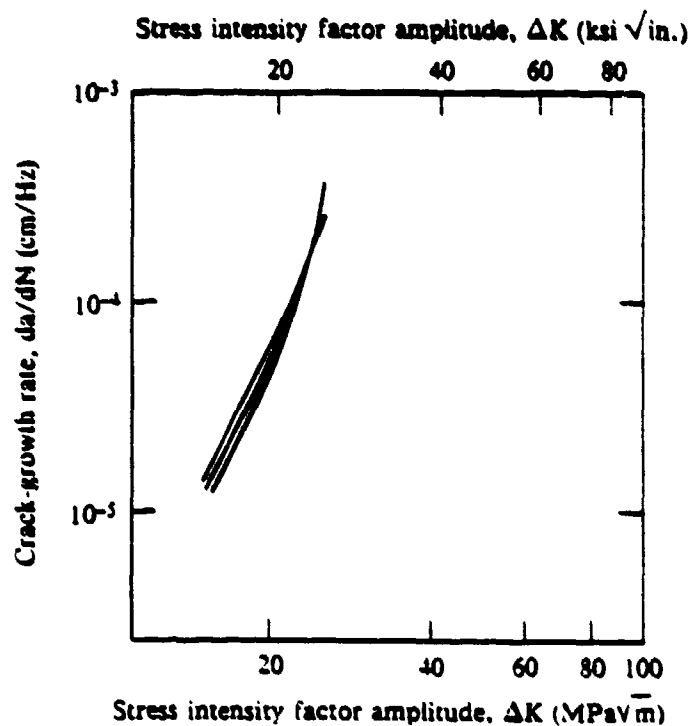


Figure C-10. Fatigue-crack-growth rate of hydrovac-processed, duplex-annealed Ti-6Al-2Sn-4Zr-2Mo at room temperature in ambient air as determined by triplicate tests.

Table C-2 lists the experimentally determined constants A and B of the crack-growth-rate equation,  $da/dN = 10^{-4} (\Delta K)^B$ . Hydrovac-processed alloys are more susceptible to crack growth as shown by the higher exponents for both equiaxed- $\alpha$  Ti-6Al-4V and Ti-6Al-2Sn-4Zr-2Mo. Representative fatigue crack-growth rates of as-received and hydrovac-processed equiaxed- $\alpha$  Ti-6Al-4V shown in Figure C-11 clearly demonstrate that hydrovac-processed alloys are more susceptible to fatigue-crack propagation.

Measurements made during the crack-initiation phase of the fatigue crack-growth test provide semi-quantitative information about crack-initiation susceptibility. The minimum values of  $\Delta K$  at which cracking was observed electrically (Table C-3) indicate that the hydrovac-processed alloys, particularly Ti-6Al-4V, are more resistant to crack initiation.

Indications of fracture toughness, K, were obtained by stopping the fatigue test before specimen failure and applying a slowly increasing load. Although plane-strain conditions were not satisfied, the K values obtained are useful for comparison because the thickness is the same for all specimens. Table C-4 shows that hydrovac processing significantly decreases the fracture toughness of the alloys.

**TABLE C-2**  
**FATIGUE-CRACK-GROWTH PARAMETERS FOR CONVENTIONAL AND HYDROVAC-  
PROCESSED Ti-6Al-4V AND Ti-6Al-2Sn-4Zr-2Mo<sup>(a)</sup>**

Alloy	A	B
Equiaxed- $\alpha$ Ti-6Al-4V	8.79	2.84
Hydrovac-processed, equiaxed- $\alpha$ Ti-6Al-4V	9.94	3.95
Duplex-annealed Ti-6Al-2Sn-4Zr-2Mo	9.16	3.15
Hydrovac-processed, duplex, annealed Ti-6Al-2Sn-4Zr-2Mo	12.00	5.74
Widmanstätten Ti-6Al-4V	9.27	3.01

(a) Crack-growth rate,  $da/dN$  (cm/Hz) as a function of stress-intensity amplitude,  $\Delta K$  (MPa $\sqrt{m}$ ), is given by the relation  $da/dN = 10^{-4} (\Delta K)^B$ .

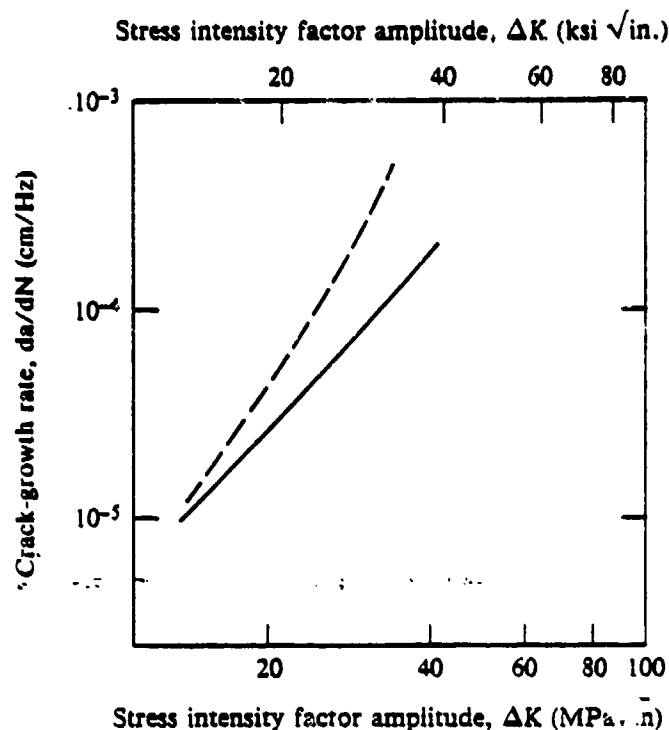


Figure C-11. Fatigue-crack-growth rates of (—) as-received and (---) hydrovac-processed equiaxed- $\alpha$  Ti-6Al-4V at room temperature in ambient air.

TABLE C-3  
MINIMUM STRESS-INTENSITY AMPLITUDE VALUES ( $\Delta K_{min}$ ) FOR THE ONSET OF  
CRACK GROWTH IN AS-RECEIVED AND HYDROVAC-PROCESSED Ti-6Al-4V AND  
Ti-6Al-2Sn-4Zr-2Mo

Alloy	$\Delta K_{min}$ [MPa $\sqrt{m}$ (ksi $\sqrt{in.}$ )]
Equiaxed- $\alpha$ Ti-6Al-4V	20 (18), 19 (17), 19 (17)
Hydrovac-processed, equiaxed- $\alpha$ Ti-6Al-4V	21 (19), 25 (23), 25 (23)
Duplex-annealed Ti-6Al-2Sn-4Zr-2Mo	18 (16), 17 (15)
Hydrovac-processed, duplex-annealed Ti-6Al-2Sn-4Zr-2Mo	19 (17), 20 (18), 20 (18)
Widmanstätten Ti-6Al-4V	20 (18), 20 (18)

**TABLE C-4**  
**FRACTURE TOUGHNESS VALUES,  $K_{IC}$ , DETERMINED FROM FATIGUE-CRACK-  
 GROWTH-RATE TESTS OF AS-RECEIVED AND HYDROVAC-PROCESSED Ti-6Al-4V**  
**AND Ti-6Al-2Sn-4Zr-2Mo**

Alloy	$K_{IC}$ [MPa $\sqrt{m}$ (ksi $\sqrt{in.}$ )]
Equiaxed- $\alpha$ Ti-6Al-4V	92 (84), 99 (90)
Hydrovac-processed, equiaxed- $\alpha$ Ti-6Al-4V	55 (50), 50 (45), 48 (44)
Duplex-annealed Ti-6Al-2Sn-4Zr-2Mo	> 62 (56), > 70 (64)
Hydrovac-processed, duplex-annealed Ti-6Al-2Sn-4Zr-2Mo	37 (34), 37 (34)
Equiaxed- $\alpha$ Ti-6Al-4V	111 (101), 109 (99)

## REFERENCES

1. T. L. Mackay, S. M. L. Sastry, and C. F. Yoltan, Metallurgical Characterization of Superplastic Forming, AFWAL-TR-80-4038 McDonnell Douglas Corporation, St. Louis, MO, September 1980.
2. M. Hansen, Constitution of Binary Alloys, McGraw-Hill, NY, 1958, p. 800.
3. Y. Mahajan, S. Nadiv, and W. R. Kerr, "Studies of Hydrogenation in Ti-6Al-4V Alloys," Scripta Metallurgica, Volume 13, 1979, pp. 695-699.
4. W. R. Kerr, P. R. Smith, M. E. Rosenblum, F. J. Gurney, Y. R. Mahajan, and L. R. Bidwell, "Hydrogen as an Alloying Element in Titanium (Hydrovac)," in Titanium '80; Science and Technology, ed. by H. Kimura and O. Izumi, Metallurgical Society of AIME, Warrendale, PA, 1980, Vol. 4, pp. 2477-2486.
5. J. Greenspan, F. J. Rizzitano, and E. Scala, "Titanium Powder Metallurgy by Decomposition Sintering of the Hydride," in Titanium Science and Technology, Proceedings of Second International Conference on Titanium, ed. by R. I. Jaffee and H. M. Burte, Plenum Press, NY, 1973, pp. 365-379.
6. N. Birla and V. Depierre, A Test Method for Evaluation of Metal Powders, AFML-TR-75-171, October 1975.
7. A. K. Miller and O. D. Sherby, "On Subgrain Strengthening at High and Low Temperatures," Scripta Metallurgica, Volume 10, 1976, pp. 311-317.
8. J. J. Kearns, J. E. McCauley and E. A. Nicols, "Effects of Alpha/Beta Phase Constitution on Superplasticity and Strength of Zircalloy-4," Journal of Nuclear Materials, Volume 61, 1976, pp. 169-184.
9. W. R. Kerr, "The Effect of Hydrogen as a Temporary Alloying Element on the Microstructure and Tensile Properties of Ti-6Al-4V," Metallurgical Transactions (submitted).
10. R. J. Lederich, S. M. L. Sastry, M. Hayase, and T. L. Mackay, "Superplastic Formability Testing," Journal of Metals, Volume 34, 1982, pp. 16-20.

11. P. R. Rios, J. R. C. Guimaraes, and K. K. Chawla, "Modeling the Stress-Strain Curves of Dual Phase Steels," *Scripta Metallurgica*, Volume 15, 1981, pp. 899-901.
12. S. M. L. Sastry, P. S. Pao, and K. K. Sankaran, "High Temperature Deformation of Ti-6Al-4V," in Titanium '80; Science and Technology, ed. by H. Kimura and O. Izumi, Metallurgical Society of AIME, Warrendale, PA, 1980, Vol. 2, pp. 873-877.
13. S. M. L. Sastry, R. J. Lederich, T. L. Mackay, and W. R. Kerr, "Superplastic Forming Characterization of Titanium Alloys," *Journal of Metals*, Vol. 35, 1983, pp. 48-53.
14. F. Dymant, "Self and Solute Diffusion in Titanium and Titanium Alloys," in Titanium '80, Science and Technology, ed. by H. Kimura and O. Izumi, Metallurgical Society of AIME, Warrendale, PA, 1980, Vol. 1, pp. 519-531.
15. K. Hauffe, Oxidation of Metals, Plenum Press, NY, 1965, p. 48.